University of Alberta

Development of block copolymer based nanocarriers for the solubilization and delivery of valspodar

by

ZIYAD BINKHATHLAN

A thesis submitted to the Faculty of Graduate Studies and Research
in partial fulfillment of the requirements for the degree of

DOCTOR OF PHILOSOPHY
in
PHARMACEUTICAL SCIENCES

Faculty of Pharmacy and Pharmaceutical Sciences

Fall 2011
Edmonton, Alberta

Dedication

I dedicate this thesis to my beloved mother, who has always been the main source of motivation for me; to my dear wife who has been in my side all the way with her love, support, and patience; and to my wonderful kids Saud and Yara.

ABSTRACT

One of the major causes of failure in cancer chemotherapy is multidrug resistance (MDR), where cancer cells become resistant to different types of anticancer drugs. Over-expression of membrane efflux pumps like P-glycoprotein (P-gp), which recognizes different chemotherapeutic agents and transports them out of the cell play a major role in MDR. One of the major reasons for shortcomings of P-gp inhibitors in clinic is their non-selective distribution to non-target organs, which leads to reduced elimination of P-gp substrates (e.g. anticancer drugs) and intolerable toxicities by anticancer drugs. The objective of this research is to develop a nanocarrier that permits a change in the pharmacokinetics of P-gp inhibitors, limiting their non-specific distribution. Polymeric micelles have shown promise in changing the pharmacokinetics of hydrophobic drugs in a favorable manner. Presented herein are the results of our investigation of self-associating poly(ethylene oxide)-*block*-poly(ε-caprolactone) (PEO-*b*-PCL) and PEO-*b*-poly(α-benzyl-ε-caprolactone) (PEO-*b*-PBCL) block copolymers as biodegradable polymeric nanocarriers for the solubilization and delivery a model P-gp inhibitor (valspodar). It is hypothesized that encapsulation of valsopdar in polymeric nanocarriers can enhance its therapeutic efficacy by providing an inert alternative to Cremophor EL for solubilizing valspodar, favorably changing its pharmacokinetics and reducing its pharmcokinetic interaction with anticancer drugs (P-gp substrates) upon co-administration. PEO-

b-PCL and PEO-*b*-PBCL were assembled to form carriers of 60-100 nm diameters, and were shown to be able to efficiently encapsulate valspodar: achieving a clinically relevant aqueous solubility of 2.8 mg/mL. Following intravenous administration of valspodar to healthy rats, there was nearly a 100% increase in plasma area under the curve (AUC) of valspodar when administered in the polymeric nanocarrier formulations as compared to when Cremophor EL formulation was used. Co-administration of doxorubicin, a model P-gp substrate anticancer agent, with valspodar in the standard Cremophor EL/ethanol formulation resulted in more than 50% reduction in doxorubicin clearance, which was accompanied by over a 100% increase in doxorubicin AUC. In contrast, no change was detected in doxorubicin clearance or AUC, when valspodar was administered in PEO-*b*-PCL polymeric nanocarrier formulation. Overall, our results suggest that PEO-*b*-PCL micelles hold great promise for solubilization of valspodar and the safe co-administration with doxorubicin.

ACKNOWLEDGEMENTS

I would like to express my gratitude to the following people:

- My supervisor Dr. Afsaneh Lavasanifar for her kindness, guidance, advice, and continuous support. I cannot thank her enough for her endless help and motivation throughout my studies.
- My co-supervisor Dr. Dion Brocks, who was as kind and caring as I was his own student. I am greatly indebited for his advice, guidance and assistance at all stages of my work.
- Dr. Ayman El-Kadi for his thoughtful comments and constructive feedback as my supervisory committee member.
- Dr. Raimar Löbenberg and Dr. Arno Siraki for accepting to be in my examining committee in such a short notice.
- My past lab mates Dr. H.M. Aliabadi, Dr. Adullah Mahmud, and Sara Elhasi for helping me in the beginning of my studies.
- My current lab mates, for the fruitful discussions and help they have given me throughout the whole program.
- All the past and the current members in Dr. Brocks's lab, in particular, Dr. Dalia A. Hamdy, Dr. Marwa Elsherbiny, and Dr. Jigar Patel for their help and support in my early pharmacokinetic studies.
- Faculty staff, in particular, Joyce Johnson, Jeff Turchinsky and Drew Price for their help and support throughout the whole program.
- My dear wife, Rana and my lovely kids, Saud and Yara who accompanied me throughout the whole journey and helped me in every way with their love, support and patience.
- My mother and my dear brothers and sisters for their love, encouragement and support throughout my whole life.
- Finally, I would like to thank the following institutions:
    - King Saud University, Riyadh, Saudi Arabia, for providing me with my scholarship.

- The Saudi Cultural Bureau in Canada, for managing my tuition fees and academic expenses.
- The Faculty of Pharmacy and Pharmaceutical Sciences, University of Alberta, Edmonton, Canada, for accepting me in the graduate studies program and providing me with the facilities, training, and qualification.

TABLE OF CONTENTS

LIST OF FIGURES

LIST OF TABLES

LIST OF ABBREVIATIONS

ABC	ATP-binding cassette
ALL	Acute lymphoblastic leukemia
AML	Acute myeloid leukemia
AUC	Area under the curve
BBB	Blood brain barrier
Bcl	B cell lymphoma
BCRP	Breast cancer resistance protein
bFGF	Basic fibroblastic growth factor
CEP	Circulating endothelial progenitor cells
CDDP	Cisplatin
CL	Clearance
CAC	Critical association concentration
CMC	Critical micellar concentraion
CNS	Central nervous system
CyA	Cyclosporine A
CYP	Cytochrome P450

DLS	Dynamic light scattering
DNA	Deoxyribonucleic acid
DOX	Doxorubicin
DOXol	Doxorubicinol
E	Extraction ratio
eNOS	Endothelial nitric oxide synthase
EPR	Enhanced permeation and retention effect
F	Drug bioavailability
f_g	Drug gastrointestinal availability
f_h	Drug hepatic availability
f_u	Drug unbound fraction in blood
g	Gravitation force
GI	Gastrointestinal
GSH	Glutathione
GST	Glutathione S-transferase
h	Hour
HDL	High-density lipoprotein
HIF	Hypoxia-inducible transcription factor
HPLC	High-performance liquid chromatography
HRE	Hypoxia-response elements

IL	Interleukin
LC/MS	Liquid chromatography/mass spectrometry
LDL	Low-density lipoprotein
LLC	Lewis lung carcinoma
LRP	Lung resistance protein
MDR	Multidrug resistance
min	Minute
$\mathbf{M_n}$	Number average molecular weight
$\mathbf{M_w}$	Weight average molecular weight
µL	Microliter
µM	Micromolar
mL	Milliliter
MMP	Matrix Metalloproteinase
MRP	Multi-drug resistance-associated protein
MTX	Methotrexate
Mw	Molecular weight
NBD	Nucleotide-binding domain
MTD	Maximum tolerable dose
NFκB	Nuclear factor κB
ng	Nanogram

nm	Nanometer
NO	Nitric oxide
NSCLC	Non-small cell lung cancer
ONOO−	Peroxynitrite
P(ASP)	Poly(L-aspartic acid)
PBLA	Poly(β-benzyl-L-aspartate)
PBCL	Poly(α-benzyl-ε-caprolactone)
PCL	Poly(ε-caprolactone)
PDLLA	Poly(D,L-lactide)
PEG	Poly(ethylene glycol)
PEO	Poly(ethylene oxide)
P(Glu)	Poly(L-glutamic acid)
pg	Picogram
P-gp	P-glycoprotein
PHSA	Poly(N-hexyl stearate-L-aspartamide)
PLA	Poly(lactic acid)
PLLA	Poly(L-amino acid)
PLGA	Poly(lactic-*co*-glycolic acid)
PLH	Poly(L-histidine)
PLL	Poly(L-lysine)

PMN	Polymorphonuclear leukocyets
PVP	Poly(N-vinylpyrrolidone)
PXR	Pregnane X receptor
PXT	Paclitaxel
RBC	Red blood cells
RES	Reticuloendothelial system
RIA	Radioimmunoassay
ROC	Reactive oxygen species
SD	Standard deviation
SEM	Scanning electron microscope
SXR	Steroid and xenobiotic receptor
TPGS	D-alpha tocopheryl polyethylene glycol 1000 succinate
TEM	Transmission electron microscope
Tf	Transferrin
THF	Tetrahydrofuran
TNF	Tumor necrosis factor
UV	Ultraviolet
Vd	Volume of distribution
Vd_{ss}	Volume of distribution at steady-state
VEGF	Vascular endothelial growth factor

VEGFR	VEGF receptor
VPF	Vascular permeability factor
WT	Wild-type

CHAPTER ONE

INTRODUCTION

1.1. Multidrug resistance (MDR) in cancer: an overview

Chemotherapy is considered a cornerstone in the management of many types of cancer. However, its effectiveness in curing cancer is partly hampered by inherent or acquired MDR, where cancer cells become resistant simultaneously to pharmacologically and structurally diverse drugs (1, 2). MDR has been linked to the poor prognosis and reduced survival rates for several types of cancer, such as leukemia, gastric, breast, ovarian, and pancreatic cancer (3-6). Studies involving the tumor microenvironment have revealed that there are several pathophysiological factors/forces that might contribute to the development of MDR. These factors/forces may include hypoxia, and changes in the regulation of oncogenes, tumor suppressors, and apoptotic factors (7). For instance, hypoxia in cancer has been linked to an increase in metastatic potential and drug resistance, and has been associated with a poor prognosis (8-15). Moreover, in several studies, hypoxia has been shown to increase the expression of P-glycoprotein (P-gp), a transporter protein associated with MDR (16, 17). Besides hypoxia, factors such as mutations in oncogenes and tumor suppressors have been shown to contribute to the development of MDR (7, 18). Further, the response of cancer cells to these genetic mutations can lead to changes in the tumor microenvironment that promote MDR (17).

1.1.1. Underlying mechanisms for tumor MDR

The underlying mechanisms behind emergence of MDR in cancer have been classified into cellular and non-cellular mechanisms (19). Non-cellular resistance is usually associated with solid tumors and occurs as a consequence of tumor growth. The mechanisms may include geometric resistance of tumor vasculature, increased interstitial fluid pressure, reduced drug penetration to the core of the tumor, insufficient nutrients and oxygen supply, existence of non-cycling cells (resistant to cell cycle-dependent anticancer drugs), and acidic environment (19). The cellular mechanisms have major roles in MDR and are categorized into: classical MDR phenotypes (reduced uptake or enhanced efflux of anticancer drugs) and non-classical MDR phenotypes (overexpression of detoxifying enzymes, underexpression or mutation of anticancer drug targets, or inhibition of apoptotic pathways) (19).

1.1.1.1. Reduced uptake or enhanced efflux of anticancer drugs

The ATP-binding cassette (ABC) transporters comprise one of the largest membrane-bound protein families (20). These transporters can reduce the cellular or nuclear accumulation of their substrates by means of reduced uptake, altered intracellular distribution or enhanced efflux of the anticancer drug. The substrates of these proteins are transported, against a concentration gradient with ATP hydrolysis as a driving force, across the membrane. The human genome encodes more than 40 ABC transporters divided into five different subfamilies: ABCA, ABCB, ABCC, ABCD and ABCG. So far, only 10 transporters have been shown

to be involved in MDR (21), belonging to the subfamilies ABCA, ABCB, ABCC and ABCG (Table 1.1) (21-24). Examples of those transporters may include P-glycoprotein (P-gp), multidrug resistance-associate protein (MRP), lung resistance protein (LRP), and breast cancer resistance protein (BCRP). They can be overexpressed in tumor cells and serve to transport anticancer drugs out of the cell, resulting in intracellular drug levels that are not enough for effective therapy (19).

Table 1.1 – ABC transporters involved in drug resistance (adopted from(21))

Gene	Protein/alias	Anticancer agents effluxed by transporter	Other drugs and substrates
ABCA2	ABCA2	Estramustine	–
ABCB1	P-GP/MDR1	Colchicine, doxorubicin, etoposide, vinblastine, paclitaxel	Digoxin, saquinivir
ABCC1	MRP1	Doxorubicin, daunorubicin, vincristine, etoposide, colchicine, camptothecins, methotrexate	Rhodamine
ABCC2	MRP2	Vinblastine, cisplatin, doxorubicin, methotrexate	Sulfinpyrazone
ABCC3	MRP3	Methotrexate, etoposide	–
ABCC4	MRP4	6-mercaptopurine, 6-thioguanine and metabolites; methotrexate	PMEA, cAMP, cGMP
ABCC5	MRP5	6-mercaptopurine, 6-thioguanine and metabolites	PMEA, cAMP, cGMP
ABCC6	MRP6	Etoposide	–
ABCC11	MRP8	5-fluorouracil	PMEA, cAMP, cGMP
ABCG2	MXR/BCRP	Mitoxantrone, topotecan, doxorubicin, daunorubicin, irinotecan, imatinib, methotrexate	Pheophorbide A, Hoechst 33342, rhodamine

1.1.1.2. Overexpression of detoxifying enzymes

This type of resistance can be caused by the overexpression of specific enzymes such as glutathione S-transferase (GST), which can decrease the activity of anticancer drugs independent of their intracellular concentrations (19). GST is an enzyme system involved in the detoxification of xenobiotics (25). It catalyzes biotransformation reactions whereby organic molecules are conjugated with glutathione (GSH), resulting in polar compounds that can be easily excreted (25). The GSTs have a major role in the metabolism of several anticancer drugs such as nitrogen mustards and cyclophosphamides (19). Several resistant cell lines have been shown to overexpress certain GST isoforms (26-29). Specifically, GST-π (GST-P1) overexpression has been a consistent feature of several tumors. Moreover, it has been associated with drug resistance and poor prognosis (30). In fact, Canfosfamide (TELCYTA®) is an investigational prodrug that has been specifically designed to exploit the elevated levels of GST-P1 (31). This prodrug is activated by GST-P1, where it is cleaved into its two active components: a GSH analog and a cytotoxic moiety which induces apoptosis (30). TELCYTA® is currently in Phase III clinical trials for the treatment of advanced tumors in combination with other anticancer agents (32, 33). In addition to GST, GSH also appears to play a key role in detoxification and cellular repair following the damaging effects of some anticancer drugs (19). Increases in GSH levels have been observed in many resistant cell lines (34-36).

1.1.1.3. Underexpression or mutation of drug targets

Topoisomerases are isomerase enzymes that control the changes in DNA structure by catalyzing the winding/unwinding of DNA during DNA transcription and replication (37). Two types of topoisomerase have been shown to be present in all eukaryotes (38, 39). Type I topoisomerase alters the DNA topology *via* single strand break, while type II topoisomerase cuts both strands of DNA (37). Thus, these enzymes have been considered as therapeutic targets in rapidly dividing tumor cells for anticancer drugs. For example, camptothecin derivatives specifically target type I topoisomerase, while doxorubicin and etoposide and their analogs target type II topoisomerase.

Although topoisomerase inhibitors are among the most efficient inducers of apoptosis (40), resistance to various topoisomerase (I and II) inhibitors has been documented (41-44). Resistance may occur alone or concurrent to P-gp overexpression (45-47). Generally, the resistance may occur due either to underexpression of topoisomerase enzyme or topoisomerase gene mutation (48-54). It has been reported that resistance to topoisomerase I inhibitors is often accompanied by a compensatory rise in the level of topoisomerase II expression and *vice versa* (55, 56). For instance, resistance to camptothecins is believed to be due to down-regulation of topoisomerase I, thereby leading to hypersensitivity to etoposide, a topoisomerase II inhibitor, as a consequence of a possible increase in topoisomerase II expression. In another instance, when the topoisomerase I inhibitor camptothecin-11 (irinotecan) was pretreated in nude mice bearing

human xenografts, enhanced activity of doxorubicin, a topoisomerase II inhibitor, was observed (57), presumably due to overexpression of topoisomerase II activity mediated by irinotecan pretreatment. Therefore, in order to circumvent topoisomerase-mediated resistance, it has been suggested to target both enzyme classes at the same time. Nonetheless, the results from preclinical and clinical studies with simultaneous or sequential exposure of tumor cells to etoposide and either topotecan or irinotecan demonstrated an antagonistic, rather than synergistic, effect in addition to severe to life-threatening neutropenia and anemia (56, 58-61). A single agent that inhibits both topoisomerases (dual inhibitor) may present the advantage of improving antitopoisomerase activity, with reduced side effects, as opposed to the combination of two inhibitors. Indeed, in recent years, a number of compounds able to target both enzymes have been identified (recently reviewed in (62)). Moreover, some of the dual topoisomerase I/II inhibitors have reached the clinical trials such as aclarubicin and intoplicin (63), in addition to batracylin, which is currently being investigated in phase I clinical trials (NCT00450502) for patients with solid tumors and lymphomas (62).

1.1.1.4. Inhibition of apoptotic pathways

Anticancer agents typically induce apoptosis, or programmed cell death. This form of cell death is characterized by certain changes in the cell morphology including nuclear condensation and DNA fragmentation. The complicated process of apoptosis is controlled by a diverse range of genes and proteins that exert a

regulatory role in cellular events (reviewed in (64)). The tumor suppressor protein, p53, encoded by *TP53* gene, is a well-characterized transcription factor that is responsible for the direct activation of numerous genes involved in apoptosis. The p53 pathway responds to intra- or extracellular stresses that disrupt DNA replication and cell division (65). Following DNA damage, such as the one caused by anticancer drugs, the transmitted stress signal leads to a response through post-translational modification and consequential activation of the p53 protein (66). As p53 levels increase, transcription of downstream target genes occurs. In addition to the transcription-dependent induction of apoptosis, p53 also induces apoptosis through the mitochondrial pathway (67). Besides p53, there is the apoptosis regulator Bcl-2 family of proteins. The Bcl-2 gene was first discovered in 1985 in human B-cell lymphomas (68). To date, there are a total of 25 genes in the Bcl-2 family. These proteins can either be pro-apoptotic (e.g. Bax and Bak) or anti-apoptotic (e.g. Bcl-2 proper and Bcl-XL) (69). Bcl-2 family proteins are able to form homo- and hetero-dimers and the balance achieved will determine the apoptotic fate of the cell (64). For instance, it has been shown that bax-bcl-2 heterodimers as well as bax homodimers promote apoptosis, whereas apoptosis is inhibited when bcl-2 forms homodimers (70, 71). Therefore, the Bcl-2 family proteins are considered the key regulators of apoptosis. Other signaling pathways that have critical role in cell survival/apoptosis may include phosphatidylinositol-3-phosphate kinase (PI3K) (72, 73), nuclear factor-kappaB (NF-κB) (74), and RAS/RAF (75) pathways.

There are many potential mechanisms whereby tumor cells can develop resistance to apoptosis. Clinically relevant examples include inactivating mutations of the gene for p53 protein (*TP53*) (76-78), activating mutations of the gene for PI3K (79-83), attenuation of expression of PTEN (a phosphatase controlling PI3K activity) (84-86), and activating mutations of the genes for the RAS/RAF pathway (87-89). Modulation of these pathways affects the balance of activity of the bcl-2 family of proteins. These findings have therefore motivated a widespread attempt to find drugs that act to counter the resistance to apoptosis. In fact, there are now several therapeutic drugs that are being evaluated in preclinical and clinical studies (90-92). Direct inhibition of bcl-2 family members, has been demonstrated (93). For instance, obatoclax interferes with bcl-2 family-mediated resistance and restores sensitivity to several new anticancer drugs (94). Examples of the other promising approaches used to overcome resistance to apoptosis include the development of inhibitors of the PI3K (95, 96) and NF-κB (97-100) signaling pathways.

1.1.2. P-glycoprotein (P-gp)

P-gp was first identified by Juliano and Ling (1976) as a surface glycoprotein expressed in drug-resistant Chinese hamster ovary cells (101). This discovery led to the finding that P-gp is an ATP-dependent efflux transporter, which has become the most studied member of ABC transporters. It can bind to a large variety of hydrophobic compounds with neutral or positive charge including

numerous anticancer agents. In fact, classical resistance to the chemotherapeutic agents is usually linked to the overexpression of P-gp (19, 102).

1.1.2.1. Structure

P-glycoprotein is the 170-kD protein product of the human gene *MDR1* (*Mdr1a/1b* in rodents) (103, 104). Although it is also encoded by another gene (*MDR3*) in human (*Mdr2* in rodents), the *MDR3* gene product is believed to be only involved in phospholipid transport (105-108). *MDR1* P-gp is comprised of 1280 amino acids divided into two symmetrical halves (cassettes) with 43% sequence homology between the two cassettes (19, 102, 103, 109). Further, each cassette contains six transmembrane domains that are separated by an intracellular flexible linker polypeptide loop with an adenosine 5′-triphosphate (ATP)-binding motif (19, 103, 106) (Figure 1.1).

One of the most interesting features of P-gp is that it can recognize and transport drugs with a wide array of chemical structures (106). Although most of the drugs transported by P-gp are basic or neutral, there are many exceptions. The only common feature is that most of the P-gp substrates are hydrophobic in nature, suggesting that partitioning of the lipid membrane of cells is an essential step for the interaction of a substrate with the active sites of P-gp. In fact, Seelig and Landwojtowicz have shown that hydrophobicity and number of hydrogen bonds are the major determinants for substrates and P-gp interaction, and that partitioning into the lipid membrane is the rate-limiting step for such interaction

(110). Additionally, the surface area and amphiphilic characteristic of the substrate also seems to play a significant role in determining its P-gp activity (111).

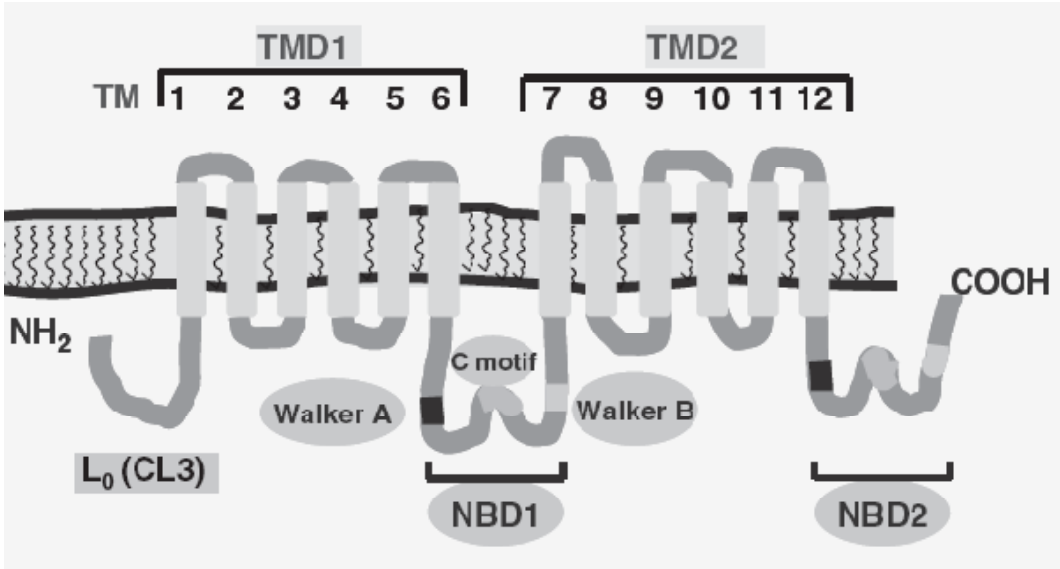

Figure 1.1 – Proposed topology and domain organization of P-gp (Adopted from ref. (112)). TMD: Transmembrane domain; NBD: Nucleotide-binding domain; CL3: Cytoplasmic loop 3.

Although in recent years there has been a great advancement in our understanding of the structure of P-gp, the precise molecular mechanism of drug transport by P-gp is still not fully understood (106). Nevertheless, several hypothetical models were proposed to explain the mechanism of substrate efflux by P-gp (113). The pore model, flippase model, and hydrophobic vacuum cleaner (HVC) model explain the efflux mechanism to a certain extent (113) (Figure 1.2). Generally, when a substrate binds to P-gp, it results in the hydrolysis of one ATP and a change in the conformation of P-gp, which is followed by the release of

bound drug to the extracellular space (114-117). Hydrolysis of the second ATP restores the native conformation of P-gp (116-118). In tumor cells that express P-gp, this would result in reduced intracellular concentrations of a wide range of anticancer agents including anthracyclines (e.g. doxorubicin), Vinca alkaloids (e.g. vincristine), epipodophyllotoxins (e.g. etoposide) and taxanes (e.g. paclitaxel). The reduction in intracellular concentrations of anticancer drugs usually results in a decrease in the cytotoxicity of these agents. The two cassettes of P-gp have two central roles in the substrate transport process. First, they form the pathway through which the substrate is translocated across the cell membrane. Second, they provide the amino acid residues which interact directly with the substrate and form substrate binding-site(s) (117, 119).

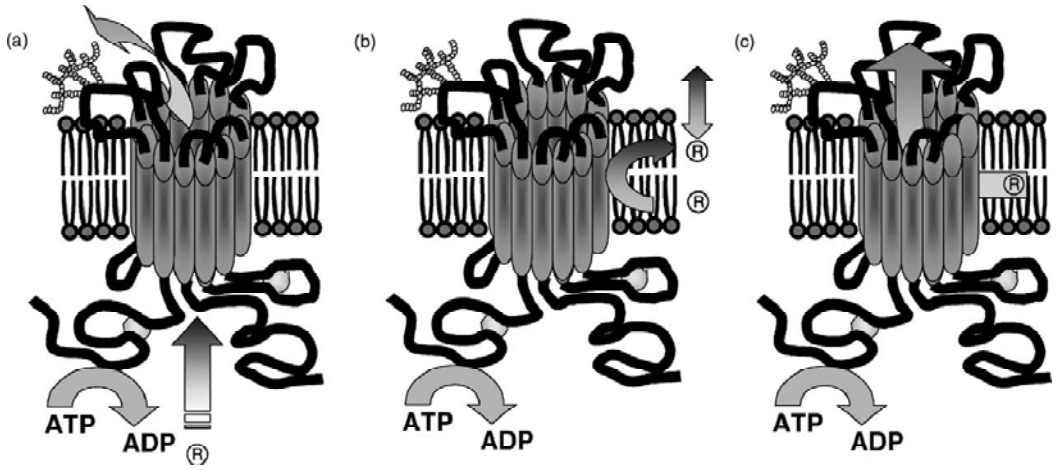

Figure 1.2 – Models proposed to explain the mechanism of drug efflux by P-gp. (a) Pore model, (b) flippase model and (c) hydrophobic vacuum cleaner model. In pore model, drugs associate with P-gp in the cytosolic compartment and are transported out of the cell through a protein channel. In flippase model, drugs embed in the inner leaflet of the plasma membrane, bind to P-gp within the plane of membrane and are translocated to the outer leaflet of the bilayer from which they passively diffuse into extracellular fluid. The hydrophobic vacuum cleaner model combines the features of 'pore' and 'flippase' models (Adopted from ref. (113)).

1.1.2.2. Tissue distribution and physiological role

In addition to MDR tumor cells, P-gp is constitutively expressed in various normal human tissues including the kidney, liver, small and large intestine, brain, testes, adrenal gland and the placenta (120-122). This tissue distribution indicates that P-gp plays an important role in excreting xenobiotics and metabolites into urine, bile and into intestinal lumen, and in preventing their accumulation in the brain and pregnant uterus (120, 122). The expression of P-gp in some of the major organs indicates that P-gp might be part of a protective role against a wide range of potentially toxic substances, serving to limit their distribution and facilitate their elimination (114). Determination of the

distribution pattern and the exact location of P-gp would lead to a better understanding of its physiological role.

In the gastrointestinal (GI) tract, P-gp is expressed on both the small and large intestine (colon) and located on the apical membrane of intestinal epithelial cells, oriented such that substrates are secreted from the cells into the intestinal lumen (123). An intriguing aspect of P-gp is the interaction with drug metabolizing enzymes, specifically the 3A4 isozyme of cytochrome P450 (CYP3A4). P-gp and CYP3A4 share many substrates and inhibitors and have a common tissue distribution (124). The considerable overlap in the substrate selectivity and tissue localization of CYP3A4 and P-gp has led to the hypothesis that this transporter - enzyme pair act as a coordinated absorption barrier against xenobiotics (124-126). In fact, several studies have shown that P-gp in the intestine not only limits parent drug absorption but also increases the access of drug to metabolism by CYP3A4 through repeated cycles of absorption and efflux (125, 127). Co-regulation of CYP3A4 and P-gp has been proposed as an explanation of the overlap of substrate specificity and tissue distribution of these two proteins. This has been confirmed by the identification of the human nuclear receptor SXR (steroid and xenobiotic receptor) and its rodent homolog PXR (pregnane X receptor), which have been shown to coordinately regulate *CYP3A4* and *MDR1* (127, 128).

In the liver, P-gp is located on the canalicular (apical) membrane and functions to transport substrates into the canalicular space from the interior of the hepatocyte (129). For a compound to be eliminated by means of P-gp-mediated biliary excretion, it must first pass across the sinusoidal membrane of the hepatocyte. Once in the hepatocyte, the compound may be segregated and/or trafficked to the canalicular membrane, where P-gp will transport the compound into bile; ultimately, the compound would either be reabsorbed from the intestine or eliminated in the feces. Moreover, drug metabolites may also be transported by P-gp into bile (130).

In kidney, P-gp is expressed on the apical (luminal) side of the proximal tubule cells and also in other parts of the nephron such as the loop of Henle and collecting ducts (131). Many studies have shown that P-gp plays a key role in the renal elimination of certain substrates by means of active secretion into the urine. In addition to increasing the direct flux of drugs from blood to urine (132), P-gp would likely limit the re-absorption of substrates that are filtered at the glomerulus.

The blood brain barrier (BBB), which comprises endothelial cells lining the brain capillaries, represents an important physical, biochemical, and transport barrier that serves to limit access of many xenobiotics to the central nervous system (CNS) (133). Although it is generally assumed that highly lipophilic drugs will achieve high concentrations within the CNS by passive diffusion across cell

membranes, numerous lipophilic agents penetrate the CNS poorly (e.g., loperamide, vinblastine, etoposide, domperidone, and colchicine). Interestingly, most of these compounds are substrates for P-gp (134, 135). Immunocytochemical studies revealed the presence of P-gp on the luminal (apical) membrane of brain microvessel endothelial cells (BMEC) (120). The first experimental evidence that P-gp is involved in drug transport in the BBB was reported by Tsuji and coworkers (136). Later, there has been a growing body of evidence, from studies in animal models and studies in humans, suggesting that P-gp has a significant role in limiting substrate penetration into the CNS and is an important determinant of pharmacologic effect and toxicity within the CNS (130). Functional P-gp has also been found in several types of human and murine cells/tissues such as leukocytes and pluripotent stem cells, adrenal gland, testes, and placenta.

1.1.2.3. Role of P-gp in cancer MDR

Studies performed over the last two decades have shown that intrinsic and acquired expression of P-gp plays a significant role in clinical drug resistance in specific solid tumors and hematological malignancies. For instance, Goldstein *et al.* (137) analyzed more than 400 tumors and provided a classification on the basis of their *MDR1* RNA levels. Accordingly, tumors were classified into three types: 1) ***usually positive*** for *MDR1* gene (intrinsically drug-resistant tumors, such as colon, kidney, liver and pancreas cancer); 2) ***occasionally positive*** (e.g. neuroblastoma and acute lymphocytic leukaemia in adults, untreated non-

Hodgkin's lymphoma, treated breast cancer and pheochromocytoma); 3) ***generally negative*** (e.g lung, ovary, prostate cancer, and melanoma) (137). Although the low level or absence of *MDR1* expression in some drug-resistant tumors suggests that other mechanisms of multidrug resistance exist, there is a strong correlation between *MDR1* expression and drug resistance in many types of cancer. Moreover, a recent literature review has revealed that overexpression of *MDR1* was associated with poor responses to first-line chemotherapy (138).

In breast cancer, the role of *MDR1* gene expression has been extensively investigated (139). A meta-analysis (140) performed on 31 breast cancer studies (total of 1232 treated or untreated patients) revealed two important findings: 1) it indicated that the proportion of breast tumors expressing *MDR1* gene in all studies was about 40%; and 2) patients with tumors expressing *MDR1* were three times more likely to fail to respond to chemotherapy than patients whose tumors were *MDR1* negative (140). However, due to the high variability among the different studies included in the meta-analysis, a definitive conclusion about the role of P-gp in breast cancer was not possible.

It has always been believed that the contribution of P-gp to multidrug resistance is exclusively by virtue of decreasing the intracellular concentration of chemotherapeutic agents in the tumor cells. However, there might be complementary mechanisms not directly related to anticancer drug efflux, like its counteracting influence on apoptotic stimuli (141). The work by Johnstone group

and others has demonstrated that functional P-gp can confer resistance to apoptosis induced by diverse nondrug stimuli including Fas and TNF, UVB- and γ-irradiation and serum starvation (142-144).

The exact mechanism by which P-gp inhibits apoptosis is not clear; however, different theories have been proposed including interfering with death-inducing signaling complex (DISC) and inhibition of caspase-8 activation (142, 144). Moreover, it has been suggested that P-gp could prevent apoptosis by regulating the intracellular levels of lipid factors involved in apoptotic signaling pathways such as the sphingolipids and their metabolites, particularly ceramide and sphingosin-1-phosphate (S1P) (141). Furthermore, overexpression of sphingosine kinase, the enzyme involved in the production of S1P, leads to up-regulation of P-gp (141). Therefore, it has been concluded that interplay between the lipid mediators and the transporter function and/or expression may contribute to the resistance of P-gp-positive cells to ceramide-induced apoptosis (145-147). Interestingly, two well known inhibitors of P-gp, cyclosporine A and valspodar (PSC 833) also directly affect ceramide metabolism (148, 149). Both inhibitors were shown to increase apoptotic death of P-gp expressing tumor cells (148-151).

1.1.3. P-gp inhibitors for chemosensitization of MDR tumors

P-gp inhibitors belong to a variety of chemical and pharmacological classes including calcium channel blockers, coronary vasodilators, quinolines,

cyclosporins, hormones, excipients, and antibodies (1, 152-154). In general, they have been classified into three generations (19). Examples of first generation P-gp inhibitors include verapamil, felodipine, nifidipine, chlorpromazine, quinine and quinidine, and cyclosporine A (CyA) as the most effective first generation P-gp inhibitor known. To date, a number of these inhibitors have excellent MDR-reversal activities both *in vitro* and *in vivo* (19). A unique property shared by most first generation P-gp inhibitors is that they are already existing therapeutic agents and they typically reverse MDR at concentrations much higher than those required for their individual therapeutic activity, which consequently leads to unacceptable side effects (155). Moreover, several of these agents possess an inhibitory action on cytochrome P-450 3A (CYP3A) activity as well as on biliary and renal excretion *via* effects on P-gp. Therefore, they have the potential to alter the pharmacokinetics of the anticancer drugs with which they are co-administered.

The search for non-toxic inhibitors resulted in the development of second generation inhibitors which are more potent and less toxic derivatives of first generation drugs (156-158). Examples of these agents include dexverapamil (R-enantiomer of verapamil), emopamil, and valspodar (non-immunosuppressive analog of CyA). They are very effective at lower concentrations compared to their analogs in the first generation (156-158). However, like the first generation P-gp inhibitors, several of the second generation P-gp inhibitors also inhibit CYP3A enzymes.

Later, several MDR modulators, including monoclonal antibodies targeted against P-gp, have been developed using structure-activity relationships and combinatorial chemistry approaches. These agents are considered third generation P-gp inhibitors (159-161). Examples may include tariquidar, zosuquidar, and laniquidar (24). These investigational agents have minimal effect on other members of the ABC transporter family and have no appreciable impact on CYP 3A4 (162). Moreover, they are very effective at concentrations in the nanomolar range (19). One of the most promising third-generation P-gp inhibitors is tariquidar, which binds non-competitively and with high affinity to P-gp and potently inhibits its activity (163). The inhibitory effects of tariquidar on the P-gp pump notably exceed those of first- and second-generation P-gp inhibitors with respect to potency and duration of action (163). Moreover, it did not interfere with the pharmacokinetics of paclitaxel, vinorelbine, or doxorubicin when it was administered to patients with solid tumors (164). This allowed the use of standard doses of these chemotherapeutic agents without the need for dose reduction as was the case with the older generations of P-gp inhibitors. Although several P-gp inhibitors from all generations have been evaluated in several clinical trials, none of these agents has yet been approved for clinical use.

1.1.4. Clinical trials and limitations of the use of P-gp inhibitors in MDR

Although three generations of P-gp inhibitors have emerged and a number of clinical trials have been conducted to investigate their potential to inhibit drug resistance, most of these trials have either not been successful or were terminated because of the non-specific toxicity associated with the use of these agents. Most of the early clinical studies showed that clinical drug resistance is quite complex, as the observations reported in *in vitro* models could not be reproduced *in vivo*. One of the obstacles in the successful outcome of clinical studies was the high variability in the response rate associated with P-gp inhibitors, which not only depends on the levels of the expression of the target transporter i.e. P-gp, but also on the co-expression of other ABC drug transporters in patients. Furthermore, although the plasma concentration of the P-gp inhibitors sometimes exceed the toxic level, sufficient concentration to inhibit the P-gp function may not have been achieved. Another important factor in the effectiveness of an inhibitor in clinical studies is pharmacokinetic interactions between the P-gp inhibitor and the anticancer drug(s) used in the study, which leads to enhanced toxicity of the anticancer drug(s). In many cases, co-administration of a P-gp inhibitor resulted in significantly elevated plasma concentrations of an anticancer drug by interfering with its excretion or metabolism. Moreover, inhibition of P-gp in non-target cells may increase the toxicity of the anticancer drugs in healthy tissues that express P-gp. These problems represent the major obstacles to positive outcomes and the successful use of the P-gp inhibitors in overcoming MDR in the clinic.

Different P-gp inhibitors that are presently in the clinical trials are summarized in Table 1.2.

Among the P-gp inhibitors, valspodar (PSC 833) is a second generation inhibitor, and one of the most studied compounds to date in clinical trials. It was selected on the basis of encouraging preclinical results showing a 10-fold higher potency than cyclosporine A, along with lower renal toxicity and lack of immunosuppressive activity (103, 157, 165-169). Valspodar is not a P-gp substrate, and it is believed to act in a non-competitive manner by binding to the P-gp and altering its conformation (170-174). However, there is some evidence that valspodar may serve as substrate for P-gp and its transport was demonstrated by both human and mouse P-gp although characterized by a 4-fold lower K_m (50 nM) compared to its analog, CyA (200 nM) (175). It has also been found that valspodar directly interacts with P-gp with high affinity and that it probably interferes with its ATPase activity (176). On the basis of these data it has been extensively studied in clinical trials, including phase III studies, some of which are ongoing. However, the major drawback in the clinical application of valdospar is its inhibitory action on cytochrome P-450 3A (CYP3A) as well as the non-selective action on P-gp expressed in normal tissues, which results in reduced elimination and enhanced accumulation and toxicity of several anticancer drugs (P-gp substrates) after co-administration with valspodar in patients with cancer (168, 177-180). These unwanted effects were clinically relevant (181-183). Generally, in the presence of valspodar, the suggested dose reductions were 50-

60% for paclitaxel and 30-50% for doxorubicin and etoposide (184-186). The risk of toxicity makes chemotherapy dose reductions necessary which in turn lead to an inevitable decrease in clinical activity of the treatment. In fact, that could explain in part why in recent clinical trials (187, 188), and several others (189-192), valspodar did not improve the clinical outcomes in patients with cancer.

Table 1.2 – P-gp inhibitors that are currently in clinical trials

P-gp inhibitor	Common name	Type(s) of cancer	Clinical benefit	ClinicalTrials.gov Identifier(s)
PSC 833	Valspodar	AML	No	NCT00004217; NCT00005823
XR 9576	Tariquidar	Solid tumors	Limited	NCT00020514; NCT00069160
LY 335979	Zosuquidar	AML	No	NCT00046930
R 101933	Laniquidar	Breast cancer	Not known	NCT00028873
MS 209	Dofequidar	Solid tumors	Not known	NCT00004886
Tesmilifene	–	Breast cancer	Limited	NCT00364754
CBT-1	–	Solid tumors	Limited	NCT00972205

1.1.5. Role of drug delivery systems in the treatment of MDR tumors

In 1972, Riehm and Biedler showed that the non-ionic surfactant polysorbate 80 (commercially known as Tween 80) was able to enhance the cytotoxicity of actinomycin D and daunomycin in Chinese hamster resistant cells (193). Since then, a number of lipid and polymeric excipients present in pharmaceutical formulations have been reported to modulate the activity of P-gp. Examples of those excipients may include: Cremophor EL, Solutol HS, and vitamin E TPGS (153).

Liposomes, the most extensively studied colloidal drug delivery systems, have been shown to inhibit P-gp function (194-199). Two mechanisms were proposed for this effect, namely, bypassing P-gp through an endocytosis pathway (1, 200) and direct interaction with P-gp (197). Rahman *et al.* have proved the interaction of liposomes with P-gp through P-gp photolabeling studies using azidopine (a photoactive P-gp substrate) (195). They have shown that liposome-encapsulated doxorubicin completely inhibited the photoaffinity labeling of P-glycoprotein by azidopine in membrane vesicles of human vincristine-resistant leukemia cells (HL-60/VCR), with potency comparable to that of azidopine, suggesting that circumvention of MDR by liposomes is related to their specific interaction with P-glycoprotein (195). Moreover, in the same study, blank liposomes have been shown to directly inhibit photoaffinity labeling of P-glycoprotein. However, other studies have shown that liposomes had limited

success in overcoming P-gp-mediated resistance in some *in vitro* models and in clinical studies (201-204). Recently, liposomal formulations co-encapsulating both an anticancer agent and a P-gp inhibitor have been studied. The results showed that liposomes co-encapsulating both drugs had better responses in both *in vitro* and *in vivo* resistant models compared with non-encapsulated (free) drugs (205-207). Furthermore, actively targeted liposomes have been investigated to overcome P-gp-mediated drug resistance (207). For instance, doxorubicin and verapamil were co-encapsulated into liposomes with 95 and 70% encapsulation efficiency, respectively. Human transferrin (Tf), which was used as the targeting moiety, was conjugated to the liposomes to target Tf receptors. In resistant leukemia K562 cells (Tf receptor-positive), Tf-conjugated liposomes co-encapsulating doxorubicin and verapamil showed higher cytotoxicity (IC_{50} = 4.18 μM) compared to the non-targeted ones (IC_{50} = 21.7 μM) and the targeted liposomes loaded with doxorubicin alone (IC_{50} = 11.5 μM). It was concluded that Tf-targeted liposomes co-encapsulating doxorubicin and verapamil were effective in selective targeting and reversal of drug resistance in cells (207).

The most extensively studied amphiphilic block copolymers are derivatives of poly(ethylene oxide)-*b*-poly(propylene oxide)-*b*-poly(ethylene oxide) (PEO-*b*-PPO-*b*-PEO) which are known as poloxamers or commercially as Pluronic®. Alakhov et al. have demonstrated that Pluronic® block copolymers inhibit the efflux actions of P-gp and consequently sensitizing resistant cells (208, 209). For instance, by addition of Pluronic® L61 to the doxorubicin-resistant

human breast cancer cell line (MCF-7/ADR), there was a 740-fold increase in the sensitivity towards doxorubicin compared to the drug alone (IC_{50} = 222 μg/mL *versus* 0.3 μg/mL), while the cytotoxicity in the sensitive cell line (MCF-7) was unaffected (IC_{50} = 2 μg/mL) (210). Similar effects have also been reported *in vivo* (210, 211). Specifically, there was a significant increase in lifespan (> 150%) and tumour growth inhibition (> 90%) observed in animals with daunorubicin-resistant murine myeloma ($Sp2/0^{DNR}$) tumors treated with doxorubicin/L61 compositions (211). Recently, Kabanov et al. demonstrated that Pluronic® can 1) increase tumor accumulation of the P-gp substrate; 2) induce ATP depletion and 3) promote apoptosis in animal models of MDR tumors (212). Furthermore, Pluronic® can increase the antitumor effect of the drug both in MDR and non-MDR tumors (212). Currently, there are clinical trials (Phase II) undergoing for SP-1049C (Supratek Pharma, Inc., Canada), a doxorubicin formulation based on Pluronic® (mixture of L61 and F127) (213, 214). Although results from these trials on this system reported partial response in some patients, data shows appearance of hematological and non-hematological signs of toxicity in some patients (215)

Burt and coworkers investigated the potential of low molecular weight methoxypolyethylene glycol-*block*-polycaprolactone (MePEG-*b*-PCL) to modulate P-gp function in Caco-2 cells (216). They have shown that diblock copolymers composed of $MePEG_{17}$-b-PCL_5 produced optimal enhanced cellular accumulation of Rhodamine-123 (P-gp substrate) in Caco-2 cells (216). Recently,

the same group investigated the potential of MePEG-*b*-PCL diblock copolymers to modulate P-gp function in MDR cancer cells (217). The results showed that the $MePEG_{17}$-*b*-PCL_5 diblock copolymer modulated P-gp function in P-gp over-expressing MDR cells and resulted in enhanced accumulation and retention of P-gp substrates (doxorubicin and paclitaxel) in MDR cells. Moreover, the diblock copolymer was also effective in increasing the cytotoxicity of doxorubicin in MDR cells with the reduction in IC_{50} values of doxorubicin comparable to those obtained with Pluronic® (217, 218). Interestingly, there is a notable difference between MePEO-*b*-PCL and Pluronic® in the way they exert their P-gp inhibiting activity. MePEO-*b*-PCL copolymer usually exert its effects at concentrations above CMC (in the micelles form) when a relatively hydrophilic P-gp substrate was used (e.g. doxorubicin and rhodamine 123) (216, 217) and at concentrations below CMC when a hydrophobic P-gp substrate was used (e.g. Paclitaxel and Rhodamine 6G) (217, 219), while Pluronic® has always been shown to overcome P-gp-mediated resistance at low concentrations i.e. below CMC (in the unimers form) (220, 221). The reason behind that is unclear since studies directly comparing P-gp inhibition between Pluronic® and the MePEG-*b*-PCL diblock copolymers have not been performed.

It should be noted that the ability of delivery systems to overcome drug resistance in cancer is not necessarily through an intrinsic P-gp inhibiting activity of the delivery system itself. Although the mechanisms to overcome MDR using drug delivery systems are often complex and not fully understood, it could simply

be due to the ability of these systems to by-pass the P-gp pump through endocytosis (1, 222-224), saturation of the P-gp by high concentration of the drug (225, 226), or even through mechanisms unrelated to P-gp (227). In fact, there are several delivery systems (reviewed in (228)) that have been shown to improve the anticancer efficacy in MDR tumors both *in vitro* and *in vivo* through mechanisms that are not yet fully elucidated. Examples of these delivery systems, apart from liposomes and polymeric micelles, include polymeric nanoparticles, lipid nanocapsules, and polymer-drug conjugates (228). Additional understanding of the mechanisms by which delivery systems address the biological aspects of MDR may lead to novel systems that could be effectively utilized for treatment of MDR.

1.1.5.1. Role of drug delivery systems in reducing undesirable effects of P-gp inhibitors

Several preclinical and clinical studies have demonstrated that PEGylated liposomes could overcome valspodar-doxorubicin pharmacokinetic interaction (229-232). Krishna *et al.* have studied the renal and biliary clearance properties of liposome-encapsulated doxorubicin and compared them to those for non-encapsulated doxorubicin in the presence and absence of valspodar in a rat model (232). The results suggest that liposomes may overcome valspodar-induced doxorubicin pharmacokinetic changes, and that is likely due to the slower urinary and biliary elimination of liposomal doxorubicin (232). In a phase I clinical trial, although the use of valspodar necessitated dose reductions of both anticancer

agents (liposomal doxorubicin and paclitaxel), valspodar pharmacokinetic interactions were observed with paclitaxel but not with liposomal doxorubicin (229). To further define the pharmacokinetic interactions of liposomal doxorubicin and valspodar, another phase I study was performed with liposomal doxorubicin (without paclitaxel), and with and without valspodar (230). The results showed that treatment with PEGylated liposomal doxorubicin in combination with valspodar resulted in a moderate decrease in the mean doxorubicin clearance (~ 33%) and an increase in the half-life (~ 65%) but did not increase the toxicity of this agent (230).

1.2. Polymeric micelles: an overview

Polymeric micelles are association core/shell carriers with a diameter in the nanometer range (10-100 nm) (233-236). In the last twenty years, they have gained considerable attention as versatile nanomedicine platforms that can fulfill the requirements of an ideal drug carrier for targeted drug delivery (233, 234, 237-239). Polymeric micelles are formed through self-assembly of amphiphilic block copolymers in an aqueous environment (Figure 1.3). They have a core/shell structure in which the hydrophobic core acts as a nanoreservoir for the encapsulation of hydrophobic drugs, proteins or DNA and the hydrophilic shell interfaces the biological environment. Owing to the presence of hydrophilic shell polymeric micelles can escape opsonization and further uptake by mononuclear phagocytic system (MPS) and circulate for longer periods of time in the blood and

eventually accumulate in tissues bearing leaky vasculature; a behavior that is not unique to polymeric micelles and can be achieved by other stealth nano-carriers such as stealth liposomes (240, 241). The unique feature that has made polymeric micelles superior to other colloidal delivery systems; however, is the chemical flexibility of the core/shell structure, which allows for the development of custom-made nano-carriers individually designed with respect to the physicochemical properties of the incorporated drug, individual requirements for various modes of drug release, responsiveness to internal or external stimuli and interaction with specific molecular targets (242-244).

Examples of the most commonly used block copolymers for drug delivery include 1) Poly(ethylene oxide)-*block*-poly (propylene oxide)-*block*-poly (ethylene oxide) (PEO-*b*-PPO-*b*-PEO), which are known as Poloxamers (Pluronic®); 2) PEO-*b*-poly(L-amino acids) (PEO-*b*-PLAA) such as PEO-*b*-poly(L-aspartic acid) (PEO-*b*-P(Asp)), PEO-*b*-poly(L-glutamic acid) (PEO-*b*-P(Glu)) and PEO-*b*-poly(L-lysine) (PEO-*b*-PLL); and 3) PEO-*b*-poly(ester)s such as PEO-*b*-poly(lactic-*co*-glycolic acid) (PEO-*b*-PLGA), PEO-*b*-poly(D,L-lactic acid) (PEO-*b*-PDLLA), and PEO-*b*-poly(ε-caprolactone) (PEO-*b*-PCL).

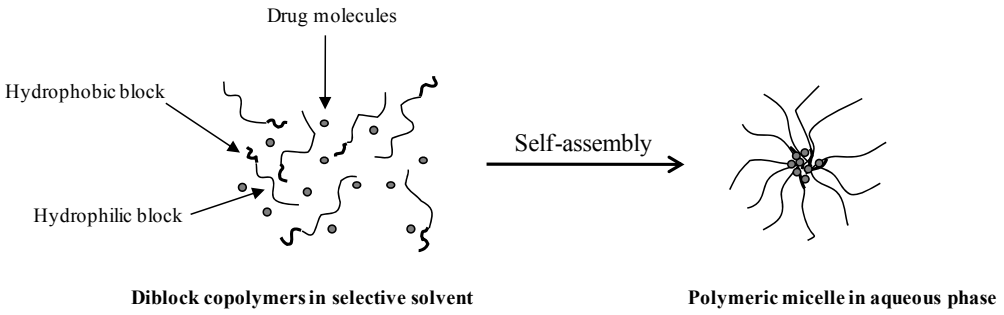

Figure 1.3 – The process of self-assembly for amphiphilic diblock copolymers

1.2.1. Design of polymeric micelles for drug delivery applications

1.2.1.1. Micelle-forming polymer-drug conjugates

In this approach, the incorporation and stabilization of drug within the micellar carrier is mediated through the formation of chemical bonds between the functional group(s) of the polymeric backbone and the drug. Numerous studies have reported on the development of different micelle-forming drug conjugates based on PEO-*b*-Poly(ester)s and PEO-*b*-PLLA block copolymers (234). Drug conjugation to PEO-*b*-poly(ester)s is usually carried out through formation of covalent bonds between the activated terminal hydroxyl group of the poly(ester) segment and reactive groups on the drug molecule (245, 246). Nonetheless, the PLLA block has clear advantage over poly(ester) block for drug conjugation owing to the presence of several functional groups, which provide multiple sites for the conjugation of drug molecules to one polymeric chain. This may help to lower the dose of the polymeric drug. Additionally, the availability of diverse functional groups in a PLLA chain (e.g. amino, hydroxyl, and carboxylic groups) allows conjugation of different chemical entities to the polymeric backbone.

1.2.1.2. Polyion complex micelles

Polyion complex micelles can incorporate and deliver different therapeutic agents that possess charge, which may include drugs, peptides, and DNA (247-256). In this approach, drug encapsulation is promoted through electrostatic interactions between oppositely charged polymer/drug combinations. Neutralization of charge on the core-forming segment of the block copolymer will then trigger self assembly of the polyion complex and lead to further stabilization of the complex within the hydrophobic environment of the micellar core.

1.2.1.3. Polymeric micellar nano-containers

Several amphiphilic block copolymers have been used to non-covalently incorporate drug molecules. In this system, the formation of hydrophobic interactions or hydrogen bonds between the micelle forming block copolymer and drug provides the basis for the solubilization and stabilization of drugs in the polymeric micelles. The physical encapsulation of drugs within polymeric micelles is generally a more attractive approach than micelle-forming polymer-drug conjugates since many polymers as well as drug molecules do not bear reactive functional groups or the free functional group may be required for the pharmacological effectiveness of the drug. The physical encapsulation of drugs in polymeric micelles may be accomplished by direct addition and incubation of drug with block copolymers in an aqueous environment, only if the block copolymer and drug are water soluble (257, 258). However, most of the block

copolymers are not soluble in water and produced poor drug loading in direct mixing method. Therefore, physical incorporation of hydrophobic drugs into polymeric micelles is usually achieved by dialysis, oil in water (o/w) emulsion, solvent evaporation, or co-solvent evaporation methods depending on the block copolymer and drug characteristics (Figure 1.4). In dialysis method (259, 260), the drug and block copolymers are dissolved in a good solvent and then dialyzed against a selective solvent. As polymeric micelles form during the dialysis process, the drug is loaded into the cores of the micelles. Unloaded drug is also removed during the dialysis process. In o/w emulsion method (261, 262), a drug dissolved in a water immiscible organic solvent (e.g. dichloromethane) is added to water in a drop-wise manner and under vigorous stirring. The polymer may be dissolved in either organic or aqueous phase. The organic solvent is then removed by evaporation. The solvent evaporation method (238, 243) is based on dissolving the drug and polymer in a volatile organic solvent and complete evaporation of the organic solvent leading to the formation of polymer/drug film. This film is then solvated in aqueous phase by gradual shaking to facilitate slow detachment of block copolymer and formation of micelle. Co-solvent evaporation method (263, 264) involves the drug and polymer being dissolved in a volatile water-miscible organic solvent (co-solvent). Micellization and drug entrapment is then triggered by the addition of aqueous phase (nonsolvent for the core forming block) to the organic phase (or *vice versa*), followed by the evaporation of the organic co-solvent.

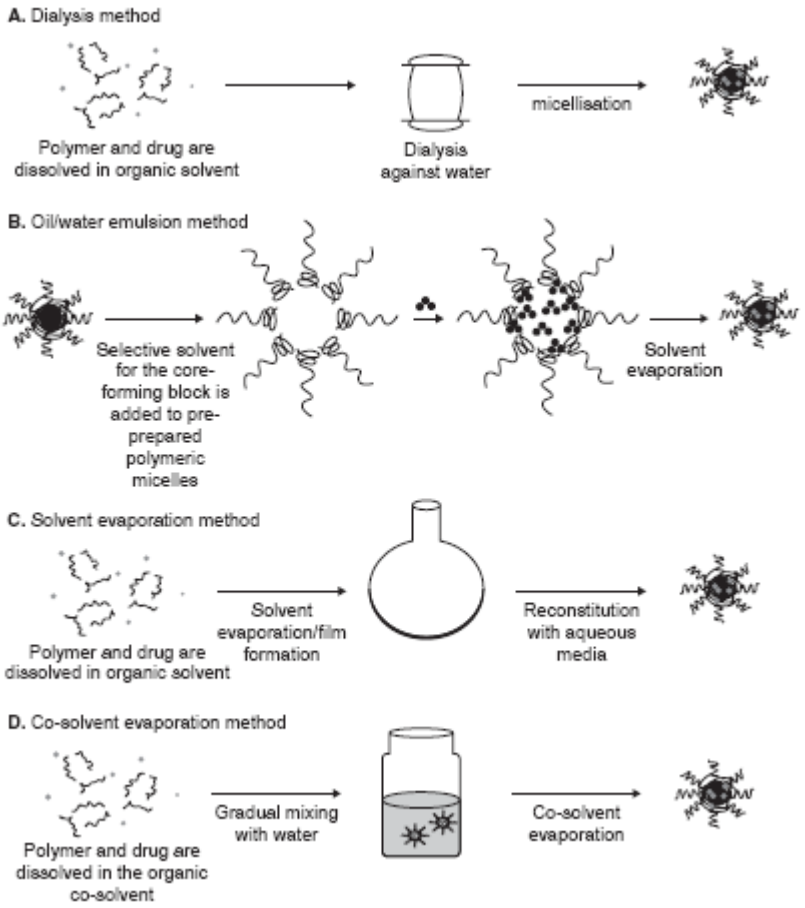

Figure 1.4 – Methods commonly used for physical drug encapsulation in polymeric micelles: A) dialysis method; B) oil/water emulsion method; C) solvent evaporation method; D) Co-solvent evaporation method (Adopted from ref. (234) with modification).

1.2.2. Applications of polymeric micelles in drug delivery

The *in vitro* and *in vivo* evaluation of drugs formulated in polymeric micelles has demonstrated that the major application of these delivery systems

lies in three major areas in drug delivery: drug solubilization, controlled drug release, and drug targeting.

1.2.2.1. Polymeric micelles as solubilizing agents

It has been estimated that approximately 40% of the existing and emerging therapeutic agents exhibit poor water solubility (265, 266), which could restrict their effective application. Drug formulation and delivery strategies provide a means to fully exploit the therapeutic benefit of these poorly soluble agents. Conventional solubilizing agents currently in use for the formulation of such agents are often ineffective or even toxic. For instance, Cremophor EL, a surfactant used for the solubilization of potent hydrophobic drugs such as paclitaxel and CyA, causes several adverse effects including hypersensitivity reactions, hyperlipidemia, neurotoxicity, and reversal of P-gp activity (267, 268). Furthermore, numerous studies have shown that Cremophor EL alters the pharmacokinetics of many drugs including CyA, paclitaxel, etoposide, and doxorubicin (267, 268). Tween 80 and deoxycholate are other examples of solubilizing agents that are not biologically inert since both agents are known to be hemolytic (237, 267, 268). Owing to the multiple advantages, including a better safety profile, polymeric micelles have been the focus of much interest as alternative vehicles for the solubilization of molecules with poor water solubility. Moreover, polymeric micelles have shown enhanced loading capacity, higher thermodynamic stability (based on the low CMC) and kinetic stability (based on the interactions between the polymer chains below CMC), and better control over

the rate of drug release. Consequently, they may have the potential to modify the pharmacokinetics and biodistribution of incorporated drug in a favorable manner.

One of the most impressive example of solubility improvement by polymeric micelles was that reported by Park and coworkers (269). They have shown that micelles composed of Poly(ethylene glycol)-*b*-poly(vinylbenzyloxy)-N,N-diethylnicotinamide) (PEG-*b*-PVBODENA) were able to load up to 37.4% (w/w) paclitaxel, thereby raising the water solubility of the drug to 38.9 mg/mL (compared to ~ 1μg/ mL) (269).

Compatibility between the drug and the core-forming block have been shown to to have a significant influence on the loading capacity and loading efficiency of micelles (270, 271). Ionic, hydrogen bonding, and pi-pi interactions between the drug and the micellar core have been employed in order to enhance the drug loading capacity of the micelles. For instance, Kataoka's group investigated PEG-*b*-poly-benzyl-L-aspartate (PEG-*b*-PBLA) micelles as a delivery system for DOX and were able to achieve loading levels of 15-20% (wt/wt) (262). The obtained high loading level was attributed to the pi-pi stacking interactions between the benzyl residues of the PBLA core-forming block and DOX. In addition, chemical conjugation of DOX to the poly(L-Aspartic acid) (P(Asp)) block of PEO-*b*-P(Asp) has been utilized as a means to increase the entrapment of DOX inside the core of the micelles (272). Further evidence for the importance of compatibility between the core-forming block and the encapsulated

drug is provided in studies by Kwon's group (273, 274). They have synthesized a series of PEO-*b*-poly(N-hexyl-L-aspartamide) (PEO-*b*-p(NHA)) acyl esters wherein the length of the acyl side chain is varied. The copolymers were explored for formulation of amphotericin B (Amp B) as it was known that this drug interacts favorably with aliphatic chains. Indeed, replacement of the aromatic core with aliphatic ones was found to effectively encapsulate Amp B while also reducing the toxicity of this compound (273, 274).

1.2.2.2. Polymeric micelles as controlled release delivery systems

The mode of drug release from polymeric micelles is mainly dependent on the chemical structure and the physico-chemical properties of the micelle-forming block copolymer and incorporated drug, the localization of the incorporated drug within the core/shell structure, and also dependent on the method utilized for drug loading and micelle prepation. Typically, the release profile includes a burst release phase that occurs over the first few hours and is attributed to the portion of the drug that resides in the shell or at the core/shell interface (275). The burst release is then followed by a slow and delayed release phase that could proceed over long period ranging from days to months. For instance, Kwon et al. have demonstrated the delayed release of DOX from PEO-*b*-PBLA micelles with only 20% of the total drug released over 100 hours (261). Moreover, Liu et al. have investigated the release profile for the hydrophobic drug ellipticine from PEO-*b*-PCL micelles, and have found that less than 40% of the total drug was released within 150 hours (271).

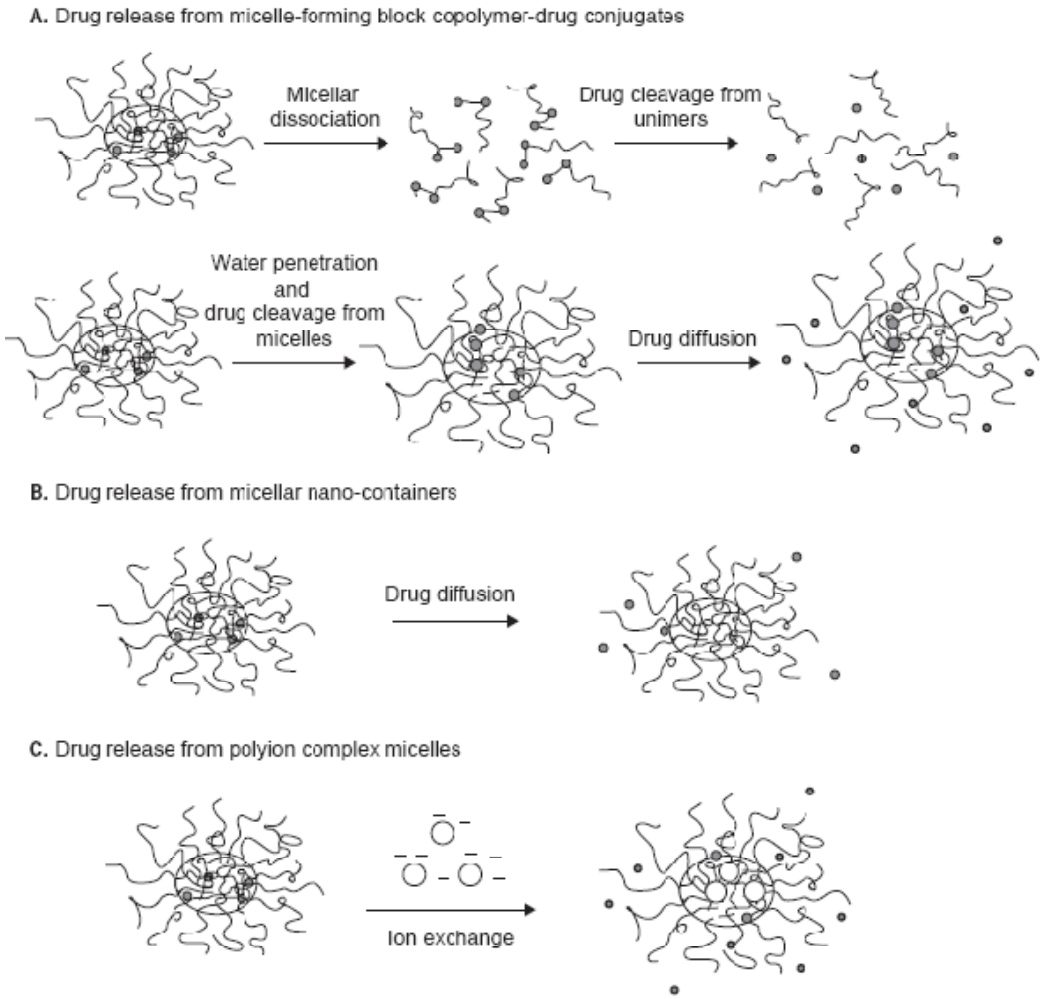

Figure 1.5 – Modes of drug release from polymeric micelles (Adopted from ref. (234)).

It is proposed that diffusion and polymer degradation are the major mechanisms for drug release, as for most polymer-based nano-sized delivery systems (276) (Figure 1.5). Previous studies have shown that most of the polymers that are commonly employed as the hydrophobic core-forming blocks such as PCL, P(Asp), PBLA, PPO, and PDLLA do not degrade to a significant extent over a one week period (275). Therefore, the diffusion of the drug may be

considered as the dominant mechanism for drug release. Potentially, it would be possible to tailor the chemical structure of the micelle-forming block copolymer and modify the physico-chemical properties of the core/shell forming blocks to adopt instant, pulsed, or delayed mode of drug release depending on the delivery requirements. For example, hydrophobicity and rigidity of the micellar core may be enhanced to restrict water penetration to the micellar core, which may lead to a sustained or even delayed mode of drug release from the carrier (277, 278). Application of polymeric micelles that have glassy cores under physiological condition (37 ºC), cross-linking of the micellar core structure, and induction of strong hydrophobic interaction or hydrogen bonds between the core-forming block and the encapsulated drug may be utilized to lower the rate of drug release from the micellar carrier (234). Furthermore, introduction of hydrophilic or stimulus-responsive groups to the core-forming block could provide an instant or pulsed mode of drug release. Finally, the method of drug encapsulation inside polymeric micelles could also be modified to improve the extent of drug loading, and localization or physical state of the loaded drug provide other means for controlling the rate of drug release from polymeric micelles.

1.2.2.3. Polymeric micelles as carriers for drug targeting

1.2.2.3.1. Passive drug targeting by means of enhanced permeation and retention (EPR) effect

The EPR effect was first reported by Matsumura and Maeda in 1986 (279) and later was described and validated by Maeda et al. (280, 281). The EPR effect (recently reviewed in (280)) is the result of the increased permeability to circulating macromolecules, which is accompanied with limited lymphatic drainage from the tumor interstitium. Together, these two effects can increase the accumulation of i.v. administrered macromolecules in solid tumors (Figure 1.6). This unique phenomenon has also been demonstrated with plasma proteins in inflammatory and tumor tissue (282).

Cancer is one of the medical conditions that cause hypoxia in the affected tissue because of the rapid growth rate and poor blood supply to tumor cells. Tumor cells that are more than 180 μm away from the blood vessels become necrotic (10). In response to hypoxia, cells will produce many factors including hypoxia-inducible transcription factor-1 (HIF-1). In the absence of oxygen, HIF-1 binds to hypoxia-response elements (HREs) which lead to the upregulation of several genes (283). Vascular endothelial growth factor (VEGF) and one of its receptors, namely VEGF receptor 1 (VEGFR1) are among the genes upregulated under the hypoxic conditions. Recent studies have emphasized on the role of VEGF (284), which is also known as vascular permeability factor (285)) in cancer growth . Furthermore, VEGF along with basic fibroblast growth factor (bFGF) are referred to as “direct angiogenic growth factors” and are considered key regulators of angiogenesis (286). Secretion of these molecules results in induction of expression of several pro-angiogenic and vascular permeability factors such as

tumor necrosis factor-α (TNF-α), interleukin 8 (IL-8), matrix metalloproteinases (MMPs), bradykinin, prostaglandins (PGs), nitric oxide (NO), peroxynitrite ($ONOO^-$) (287-292). Nitric oxide promotes angiogenesis directly and functions upstream and downstream of angiogenic stimuli. Moreover, NO mediates recruitment of perivascular cells, which leads to the maturation of blood vessels (293). Once blood supply to the tumor is established, growth proceeds at a rapid rate.

Tumor angiogenesis is remarkably different from physiological angiogenesis. Differences include abnormal vascular structure, altered endothelial cell-pericyte interactions, abnormal blood flow, increased permeability, and delayed maturation (294). Formation of fenestrated and discontinuous membrane in tumor capillaries (with a cut-off size of 380-780 nm (295, 296)) is the main reason for the enhanced permeation of tumor vasculature, which facilitates the extravasation of macromolecules and nanoparticles into tumor interstitium. The absence of a functional lymphatic drainage at the tumor site, on the other hand, is the reason for the retention of the extravasated particles in the tumor.

The EPR effect has been observed in numerous experimental and human solid tumors, including hepatoma, renal cancer, lung cancer, and brain tumors (297, 298). Moreover, the EPR effect is believed to be responsible for increased accumulation of many drug delivery systems in solid tumors including dextran-peptide-methotrexate conjugates (299), liposomal DOX (300), PEO-modified

poly(β-amino ester) nanoparticles (301), platinum conjugates (302), micellar formulations of pirarubicin (303), and DOX-loaded PEO-poly (L-histidine) (PEO-PLH) polymeric micelles (304) (Figure 1.6).

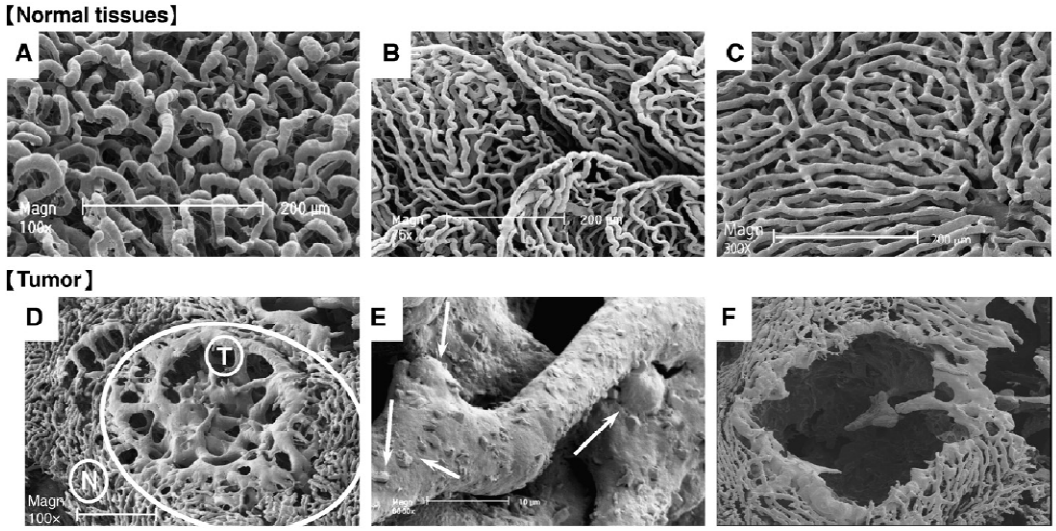

Figure 1.6 – SEM images of blood vessels in various normal tissues (A–C) and metastatic liver tumors (D–F). Normal capillaries of the pancreas (A), colon (intestinal villi) (B), and liver (sinusoid) (C) are shown. (D) Metastatic tumor nodule (circled area identified with T) in the liver, the normal liver tissue is indicated with "N." (E) Tumor vessels at the capillary level (larger magnification), with a rough surface and an early phase of polymer-extravasating vessels (arrows). Normal tissues show no leakage of polymeric resin (A–C), whereas the tumor nodules clearly demonstrate tumor-selective extravasation of polymer (via the EPR effect) (D, E). After i.v. injection of the macromolecular anticancer drug (Styrene maleic acid (SMA)-pirarubicin micelles), the tumor vascular bed (visible in D) was completely disintegrated, as shown by an empty void (F) (Adopted from ref. (280, 305)).

The EPR effect is the basic mechanism of passive targeting and is now the "gold standard" in the design of effective targeted delivery systems in cancer therapy (306). Although polymeric micelles are very promising carriers for passive targeting by EPR, only a few polymeric micellar formulations have demonstrated

success in passive targeting of the loaded drug in solid tumors (234). This is likely due to either the premature drug release from the micelles before the carrier reaches the tumor targets, or insufficient intracellular delivery of the encapsulated anticancer drug to the tumor cells (234). Finding the right polymeric micellar system that can provide a proper balance between the two properties, i.e. avoiding premature drug release outside tumor site, but promoting cellular internalization and/or obtaining triggered drug release at the tumor site poses a challenge for efficient targeted drug delivery by polymeric micelles.

1.2.2.3.2. Polymeric micelles for active or stimuli responsive targeting

The second generation of polymeric micelles (micelles for active targeting) can be categorized to immunomicelles and ligand-modified micelles (307, 308). Immunomicelles are prepared through chemical conjugation of monoclonal antibodies to the micellar surface, whereas the ligand-modified micelles are prepared through attachment of receptor-specific probes (e.g. small peptides, transferrin, or folate) on the micellar surface. Polymeric micelles can also offer an alternative targeting strategy through the responsiveness of their micellar structure to internal or external stimuli (e.g. temperature (309, 310), pH (311, 312), ultrasound (313)). Recently, a third generation of these nanocarriers has emerged that are known as multifunctional polymeric micelles (314-317). These micelles are usually designed to bear a combination of structural components required for various targeting strategies on an individual carrier,

which in turn is expected to enhance the selectivity of the delivery system for the target site. Polymeric micelles with multiple ligands on the surface and block copolymers bearing a ligand and stimulus responsive moiety in their structure are example designs of multifunctional polymeric micelles.

1.2.3. Polymeric micellar delivery systems in clinical trials

Currently, there are seven polymeric micellar formulations in the clinical trials, all of which have been developed for the delivery of anticancer agents (Table 1.3). Among these formulations, only few have shown a favorable pharmacokinetic pattern for the encapsulated drug to achieve passive drug targeting.

Physically-loaded DOX in PEO-*b*-P(Asp)-DOX micelles, namely NK911, is one of the few polymeric micellar formulations that have shown a favorable change in the pharmacokinetic parameters and biodistribution pattern of the incorporated drug in animal studies (318). Compared to free drug, NK911 exhibited an increase the half-life and plasma AUC, and a decrease in CL and Vd. Although a similar trend was observed for NK-911 in humans, the changes in the pharmacokinetic parameters were modest (319). In the phase I clinical trials, NK-911 was well tolerated and produced only moderate nausea and vomiting at myelosuppressive dosages (319). Moreover, among 23 patients, a partial response was obtained in one patient with metastatic pancreatic cancer. NK-911 is

currently undergoing phase II clinical trials for the treatment of metastatic pancreatic cancer.

Pluronic® formulation of DOX, known as SP-1049C, was developed for circumvention of MDR. In this system, DOX was physically encapsulated inside the micelles. The formulation consists of a hydrophobic copolymer, L61, combined with a more hydrophilic Pluronic® F127 at a ratio of 1:8 to avoid micellar aggregation (210). Following intravenous administration, DOX was very rapidly released from the micelles resulting in a pharmacokinetic profile comparable to the conventional DOX (320). Although results of Phase II trials on this system reported partial response in some patients after four to six cycles of treatment, data shows appearance of hematological and non-hematological signs of toxicity in some patients (213, 215).

In 1996, Burt and coworkers reported on the application of PEO-*b*-PDLLA for physical encapsulation of paclitaxel by a solvent evaporation method (238). Following intravenous administration to tumor-bearing mice, paclitaxel micellar formulation showed an 82% decrease in the AUC of the drug in blood in comparison to the Cremophor EL formulation (Taxol®) (321). The results of biodistribution studies in healthy rats using radiolabeled paclitaxel demonstrated a rapid loss of drug from the micellar carriers. Nonetheless, because of a higher maximum tolerable dose (MTD), this formulation (Paxceed®) was developed by Angiotech Pharmaceuticals in Canada (321), and underwent clinical trials. In

2000, the results of a phase II clinical trial of Paxceed® in patients with severe psoriasis demonstrated positive tolerability and therapeutic activity of this formulation (322). Moreover, in 2002, another Phase II trial was initiated to determine the effectiveness of Paxceed® in patients with rheumatoid arthritis (ClinicalTrials.gov identifier: NCT00055133); however, there is no report in the literature regarding results of this study.

Table 1.3 – Polymeric micellar delivery systems in clinical trials

Trade name	Polymer	Incorporated drug	Progress	References
NK-911	PEO-*b*-P(Asp)-DOX	DOX	Phase II	(319)
SP-1049C	PEO-*b*-PPO-*b*-PEO	DOX	Phase II	(213, 320)
Paxceed®	PEO-*b*-PDLLA	Paclitaxel	Phase II	(322)
Genexol®-PM	PEO-*b*-PDLLA	Paclitaxel	Phase II	(323-325)
NK-105	PEO-*b*-PPBA	Paclitaxel	Phase II	(326)
NK-012	PEO-*b*-P(Glu)	SN-38	Phase II	(www.ClinicalTrials.gov; identifier: NCT0095105)
NC-6004	PEO-*b*-P(Glu)	Cisplatin	Phase I/II	(327)

In 2001, Kim and coworkers reported on the pharmacokinetics, biodistribution, and toxicity profile of Genexol®-PM, which is similar to Paxceed®, i.e., paclitaxel loaded-PEO-*b*-PDLLA micelles prepared by an identical

solvent evaporation technique (260). In the Phase I trials, the Genexol®-PM dose was escalated from 135 to 390 mg/m^2 (324). The MTD was determined to be 390 mg/m^2. Despite a 2.5-fold increase in the administered dose, the C_{max} and plasma AUC were found to be lower than those obtained from the Cremophor EL-based formulation (324). In a phase II trial performed in patients with metastatic breast cancer, the overall response rate was 58.5%, with 5 complete responses and 19 partial responses (325). Moreover, another phase II study was conducted to evaluate the efficacy and safety of the combination of Genexol®-PM and cisplatin for the treatment of advanced non-small cell lung cancer (323). The overall response rate was 37.7%. Furthermore, the investigators reported that the use of Genexol-PM® allowed administration of higher doses of paclitaxel compared with the Cremophor EL-based formulation without causing significantly increased toxicity (323).

One of the most promising clinical results for a polymeric micellar system has been achieved using a formulation named NK-105. It consists of PEO-*b*-poly(4-phenyl-1-butanoate-L-aspartamide) (PEO-*b*-PPBA) micelles containing physically loaded paclitaxel. Following an intravenous administration in a tumor bearing mice, NK-105 has shown an 86-fold increase in paclitaxel plasma AUC, a 99% decrease in CL and a 93% decrease in its Vd_{ss} compared with Taxol® formulation (328). In a phase I clinical trial, the pharmacokinetic profile matched the preclinical data in terms of CL and Vd_{ss}; however, the increase in the plasma AUC was not as significant in humans as in animals (326). A phase II study of

NK105 against advanced stomach cancer as a second-line therapy is currently underway.

NK-012 is the first example of a polymeric micellar drug conjugate, as the only source of drug release, to enter clinical trials (329). NK-012 is a polymeric micellar formulation for SN-38 (7-ethyl-10-hydroxycamptothecin), which is an active metabolite of the anticancer drug irinotecan. In this system, SN-38 is chemically conjugated to the P(Glu) block of PEO-*b*-P(L-glutamic acid) (PEO-b-P(L-Glu)) as pendant groups through formation of ester bonds. Preclinical studies in tumor-bearing mice have shown promising results in terms of pharmacokinetic and tumor distribution profiles (329). A phase II clinical trial of NK-012 is currently undergoing in patients with advanced, metastatic triple negative breast cancer (ClinicalTrials.gov identifier: NCT0095105).

The most recent polymeric micellar formulation that has entered clinical trials and has shown impressive results in passive drug targeting is the PEO-*b*-P(L-Glu) micellar formulation of cisplatin, which is known as NC-6004. Preclinical studies have shown that NC-6004 were able to significantly reduce the CL and Vd_{ss} of cisplatin by 95 and 99%, respectively (330). It has also demonstrated a higher AUC in tumors, and anti-tumor activity that are comparable or higher than free cisplatin in tumor-bearing mice (330). In a phase I clinical trial performed in patients with refractory solid tumors, it was reported that NC-6004 was well tolerated in an outpatient setting and provided sustained

release of potentially active platinum species (327). A phase I/II clinical trial is undergoing for NC-6004 in combination with gemcitabine to treat pancreatic cancer in Asia (ClinicalTrials.gov identifier: NCT00910741).

1.2.4. PEO-*b*-PCL polymeric micelles for drug solubilization and delivery

PEO-*b*-PCL is one of the block copolymers in the PEO-b-poly(ester)s category. Compared to other core-forming blocks in the poly(ester)s groups, such as poly(glycolic acid) and PDLLA, PCL is more hydrophobic, which makes it more compatible with hydrophobic drugs. The semi-crystalline structure of PCL (331) may be considered as an advantage over PDLLA leading to kinetic stabilization and consequently a potential for sustaining the rate of the drug release for PCL-based micelles.

Similar to other PEO-*b*-poly(ester)s, PEO-*b*-PCL copolymers are biocompatible and biodegradable (332, 333). PCL has shown low toxicity and no immunogenicity with possible degradation products of caprolactone, succinic, butyric, valeric and hexanoic acid (334). The PCL polymer degrades by end chain scission at higher temperatures while it degrades by random chain scission at lower temperatures (335). Moreover, PCL degradation is autocatalyzed by the carboxylic acids liberated during hydrolysis (336), but it can also be catalyzed by enzymes, resulting in faster decomposition (337).

PEO-*b*-PCL has been extensively used in solubilization of hydrophobic drugs (234), and have shown potential for passive tumor targeting. Shi et al. have demonstrated that PEO-*b*-PCL were able to increase the AUC of hydroxycamptothecin (HCPT) up to 21-fold compared with the free drug following i.v. administration to rats (338). Moreover, in the same study, HCPT was inravenously administered to tumor-bearing mice, and the polymeric micellar formulation has shown about an 8-fold higher tumor accumulation of HCPT compared to free drug (338). Furthermore, in our lab, we have been exploring the potential of PEO-*b*-PCL micelles as vehicles for the solubilization and controlled delivery of CyA as a model P-gp inhibitor (339, 340). The results of our previous studies showed that PEO-*b*-PCL micelles were not only able to solubilize CyA at clinically relevant concentrations, but favorably change the plasma protein binding, pharmacokinetic and biodistribution profile of CyA after a single i.v. dose to rats keeping the incorporated CyA mainly in blood circulation and away from sites of CyA toxicity, i.e., kidneys (341, 342). This has led to a reduction in the nephrotoxic side effects of CyA upon multiple dosing of its polymeric micellar formulation compared to the Cremophor EL formulation.

1.3. Polymeric vesicles (Polymersomes):

Polymersomes are self-assembled polymeric vesicles in which the vesicle shell is composed of double layers of amphiphilic block copolymers (Figure 1.7) (343). The self-assembly mechanism of amphiphilic diblock copolymers to form polymersomes is similar to that of lipids that self-assemble to form liposomes.

Specifically, the hydrophobic blocks of each molecule tend to associate with one another to minimize direct exposure to bulk aqueous environment, whereas the more hydrophilic blocks face inner and outer hydrating solutions, which thereby define the two interfaces of a typical bilayer membrane (Figure 1.7). The advantage of using polymersomes over liposomes is that the bilayer of polymersomes can be engineered to be much thicker (up to 40 nm) than that of liposomes (4 nm). This could, in theory, improve both the hydrophobic drug solubility as well as the mechanical stability (344). Additionally, the feasibility of readily tailoring the physico-chemical and biological properties of block copolymers makes the polymersomes ideal candidates for drug delivery (345).

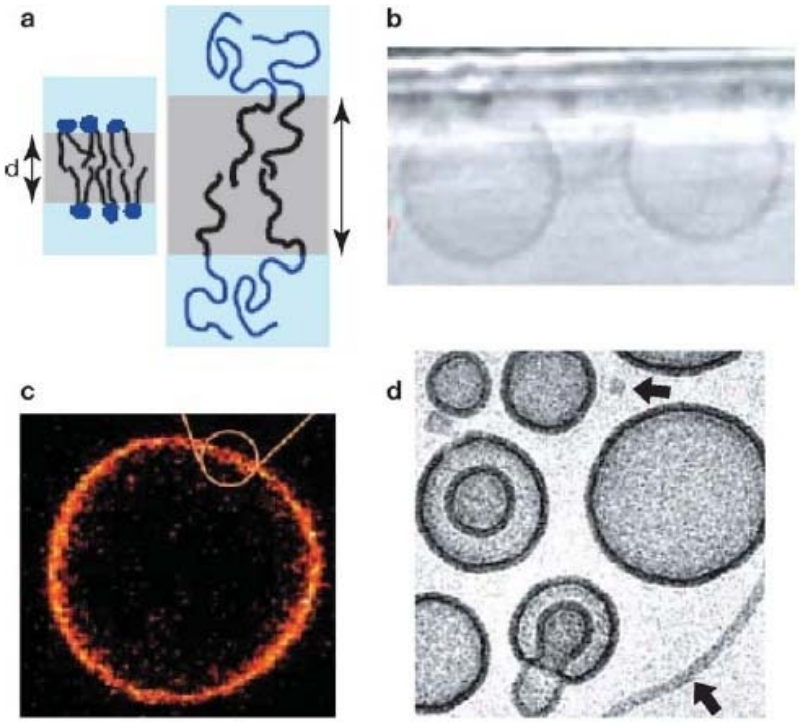

Figure 1.7 – (a) Natural lipid versus synthetic polymer assemblies. (b) Self-directed assembly of polymersomes from hydrated films. (c) Fluoro-polymersome. (d) Cryogenic transmission electron microscopy of ~100-nm polymersomes. The two arrows point to spherical and rod-like micelles that sometimes coexist with polymersomes (Adopted from ref. (343)).

1.4. Vaslpodar (PSC 833)

Valspodar is a highly lipophilic cyclic undecapeptide (practically insoluble in water) (Figure 1.8). It is a more hydrophobic derivative of cyclosporine A (CyA) that displays no evidence of nephrotoxicity or immunosuppressive activity (103, 157, 165-167, 346). Moreover, its P-gp inhibiting activity is superior to CyA both *in vitro* and *in vivo* (157, 167-169). Valspodar has shown to significantly prolong the survival rates of several oncologic disease animal models (347, 348). Furthermore, the P-gp-inhibiting activity of valspodar has

been demonstrated in clinical trials in combination with chemotherapeutic agents (182, 184, 349, 350).

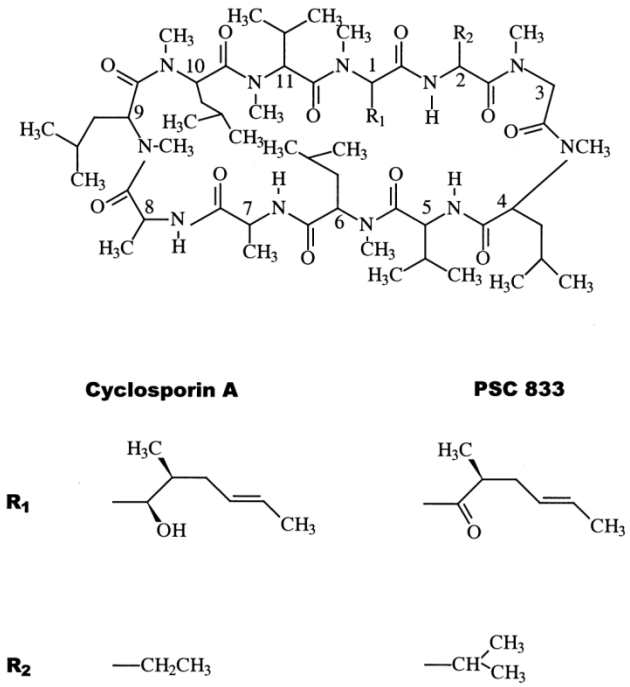

Figure 1.8 – Chemical structures of CyA and valspodar (Adopted from ref. (351)).

The quantification of valspodar in blood or plasma is usually performed either by radio-immunoassays (RIA) (181, 182, 352, 353) or by high-performance liquid chromatography (HPLC) (354-357). However, some of these RIA kits are beset by cross reactivity with valspodar metabolites, which can lead to an over-estimation of the parent drug concentration (358). HPLC assays are capable of separating intact cyclosporine analogues from their metabolites, although use of conventional HPLC is itself not without limitations. It has proved difficult for

HPLC methods to elute valspodar from the columns as a single peak (354, 356). Moreover, the lack of a suitable chromophore in valspodar for UV-absorbance necessitates the use of short wavelength (e.g. 210 nm) for detection. Because numerous molecular species absorb energy in this wavelength, sample preparation usually is complex and involves several steps including protein precipitation followed by solid-phase extraction in order to remove potentially-interfering compounds. The reported valspodar recoveries from different extraction procedures were relatively low (~ 50%) which restricts the limit of quantification (LOQ) to concentrations above 100 ng/mL (354, 356). In addition, all the reported HPLC methods for valspodar require a relatively long run time of analysis (valspodar retention time ≥ 15 min).

1.4.1. Pharmacokinetics of Vaslpodar

The majority of the published valspodar pharmacokinetic studies were those obtained from human subjects in clinical trials (181, 355, 357, 359, 360), although there are some pharmacokinetic data available for valspodar in mice, dogs, and rabbits (347, 348, 361). Nevertheless, the main objective of those studies was to assess the toxicity and pharmacokinetic interactions between valspodar and the co-administered chemotherapeutic agents.

1.4.1.1. Absorption

In the early Phase I/II clinical trials, oral dosing of valspodar was usually combined with a bolus dose of i.v. formulation, which composed of drug in Cremophor EL (PEGylated castor oil). In such studies, the oral dosage form was the conventional oral formulation consisting of the drug dispersed in a labrafil-based corn oil solution, formerly used for CyA in transplantation (185, 355). Similar to CyA, this formulation was associated with poor and erratic absorption, resulting in a mean bioavailability of 34% with a large inter-individual variability ranging from 3 to 58% (355). Later, as with the optimization of the CyA formulation gave Neoral®, a new micro-emulsion formulation (Cremophor RH40/ethanol) became available which improved the bioavailability to reach approximately double that of the conventional oral solution (60 versus 34%) with a lower variability (10-20% versus 3-58%) (352, 357).

1.4.1.2. Distribution

Following a single i.v. dose of valspodar to healthy individuals, the mean volume of distribution at steady-state (Vd_{ss}) was 1.78 L/kg (355). This was very close to the value reported for CyA, which was 1.23 L/kg (362). In mice, Desrayaud et al. (363) have studied the influence of *mdr1a* P-gp on the tissue distribution of valspodar. In this study, valspodar was administered intravenously by a constant-rate infusion to wild-type (*mdr1a* (+/+)) and knockout (*mdr1a* (–/–)) mice for four hours. At various times during infusion and after infusion, blood and tissues were sampled for total radioactivity and parent drug analysis (363).

The results, interestingly, showed a lack of effect of *mdr1a* gene disruption on the valspodar distribution in most P- gp-expressing tissues except for a larger uptake in the brain (363). Moreover, the difference between *mdr1a* (–/–) and (+/+) brain penetration was concentration-dependent. This finding was in agreement with a previous study performed in rat (166), where valspodar showed a similar dose-dependent brain penetration. Thus, these findings support the hypothesis of valspodar governing its own brain penetration. It is worth noting that to obtain a similar degree of brain penetration, the i.v. dose of CyA has to be roughly 10 times higher than the valspodar dose (166). This difference in the brain distribution of these two cyclosporines may be attributed to the higher lipophilicity of valspodar compared with CyA or that valspodar may have a higher *in vivo* potency than CyA in blocking the P-gp at the BBB (166). It could also be due to a difference between valspodar and CyA in the unbound fractions in rat blood.

1.4.1.3. Metabolism and excretion

In view of their molecular weight largely above 500 Da (1214.65 Da), cyclosporines are possibly predisposed to follow the biliary pathway of elimination. After a single oral dose in human subjects, intact valspodar appears as less than 0.1% of the dose in the urine and as around 14% of the dose in the feces, presumably the result of unabsorbed drug (168). In a study conducted by Vickers et al. (364), where cyclosporine metabolism by human liver and kidney

slices was compared, liver metabolism exceeded kidney metabolism for all tested cyclosporines, including CyA and valspodar.

Like CyA, and other cyclosporines, valspodar is metabolized by human CYP3A enzymes (168). *In vitro*, human liver microsomes were found to metabolize valspodar into several monohydroxylated, dihydroxylated, and N-desmethylated metabolites (168). Besides the *in vitro* microsomal studies (168), it has been found clinically that the major valspodar metabolite in the human blood is PSC M9 (168, 355), which is the monohydroxylated derivative at the γ-position of L-methyl leucine (the ninth amino acid). Furthermore, this metabolite (PSC M9) was found to be much less potent than the parent compound (valspodar) for restoring paclitaxel toxicity or R-123 efflux, and for inhibiting CyA binding to P-gp, suggesting that PSC M9 is not expected to significantly contribute to P-gp inhibition *in vivo* (168).

In the *mdr1a* knockout mice study, it was found that in both *mdr1a* (–/–) and wild-type mice, the metabolism and the excretion were not significantly different as described by the blood, tissue and bile concentrations of parent compound and radioactive metabolites (363). The reason behind the lack of difference in valspodar metabolism and excretion might be attributed to the fact that the major route of elimination of valspodar is through metabolism by CYP3A or that other factors such as the *mdr1b* P-gp could be involved in the pharmacokinetics of this drug. Nonetheless, in another study performed in

mdr1a/1b (–/–) mice (365), plasma valspodar concentrations did not differ significantly between wild-type and *mdr1a/1b* (–/–) mice at the different time point used (2, 6, and 26 h after valspodar administration), which could eliminate the possible involvement of *mdr1b* P-gp in the pharmacokinetics of valspodar. As a matter of fact, there is a debate whether valspodar is a P-gp substrate or not. There are reports that support valspodar being a P-gp substrate (175, 185), while others claim that it is not (166, 174). However, based on the results of several studies, it was suggested that valspodar is a slow substrate with high affinity for P-gp (185). For instance, Smith et al. (175) have shown that valspodar has a high affinity for the P-gp with a Michaelis constant (K_m) of 50 nM, four-fold lower than that of CyA.

1.4.1.4. Protein binding

Since valspodar is highly lipophilic and nonspecifically adsorbs to various materials, it was not feasible to determine its protein binding using the traditional methods such as ultrafiltration and dialysis (366). Moreover, the ultracentrifugation method may be impractical due to lipoprotein contamination of the plasma water supernatant (366). Therefore, Urien and coworkers (366) have investigated the plasma and erythrocyte binding of valspodar using blood from healthy volunteers and cancer patients using an alternative method which measures the partitioning of the drug between plasma and erythrocyte. They have also studied the role of lipoproteins in valspodar plasma binding. As expected, the plasma protein binding of valspodar was high reaching 98% (366). Furthermore,

the values were comparable between the plasma samples used from healthy volunteers and cancer patients. Similar to CyA, the valspodar plasma binding was mainly determined by lipoproteins, which contributed to 97% of the bound fraction. However, unlike CyA, valspodar association to erythrocytes was found to be low with a binding coefficient of 1.5, while it was around 61 in the case of CyA (367). This suggests a low affinity of valspodar for erythrocytic cyclophilin. Indeed, data in humans shows that valspodar binds at least 100-fold less to human cyclophilin A and 65- to 85-fold less to cyclophilin B and C, in comparison to CyA (185). It is the low valspodar binding to cyclophilin, which is involved in calcineurin antagonism in lymphocytes, that is believed to be the basis for its lack of immunosuppression and nephrotoxicity (185).

1.4.2. Valspodar as an MDR modulator

The search for MDR modulators among immunosuppressants was initiated by reports showing that CyA (Sandimmune®) could reverse MDR *in vitro*. Consequently, more than a hundred cyclosporine analogs were investigated (368). Valspodar, which was developed in 1991, was selected through a screening program to find cyclosporines which were more potent MDR modulation than CyA, but with less nephrotoxicity (185, 347). The extensive research at Novartis (Sandoz at the time) had revealed that structure-activity relationships for nephrotoxicity tended to parallel those of immunosuppressive activity, since the latter activity and the MDR modulation have been shown to be unrelated (369).

Results of both *in vitro* and *in vivo* studies showed that the maximal MDR modulation could be achieved with blood levels as low as 1 μM of valspodar (185). Indeed, in comparison with several other MDR modulators, valspodar is a more efficient restorer of anticancer drugs retention in Pgp-expressing cells; as first shown for daunomycin retention in MDR-P388 cells (157), and later confirmed for a variety of anticancer drugs in a range of animal and human Pgp-expressing MDR-cells (158, 165, 167, 169, 174, 348). It significantly prolonged survival rates of MDR-P388 tumor bearing mice and dogs with canine osteosarcoma when combined with doxorubicin (347, 348). It also increased the sensitivity toward etoposide of human carcinoma xenografts in nude mice (370). Furthermore, clinical treatment with valspodar resulted in increased intracellular accumulation of doxorubicin and vincristine in Pgp-positive myeloma cells (371). However, the major drawback in the clinical application of valdospar is its inhibitory action on CYP3A as well as the non-selective action on P-gp expressed in normal tissues, which results in reduced elimination and enhanced accumulation and toxicity of several anticancer agents (P-gp substrates) after co-administration with valspodar in patients with cancer (168, 177-180). For more detailed discussion on the clinical trials of P-gp inhibitors in MDR cancer please refer to section 1.1.4.

1.4.3. Toxicity associated with the co-administration of valspodar and anticancer agents

Valspodar itself showed a good tolerability without the immunosuppressive effects or nephrotoxic side effects shown by CyA. Its dose-limiting toxicity was a mild central nervous system (CNS) side effects which has been shown to be a reversible ataxia particularly at valspodar plasma concentrations above 3 μM (185, 352, 357). Besides ataxia, other reported side effects that were reversible and only seen at highest doses may include mild perioral numbness, peripheral neuropathy, and reversible hyperbilirubinemia (185, 352, 357). Nonetheless, when valspodar was administered concomitantly with anticancer drugs, it led to an increase in the anticancer drugs exposure and toxicity. Specifically, myelosuppression was the most commonly reported toxicity (182, 185, 190, 372). Therefore, in the presence of valspodar, it has been suggested to reduce the dose of anticancer agents (e.g. 50-60% for paclitaxel and 30-50% for etoposide and doxorubicin) to compensate for the increase in anticancer drug exposure and toxicity (185).

1.5. Thesis proposal

Encapsulation of valsopdar in polymeric nanocarriers can enhance the therapeutic benefit of valspodar in overcoming MDR in cancer by providing an inert alternative to Cremophor EL for solubilization of valspodar, favorably changing the pharmacokinetics of encapsulated drug and reducing its

pharmcokinetic interaction with anticancer drugs (that are P-gp substrates) upon co-administration.

1.5.1. Rationale and significance

Multidrug resistance is known to be the major cause for cancer chemotherapy failure. Over-expression of P-gp is one of the most important mechanisms responsible for MDR. Despite development of three generations of P-gp inhibitors, none is currently approved for clinical use. This is partly due to the emergence of severe toxicities by anticancer drugs when co-administered with the P-gp inhibitors. Non-specificity of P-gp inhibitors and their interaction with other cellular targets such as metabolizing enzymes involved in the elimination of anticancer agents can lead to elevated plasma levels of the chemotherapeutic agent leading to sever toxicity. More specific second and third generation P-gp inhibitors still suffer from the lack of selectivity for tumor P-gp. In this context, non-selective distribution of more specific P-gp inhibitors may lead to the accumulation and toxicity of P-gp substrates, including anticancer agents, in normal cells. Thus, redirecting P-gp inhibitor from normal tissues expressing P-gp towards tumor site may reduce the risk of pharmacokinetic interaction with anticancer drug and at the same time enhance the therapeutic benefit of P-gp inhibitors in the modulation of MDR.

In this project, the potential of PEO-*b*-PCL and PEO-*b*-poly(α-benzyl-ε-caprolactone) (PEO-*b*-PBCL) based nanocarriers for enhancing the therapeutic

benefit of valspodar was evaluated. In this context the efficacy of polymeric nanocarriers as solubilizing agents for intravenous and oral administration of valspodar was assessed. The effect of formulation on the pharmacokinetics of incorporated valspodar and its interaction with a model anti-cancer agent, DOX, was investigated. Previously, in our lab, we have shown that CyA in the polymeric micellar formulation can reduce the toxicity of CyA (373, 374). In this project, however, valspodar was selected since it has a better safety profile (no evidence of nephrotoxicity or immunosuppressive activity) and higher specificity toward P-gp compared to CyA (185, 375).

For clinical administration, valdospar is solubilized with the aid of Cremophor EL and ethanol. It has been demonstrated that Cremophor EL can profoundly alter the plasma pharmacokinetics of anticancer drugs such as doxorubicin and etoposide in animals as well as in humans (376-378). Since the clinical formulation of valspodar for i.v. administration also contains substantial amounts of Cremophor EL, it can be postulated that pharmacokinetic interactions with such inhibitor (184, 353) is at least partially attributable to the use of this vehicle. Moreover, the use of Cremophor EL has been associated with several adverse effects such as hypersensitivity reactions (267, 379) and neurotoxicity (267, 380).

Clinical application of valspodar resulted in the non-selective inhibition of P-gp expressed in normal tissues, which lead to reduced elimination and enhanced

accumulation and toxicity of several anticancer agents (P-gp substrates) after co-administration with valspodar in patients with cancer (168, 177-180).

We propose to develop a polymeric nanocarrier for the delivery of valspodar that can: a) provide a safe replacement for Cremophor EL as solubilizing agent; b) change the pharmacokinetics of valspodar in a favorable manner; and c) reduce the extent of pharmacokinetic interaction of encapsulated valspodar with anticancer drug.

Micelles of PEO-*b*-PCL were chosen as potential carrier due to the good biocompatibility and biodegradability profiles of the PEO and PCL blocks, thermodynamic stability of the micellar structure, and distinct properties of the PEO/PCL segments. Additionally, micelles of PEO-*b*-PCL have been shown to be successful carriers efficiently solubilizing CyA and changing its pharmacokinetic and biodistribution profile by reducing CyA accumulation in normal tissues (e.g. spleen and kidneys) and increasing its levels in blood by decreasing CL after a single i.v. dose to rats (373, 374, 381).

1.5.2. Objective

To design and develop a block copolymer based nanocarrier that can enhance the therapeutic performance of valspodar upon systemic administration.

1.5.3. Hypotheses

1- Nanocarriers based on PEO-*b*-PCL and PEO-*b*-PBCL are capable of encapsulating valspodar at clinically relevant levels.

2- Nanocarriers based on PEO-*b*-PCL and PEO-*b*-PBCL can modify the pharmacokinetics of valspodar upon intravenous administration in a favorable manner.

3- Nanocarriers of based on PEO-*b*-PCL can serve as alternative solubilizing agents for oral administration of valspodar.

4- Encapsulation of valspodar by polymeric nanocarriers can reduce the adverse pharmacokinetic interaction of this drug with DOX upon intravenous co-administration.

1.5.4. Specific aims

1- To develop and validate a reliable and sensitive method for the quantification of valspodar in biological fluids based on liquid chromatography–mass spectrometry (LC/MS).

2- To develop polymeric micellar formulations of valspodar and characterize these formulations for their size and drug loading.

3- To assess the pharmacokinetic profiles following both intravenous and oral administration of the micellar formulations compared to the clinically used formulation of valspodar (control formulation) in healthy Sprague-Dawley rats.

4- To assess the pharmacokinetic parameters of DOX administered in combination with polymeric nano-formulation of valspodar in healthy Sprague-Dawley rats.

CHAPTER TWO

EXPERIMENTAL PROCEDURES

2.1. Materials

Valspodar (PSC 833) was a kind gift from Novartis (Basel, Switzerland). Cyclosporine A (CyA) was purchased from Wuhan Zhongxin Company, China. Commercially available CyA for injection (Sandimmune®; 50 mg/mL, Novartis, Dorval, QC, Canada) was obtained from University of Alberta Hospital in-patient pharmacy. Doxorubicin hydrochloride for injection (Adriamycin® PFS; 2 mg/mL, Pfizer, Kirkland, QC, Canada) was obtained from University of Alberta Hospital in-patient pharmacy. Doxorubicinol hydrochloride and daunorubicin hydrochloride were obtained from Toronto Research Chemicals (Toronto, ON, Canada). Methoxy-PEO (average molecular weight of 5000 g mol^{-1}), diisopropylamine (99%), benzyl chloroformate (tech 95%), sodium (in kerosin), butyl lithium (Bu-Li) in hexane (2.5 M solution), pyrene, Cremophor EL, amiodarone HCl (98%), and formic acid (~ 98%; grade: eluent additive for LC-MS) were purchased from Sigma-Aldrich (St. Louis, MO, USA). Acetonitrile, ammonium hydroxide, methanol, diethyl ether, and water were all HPLC grades and were purchased from Caledon Laboratories (Georgetown, ON, Canada). HPLC-grade tetrahydrofuran (THF) was purchased from Fisher Scientific (Nepean, ON, Canada). Fluorescent probe 1,3-bis-(1-pyrenyl)propane was purchased from Molecular Probes (Invitrogen®) (Eugene, OR, USA). ε-Caprolactone was purchased from Lancaster Synthesis (UK). Stannous octoate was purchased from MP Biomedicals Inc. (Germany). Sodium chloride injection (USP) 0.9% was obtained from Hospira Healthcare Corporation (Montreal, QC, Canada). Heparin sodium for injection, 1000 IU/mL was purchased from Leo

Pharma Inc. (Thornhill, ON, Canada). Potassium dihydrogen orthophosphate, dipotassium hydrogen orthophosphate, and potassium chloride were obtained from Caledon Laboratories (Georgetown, ON, Canada). All other chemicals were of reagent grade.

2.2. Methods

2.2.1. Development of a liquid chromatography/mass spectrometry (LC/MS) method for quantification of valspodar *in vitro* and in biological samples

2.2.1.1. LC/MS conditions

LC/MS analyses were done using a Waters Micromass ZQ™ 4000 mass spectrometer coupled to a Waters 2795 separations module with an autosampler (Milford, Ma, USA). The mass spectrometer was operated in positive ion mode with selected ion recording (SIR) acquisition mode. The nebulizing gas was obtained from an in house high purity nitrogen source. The temperature of the source was set at 150° C and the voltage of the capillary and cone were 3.1 KV and 30 V, respectively. The gas flow of desolvation and the cone were set at 550 and 80 L/h, respectively. Chromatographic separation was achieved using a C_8 3.5 μm (2.1×50 mm) column as the stationary phase (Agilent® Eclipse XDB-C8, USA). Mobile phase was pumped as an isocratic acetonitrile: ammonium hydroxide 0.2% at a ratio of 90:10 v/v, respectively. Total analytical run time was 10 min. A constant flow rate of 0.2 mL/min was used throughout the run. The

column was heated to 60°C during the chromatographic run. Amiodarone was used as internal standard (IS).

The mixture of valspodar and IS was analyzed on the mass spectrometer using flow injection in scan mode to determine optimal fragmentation for each compound and establishment of the mass-to-charge ratio (*m/z*) values of the molecular ions. The analysis was carried out using SIM at the protonated molecular ions *m/z* 1214.81 (valspodar) and 645.84 (IS).

2.2.1.2. Standard and stock solutions

The stock solution of valspodar (200 µg/mL) was prepared by dissolving 20 mg of valspodar in 100 mL of methanol. Amiodarone (IS) stock solution (200 µg/mL) was prepared by dissolving 5 mg of amiodarone powder in 25 mL of methanol. Standard solutions were freshly prepared each day by serial dilutions in methanol. All of the stock solutions were stored at 4°C between uses. Standard samples were prepared by spiking appropriate amounts of valspodar in 100 µL of rat plasma at a concentration range of 10-5000 ng/mL. Blank plasma for the preparation of standard solutions was collected from drug-free Sprague-Dawley rats.

2.2.1.3. Extraction procedures

A published method (originally used for the extraction of CyA) was used for the extraction of valspodar, with minor modification (382). To each 100 µL

plasma sample in a glass tube, 500 μL HPLC water, 100 μL sodium hydroxide (1 *M)*, and 50 μL of IS (0.25 μg/mL) were added. Valspodar and IS were then extracted into 4 mL of an ether/methanol (95:5) solution by vortex-mixing for 30 seconds. After centrifugation at 3000 × *g* for 5 min, the organic layer was transferred to new glass tubes and evaporated in vacuum (ISS 110 Speedvac system, Thermosavant). The residues were reconstituted using 0.25 mL of methanol. Aliquots of 10 μL from this solution were injected into the LC/MS system.

To determine the recovery of valspodar after extraction from plasma, the peak height obtained from extracts of spiked plasma samples was compared to that obtained from direct injection of known amounts of drug using standard valspodar solutions. The recovery was assessed at valspodar concentrations of 50, 1000, and 5000 ng/mL, using four replicates for each concentration.

2.2.1.4. Calibration, accuracy, and validation

Complete validation assessment was undertaken using drug-spiked rat plasma. Calibration samples of 100 μL containing valspodar and IS were constructed over the concentration range of 10-5000 ng/mL. The sample to standard solution ratio was constantly 1:2.5 (100 uL plasma and 250 uL of varying standard solution). The ratios of valspodar to IS peak height were calculated and plotted versus nominal valspodar concentrations. Due to the wide

range of concentrations, data for calibration curves was weighted by a factor of 1/concentration.

Intraday accuracy and precision of the assay were determined using five different concentrations of valspodar in rat plasma, namely, 10, 25, 100, 500, 1000 ng/mL. Each concentration was prepared in five replicates. To assess the interday accuracy and precision, the assay was repeated on three separate days. For each daily run, a set of calibration samples separate from the validation samples was prepared to allow quantification of the peak height of valspodar to IS ratios.

Precision was assessed by percentage coefficient of variation (CV%), which was calculated as:

$$CV\%_{intraday} = \frac{100 \times SD}{Mean\ \ measured\ \ concentration}$$

, and

$$CV\%_{interday} = \frac{CV\%_{run\,1} + CV\%_{run\,2} + CV\%_{run\,3}}{3}$$

Bias was assessed by determining percent error, which was calculated as:

$$\text{Mean}\,\%\,\text{error}_{\text{intraday}} = 100 \times \frac{\text{measured concentration} - \text{expected concentration}}{\text{expected concentration}}$$

, and

$$Mean\ \%\ error_{interday} = \frac{error\ \%_{run\,1} + error\ \%_{run\,2} + error\ \%_{run\,3}}{3}$$

2.2.2. Synthesis of block copolymers and their characterization

2.2.2.1. Synthesis of PEO_{114}-*b*-PCL_{114} block copolymer

Poly(ethylene oxide)$_{114}$-*block*-poly(ε-caprolactone)$_{114}$ copolymer was synthesized by ring opening polymerization of ε-caprolactone using methoxy PEO (molecular weight of 5000 g.mol^{-1}) as an initiator and stannous octoate as a catalyst (263). Methoxy PEO (1.92 g), ε-caprolactone (5 g), and stannous octoate (0.035 g) were added to a previously flamed 10 mL ampoule, nitrogen purged, then sealed under vacuum. The polymerization reaction was allowed to proceed for 4 h at 140 ºC in oven. The reaction was terminated by cooling the product to room temperature (263).

2.2.2.2. Synthesis of PEO-*b*-PBCL block copolymers

Three block copolymers with different chain lengths of the core-forming block were synthesized by ring-opening polymerization of α-benzyl carboxylate-ε-caprolactone using methoxy PEO (molecular weight of 5000 g.mol^{-1}) as initiator and stannous octoate as catalyst (244). To synthesize the monomer (α-benzyl carboxylate-ε-caprolactone), Bu-Li (24 mL) in hexane was slowly added to dry diisopropylamine (8.4 mL) in 60 mL of dry THF in a 3 neck round bottomed flask at – 30 °C under vigorous stirring with continuous argon supply. The solution was then cooled to – 78 °C. ε-caprolactone (3.42 g) was dissolved in 8 mL of dry THF and added to the above mentioned mixture slowly, followed by the addition of benzyl chloroformate (5.1 g). The temperature was allowed to rise to 0 °C and the

reaction was quenched with 5 mL of saturated ammonium chloride solution (383). The reaction mixture was diluted with water and extracted with ethyl acetate. The combined extracts were then dried over Na_2S0_4 and evaporated. The yellowish oily crude mixture was purified twice over a silica gel column using a mixture of hexane and ethyl acetate at a ratio of 3:1, respectively, as a mobile phase. The purity of the compound was confirmed with thin layer chromatography (TLC).

Methoxy PEO (1 g), α-benzyl carboxylate-ε-caprolactone (different molar ratios to methoxy PEO) and stannous octoate (0.002 eq of monomer) were added to a 10 mL previously flamed ampoule, nitrogen purged and sealed under vacuum. The polymerization reaction was allowed to proceed for 4 h at 140 ºC in oven. The reaction was terminated by cooling the product to room temperature. The molar feed ratio of monomer (α-benzyl carboxylate-ε-caprolactone) to initiator was altered to achieve PEO-*b*-PBCL block copolymers with PBCL average molecular weights of 8,000, 16,000, and 24,000 $g.mol^{-1}$corresponding to degrees of polymerization of 30, 60, and 95, respectively.

2.2.2.3. Characterization of the block copolymers

^1H NMR spectrum of PEO-*b*-PCL or PEO-*b*-PBCL in deuterated chloroform ($CDCl_3$) at 300 MHz was used to assess the conversion of ε-caprolactone or α-benzyl carboxylate-ε-caprolactone to PCL or PBCL, respectively. The NMR spectrum of each block copolymer was obtained by Bruker Unity-300 NMR spectrometer at room temperature and used to determine

the number average molecular weight (M_n) of the block copolymers. The percentage of ε-caprolactone conversion to PCL was determined comparing peak intensity of -O-CH_2- (δ = 4.223 ppm) for ε-caprolactone monomer to the intensity of the same peak for PCL (δ = 4.075 ppm) in the ^{1}H NMR spectrum of PEO-*b*-PCL. The percentage of α-benzyl carboxylate-ε-caprolactone conversion to PBCL was determined comparing peak intensity of -O-CH_2- (δ 4.25 ppm) for α-benzyl carboxylate-ε-caprolactone monomer to the intensity of the same peak for PBCL (δ 4.05 ppm) in the ^{1}H NMR spectrum of PEO-*b*-PBCL. The weight and number average molecular weight as well as polydispersity of prepared PEO-*b*-PBCL block copolymers were also assessed by gel permeation chromatography (GPC). Twenty μL of polymer solution (20 mg/mL in THF) was manually injected into a 7.8 × 300 mm Styragel HMW 6E column (Waters Inc. Milford, MA, USA) which was attached to an HP 1100 pump. The column was eluted with 1 mL/min THF. The elution pattern was detected by refractive index (Model 410; Waters Inc.) and dynamic light scattering detectors (PD 2000 DLS; Precision Detectors, Franklin, MA, USA) using polystyrene standards.

2.2.3. Assembly of block copolymers to nano-carriers and their characterization

2.2.3.1. Assembly of PEO-*b*-PCL and PEO-*b*-PBCL block copolymers

Assembly of PEO-*b*-PCL and PEO-*b*-PBCL was triggered through a co-solvent evaporation method (263). The prepared block copolymers (60 mg) were first dissolved in acetone (1 mL) and then added to distilled water (6 mL) in a

drop-wise manner (1 drop/15 seconds) under moderate stirring, followed by the evaporation of acetone under vacuum.

2.2.3.2. Encapsulation of valspodar in PEO-*b*-PCL and PEO-*b*-PBCL nanocarriers

Valspodar and polymer were dissolved in acetone with an initial concentration of 3 and 10 mg/mL, respectively, followed by drop-wise addition of acetone to distilled water in a ratio of 1:6. All formulations were stirred for 4 h at room temperature, and then vacuum was applied to facilitate the removal of the organic solvent. The colloidal solutions were then centrifuged (11,600 ×*g*, 5 min) to remove any valspodar precipitate. To make the colloidal formulations isotonic, concentrated sucrose solution (1.5 g/mL) was added to achieve a final sucrose concentration of 95.76 mg/mL.

2.2.3.3. Characterization of PEO-*b*-PCL nanocarriers

Average diameter and size distribution of self-assembled structures (with or without valspodar) were estimated by dynamic light scattering (DLS) technique using Malvern Zetasizer™ 3000 (Malvern Instruments Ltd, UK). The level of encapsulated valspodar was determined in the supernatant using an HPLC assay, originally developed for CyA (263, 373), after destroying the nanostructures through addition of 40 times volume of methanol. The HPLC instrument consisted of a Chem Mate pump and Basic-marathon auto-sampler (Spark Holland, Netherlands). An LC1 column (Supleco, Bellefonte, PA, USA) was

equilibrated with a mobile phase of KH_2PO_4 (0.01 M), methanol and acetonitrile (22:50:28) at a flow rate of 1 mL/min. The column was heated at 65 °C using an Eppendorf CH-30 column heater (Westbury, NY, USA). Valspodar concentrations were estimated by UV detection at 205 nm (Waters, model 481, Millipore Corporation, Milford, MA, USA) after injection of 100 µL samples. Valspodar loading content and encapsulation efficiency were determined using the following equations:

$$\text{Valspodar loading content (w/w)} = \frac{\text{Amount of loaded valspodar (mg)}}{\text{Amount of polymer (mg)}}$$

$$\text{Valspodar loading content (mol/mol)} = \frac{\text{Moles of loaded valspodar}}{\text{Moles of polymer}}$$

$$\text{Encapsulation efficiency (\%)} = \frac{\text{Amount of loaded valspodar (mg)}}{\text{Amount of valspodar added (mg)}} \times 100$$

2.2.3.4. Characterization of PEO-*b*-PBCL nanocarriers

The critical association concentration (CAC) of each block copolymer was determined by following changes in the fluorescence excitation spectra of pyrene in the presence of varied concentrations of block copolymers. Pyrene was dissolved in acetone and added to 5 mL volumetric flasks to provide a concentration of 6×10^{-7} M in the final solutions. Acetone was then evaporated and replaced with aqueous polymeric micellar solutions with concentrations ranging from 0.05 to 1000 µg/mL. Samples were heated at 65 °C for an hour,

cooled to room temperature overnight, and deoxygenated with nitrogen gas prior to fluorescence measurements (384). The excitation spectrum of pyrene for each sample was obtained at room temperature using a Varian Cary Eclipse fluorescence spectrophotometer (Victoria, Australia). Emission wavelength and excitation/emission slit were set at 390 nm and 5 nm, respectively. The intensity ratio of peaks at 338 nm to those at 334 nm was plotted against the logarithm of copolymer concentration. CAC was measured from a sharp rise in intensity ratios (I_{338}/I_{334}) at the onset of micellization.

The rigidity of the hydrophobic domain in the prepared nanostructures was estimated by measuring excimer to monomer intensity ratio (I_e / I_m) from the emission spectra of 1,3-(1,1′-dipyrenyl) propane at 480 and 373 nm, respectively. 1,3-(1,1′-dipyrenyl)propane was dissolved in a known volume of chloroform to give a final concentration of 2×10^{-7} M. Chloroform was then evaporated and replaced with 5 mL of nanostructures solutions at a concentration of 1 mg/mL. Samples were heated at 65 °C for an hour and cooled to room temperature overnight. A stream of nitrogen gas was used to deoxygenate samples prior to fluorescence measurements. Emission spectrum of 1,3-(1,1′-dipyrenyl)propane was obtained at room temperature using an excitation wavelength of 333 nm. Excitation/emission slit was set at 5 nm.

Morphology of the assembled structures in the present study was characterized by transmission electron microscopy (TEM). An aqueous droplet of

micellar solution (20 μL) having a polymer concentration of 1 mg/mL was placed on a copper-coated grid. The grid was held horizontally for 20 s to allow the colloidal aggregates to settle. A drop of 2 % solution of phosphotungstic acid in PBS (pH = 7.0) was then added to provide the negative stain. After 1 min, the excess fluid was removed by a strip of filter paper (385). The samples were then allowed to dry at room temperature and loaded into a Philips FEI-Morgagni™ 268 TEM operating at an acceleration voltage of 75 kV. Images were recorded with an SIS MegaView II digital camera and processed with AnalySIS software (Soft Imaging System, Olympus®).

The level of encapsulated valspodar was determined as described in section 2.2.3.3.

2.2.4. Pharmacokinetic studies

2.2.4.1. Animals

All animal studies were performed according to the guidelines approved by Canadian Council of Animal Care (CCAC) and direct supervision of Health Sciences Laboratory Animal Services (HSLAS), University of Alberta, using male Sprague-Dawley rats (Charles River Laboratories, Montreal, QC, Canada) with body weights ranging from 250 to 350 g. All rats were housed in temperature-controlled rooms with 12 h of light/dark cycle for at least a week prior to study. The animals were fed a standard rodent chow containing 4.5% fat (LabDiet1 5001, PMI nutrition LLC, Richmond, IN, USA). Free access to food

and water was permitted prior to experimentation. On the day before the pharmacokinetic experiment, the right jugular vein of all rats was cannulated with Silastic® Laboratory Tubing (Dow Corning Corporation, Midland, MI, USA) under isofluorane/O_2 anesthesia administered by anesthetic machine (386). After surgery, the rats were transferred to their regular holding cages and allowed free access to water, but food was withheld overnight. The next morning, rats were transferred to the metabolic cages and dosing and blood sampling were performed.

2.2.4.2. Assessing the pharmacokinetics of valspodar-loaded polymeric nanocarriers

2.2.4.2.1. Intravenous administration

Cannulated rats were transferred to metabolic cages and divided into five groups (4-8 rats/group). Valspodar, from each formulation, was administered as single dose of 5 mg/kg intravenously (i.v.).

Animals administered valspodar either in its standard Cremophor EL formulation (5 mg/mL, diluted in 0.9% NaCl for injection (154)) or in the polymeric nanocarriers. The dose was injected over 2 min via the jugular vein cannula, immediately followed by injection of normal saline solution. At the time of first sample withdrawal, the first 0.2 mL volume of blood was discarded. Food was provided to animals 4 h after the drug administration. Serial blood samples (0.15–0.25 mL) were collected at 0.08, 0.33, 0.67, 1, 2, 4, 6, 9, 12, and 24 h after

dosing. Heparin in normal saline was used to flush the cannula after each collection of blood. Blood samples were immediately centrifuged for 3 min; plasma was separated and stored at – 20º C until analysis. The plasma concentrations of valspodar were analyzed by the LC/MS assay (as described in section 2.2.1) and the plasma concentration versus time curve was profiled.

2.2.4.2.2. Oral administration

Cannulated rats were transferred to metabolic cages and divided into two groups (5-6 rats/group). Valspodar, from Cremophor EL and PEO-*b*-PCL formulations, was administered as single dose of 10 mg/kg.

The rats received the desired dose by oral gavage. Food was provided to animals 4 h after the dose administration. Serial blood samples (0.15–0.25 mL) were collected at 0.5, 1, 1.5, 2, 3, 4, 6, 8, 10, 24, and 48 h after oral dose. Heparin in normal saline was used to flush the cannula after each collection of blood. Blood samples were immediately centrifuged for 3 min; plasma was separated and stored at – 20º C until analysis. The plasma concentrations of valspodar were analyzed by the LC/MS assay.

2.2.4.3. Determination of valspodar blood to plasma ratio

Known amounts of valspodar in Cremophor EL or PEO-*b*-PCL micellar formulation were added to heparinized tubes containing freshly obtained rat blood to provide final concentrations of 0.5 and 2.5 µg/mL. The tubes were placed in a

shaking water bath at 37 ºC for 1 h. Thereafter, the tubes were removed and 100 µL of blood was transferred to new glass tubes (n = 5) containing 100 µL of water. The remaining blood was centrifuged at 2500 ×*g* for 10 min. A volume of 100 µL of the plasma layer was transferred to new glass tubes (n = 5). Samples were kept frozen at – 20 ºC until being assayed for valspodar concentrations.

2.2.4.4. Determination of valspodar unbound fraction

For determination of valspodar plasma protein binding *in vitro*, an erythrocyte vs. buffer or plasma partitioning method was used. This method has been used previously for valspodar (366) as well as for other drugs, including cyclosporine A, its closely related structural analog (387-389). The partitioning method intuitively assumes that the mechanism of drug entry into the erythrocytes is by passive diffusion. Male Sprague–Dawley rats (Charles River Laboratories, Montreal, QC, Canada) were anesthetized using isoflurane/O_2 administered by anesthetic machine, and blood was collected by cardiac puncture into heparinized tubes. The collected blood (~12 mL/rat) was splitted equally into two tubes. Plasma was separated from blood cells by centrifugation of the whole blood at 2500 ×g for 10 min. After removal of the plasma, the buffy coat layers were discarded using a Pasteur pipette, and the blood cells were washed in an equal volume of isotonic Sørenson's phosphate buffer (pH 7.4), followed by centrifugation at 2500 ×*g* for 8 min. This washing procedure was repeated twice. After the third wash, the volume of total erythrocytes was estimated in each of the tubes using a calibrated tube, and either isotonic phosphate buffer (pH 7.4) or

undiluted plasma was added to make a hematocrit (HCT) of 0.4 (387). Valspodar in the different formulations was added to the erythrocytes-plasma and erythrocytes-buffer mixtures. The final concentration of valspodar was 2.5 μg/mL, which is within the range of plasma concentrations attained after administration of 5 mg/kg valspodar to rats (390). Erythrocyte suspensions were then incubated for 1 h in a shaking water bath at 37 °C. At the conclusion of the incubation, replicates of 4 blood samples (50 μL each) were set aside for assay with an additional 50 μL of water added to each tube before freezing. For the remainder of the blood the plasma and buffer were isolated by centrifugation for 8 min at 2500 ×*g*. Replicates of four at 100 μL volume from each sample was set aside for assay. All samples were frozen at – 20ºC until assayed for valspodar.

2.2.4.5. Pharmacokinetic data analysis

Non-compartmental methods were used to calculate the pharmacokinetic parameters. The elimination rate constant (λ_z) was estimated by linear regression of the plasma concentrations in the log-linear terminal phase and the corresponding half-life ($t_{1/2}$) was calculated by dividing 0.693 by λ_z. The $AUC_{0-\infty}$ was calculated using the combined linear-log trapezoidal method (391) from time 0 h post dose to the time of the last measured concentration, plus the quotient of the last measured concentration divided by λ_z. The concentration at time 0 h after i.v. dosing (Cp_0) was estimated by extrapolation of the log-linear regression line using the first three measured plasma concentrations to time 0. The mean residence time (MRT) was calculated by dividing area under the first moment

curve ($AUMC_{0-\infty}$) by $AUC_{0-\infty}$, clearance (CL) by dividing dose by $AUC_{0-\infty}$, and volume of distribution at steady-state (Vd_{ss}) by multiplying CL by MRT.

The maximum plasma concentration (C_{max}) and the time at which it occurred (t_{max}) were determined by visual examination of the data. The oral bioavailability (F) for each formulation was calculated as follows:

$$F = \frac{mean\ AUC_{oral}}{mean\ AUC_{iv}} \times \frac{Dose_{iv}}{Dose_{oral}}$$

The mean blood CL of valspodar was estimated by dividing the mean plasma CL by the blood to plasma ratio. The hepatic extraction ratio (E) was estimated, assuming negligible extrahepatic CL, by taking the quotient of i.v. blood CL divided by average hepatic blood flow of 55.2 mL/min/kg (392). The gastrointestinal availability (f_g) in turn was calculated as the quotient F divided by (1 - E), where 1 - E represents the hepatic availability (f_h).

The plasma unbound fraction (f_u) was calculated by using the equations outlined by Schuhmacher et al. (388). The concentrations of valspodar within erythrocytes of erythrocyte-plasma samples (CE) and erythrocyte-buffer samples (CE*) were determined by using the following equations:

$$CE = \frac{CB - Cp(1 - HCT)}{HCT} \qquad CE^* = \frac{CB^* - Cb(1 - HCT)}{HCT}$$

Where CB and CB* are the concentration of valspodar in the blood cell–plasma and blood cell–buffer suspensions, and Cp and Cb are the concentration of drug in the plasma and buffer, respectively. The partition coefficients for erythrocyte:plasma (Pp) and erythrocyte:buffer (Pb), and (f_u) were determined by:

$$Pp = \frac{CE}{Cp}, Pb = \frac{CE*}{Cb}, \text{ and } f_u(\%) = 100 \times \frac{Pp}{Pb}$$

2.2.5. Pharmacokinetic interaction studies

2.2.5.1. Assessing the effect of valspodar and CyA formulations on the pharmacokinetics of DOX upon i.v. co-administration

Rats used in this study had the same specification as described in section 2.2.4.1. Cannulated rats were transferred to metabolic cages and divided into seven groups (6 rats/group) receiving i.v. administration of the following in each group:

I. DOX only (5 mg/kg)

II. DOX (5mg/kg) *plus* CyA (Sandimmune®; 10 mg/kg)

III. DOX (5mg/kg) *plus* CyA (PEO-*b*-PCL micellar formulation; 10 mg/kg)

IV. DOX (5mg/kg) *plus* Valspodar (standard Cremophor EL/ethanol formulation; 10 mg/kg)

V. DOX (5mg/kg) *plus* Valspodar (PEO-*b*-PCL micellar formulation; 10 mg/kg)

VI. DOX (5 mg/kg) *plus* Unloaded PEO-*b*-PCL polymeric micelles (equivalent dose received by animals in 10 mg/kg CyA polymeric micellar formulation group)

VII. DOX (5mg/kg) *plus* Cremophor EL/ethanol vehicle (equivalent dose received by animals in group II and IV)

The commercially available DOX (Adriamycin® PFS) was administered as a single i.v. dose either alone or 30 minutes following a single i.v. dose of CyA, valspodar, or equivalent volume of the vehicle. Serial blood samples (0.15-0.25 mL) were collected at 0.08, 0.33, 0.67, 1, 2, 4, 6, 9, 12, 24, 48, and 72 h after i.v. dosing. Heparin in normal saline was used to flush the cannula after each collection of blood. Blood samples were immediately centrifuged for 3 min; plasma was separated and stored at – 20º C until analysis.

The pharmacokinetic parameters of AUC, $t_{1/2}$, and CL were calculated by using the non-compartmental approach as decribed in section 2.2.4.6.

2.2.5.2. Determination of doxorubicin and its major metabolite doxorubicinol levels in plasma

2.2.5.2.1. Standard and stock solutions

The commercially available formulation for DOX (Adriamycin®, 2 mg/mL) was used as a stock solution (stored at 4º C). DOXol (TRC, Toronto, Canada) stock solution was prepared by dissolving 1 mg in 10 mL methanol (100 µg/mL) and stored in amber glass containers at – 20º C. Daunorubicin HCL,

which was used as an internal standard (IS), was prepared by dissolving 4 mg of the powder in 100 mL of methanol (40 μg/mL) and was also kept in amber glass container at –20º C. Working solutions containing DOX and DOXol were prepared by serial dilution of the related stock solutions in methanol. Standard samples were prepared by spiking appropriate amounts of DOX and DOXol in 100 μL of rat plasma at concentration ranges of 50-5000 ng/mL for DOX and 25-2500 ng/mL for DOXol.

2.2.5.2.2. Sample preparation and HPLC conditions

The levels of DOX and doxorubicinol (DOXol) were determined using an HPLC method after drug/metabolite extraction. To 100 μL of plasma containing DOX and DOXol in polypropylene tubes, 50 μL of IS (1/10 dilution) and 300 μL of acetonitrile were added. The mixture was then vortex mixed briefly and centrifuged at 2500 ×*g* for 3 min. The supernatant of each tube was transferred to new glass tubes containing 1 mL of HPLC water. DOX, DOXol and internal standard were then extracted into 4 mL of chloroform and isopropanol mixture (1:1) by vortex-mixing for 60 S. After centrifugation the tubes for 3 min at 2500 ×*g*, the organic lower layer from each tube was carefully transferred into new tubes and dried in vacuum. Finally, the residue was reconstituted in 150 μL of methanol and injected to the HPLC. The HPLC system consisted of two LC-10 AD Shimadzu® pumps, a Mandel® 234 auto sampler and an RF-10A XL Fluorescence detector. The stationary phase was composed of a 10 μm particle size μBondapak® C_{18} column material packed in a 125 A°, 3.9 x 300 mm column

(Waters®). The mobile phase consisted of a gradient solution system containing 0.1% formic acid (A) and acetonitrile (B) running over a 30 minute period. The flow rate was set at 1 mL/min and the eluent was monitored using fluorescence detection with an excitation wavelength set at 470 nm and emission wavelength of 560 nm. Detection and integration of chromatographic peaks was performed by Data Apex Clarity system. Calibration curves were computed and plotted using the ratio of the corresponding peak area of DOX or DOXol to that of internal standard versus the nominal DOX or DOXol concentration. Data for calibration curves was weighted by a factor of 1/concentration.

2.2.6. Statistical analysis

Compiled data are presented throughout the thesis as mean ± standard deviation (SD). The data were analyzed for statistical significance by unpaired Student's *t*-test except for cases specified in the following section.

In the characterization studies of drug-free as well as the characterization and pharmacokinetic studies of valspodar-loaded PEO-*b*-PBCL nanocarriers, the differences between the means were compared by one-way analysis of variance (ANOVA) followed by a *post-hoc* analysis using Bonferroni test (SSPS for Windows v.16, Cary, NC).The level of significance was set at $\alpha = 0.05$.

In the DOX pharmacokinetic interaction study, the differences between the means were compared by one-way ANOVA followed by Bonferroni *post-hoc* analysis (SigmaPlot 11, Systat Software, CA, USA). The level of significance was set at $\alpha = 0.05$.

CHAPTER THREE

RESULTS

3.1. Liquid chromatography/mass spectrometry (LC/MS) assay

The chemical structures of valspodar and the IS are shown in Figure 3.1. The mass spectra of valspodar and IS dissolved in methanol with 0.2% ammonium hydroxide are shown in Figure 3.2 A and B, respectively. The molecular ion at *m/z* 1214.81 and 645.84 were selected for quantification of valspodar and IS, respectively. Figure 3.3 A represents the chromatogram of blank rat plasma after the extraction procedure showing no endogenous peaks that might interfere with IS or valspodar peaks (Figure 3.3 B and C, respectively). Valspodar and IS peaks were well separated with retention times of approximately 2.4 and 3.1 min, respectively. The run time of analysis was 10 min. Under the experimental condition, one peak was detected for valspodar.

(A)

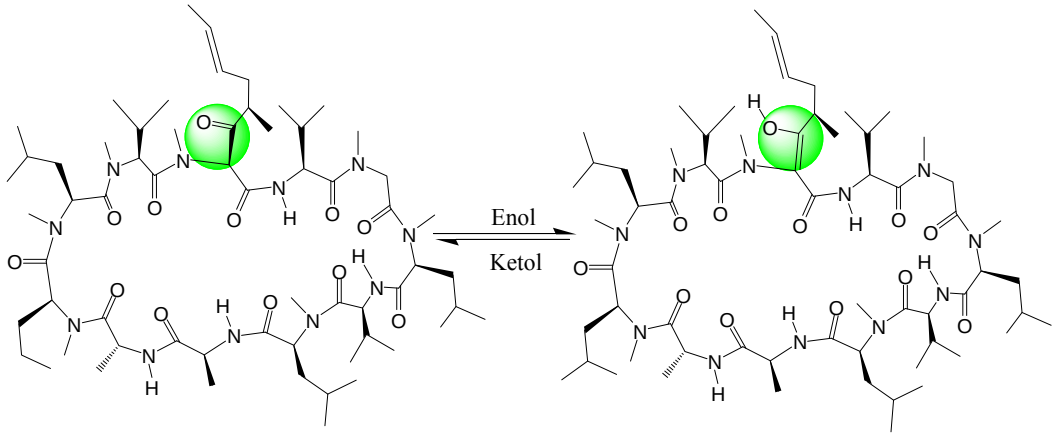

(B)

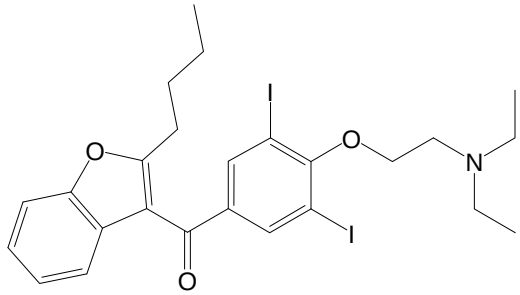

Figure 3.1 – Chemical structures of (A) vaslpodar in keto-enol tautomerism and (B) amiodarone (IS).

(A)

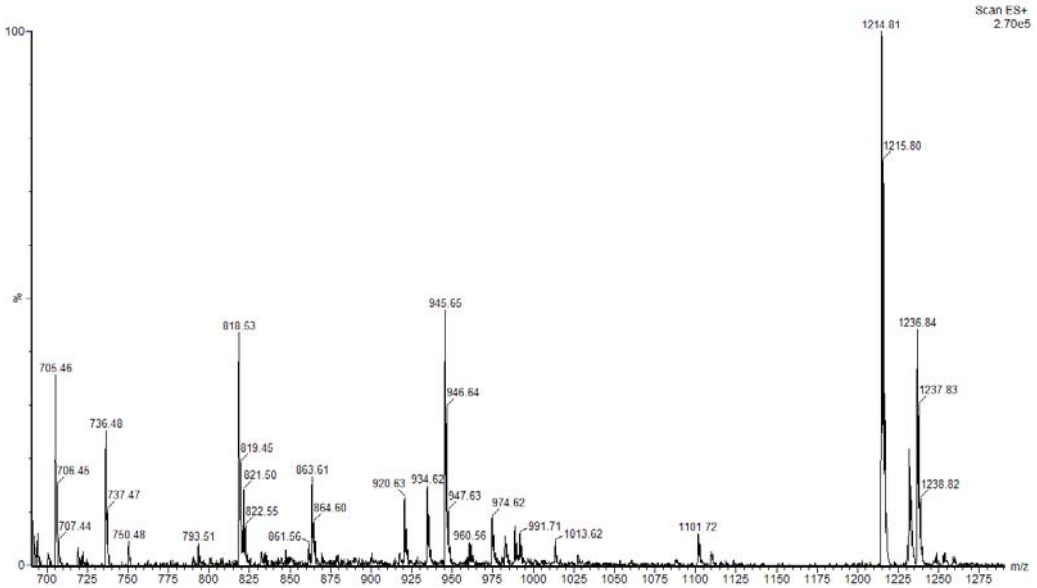

(B)

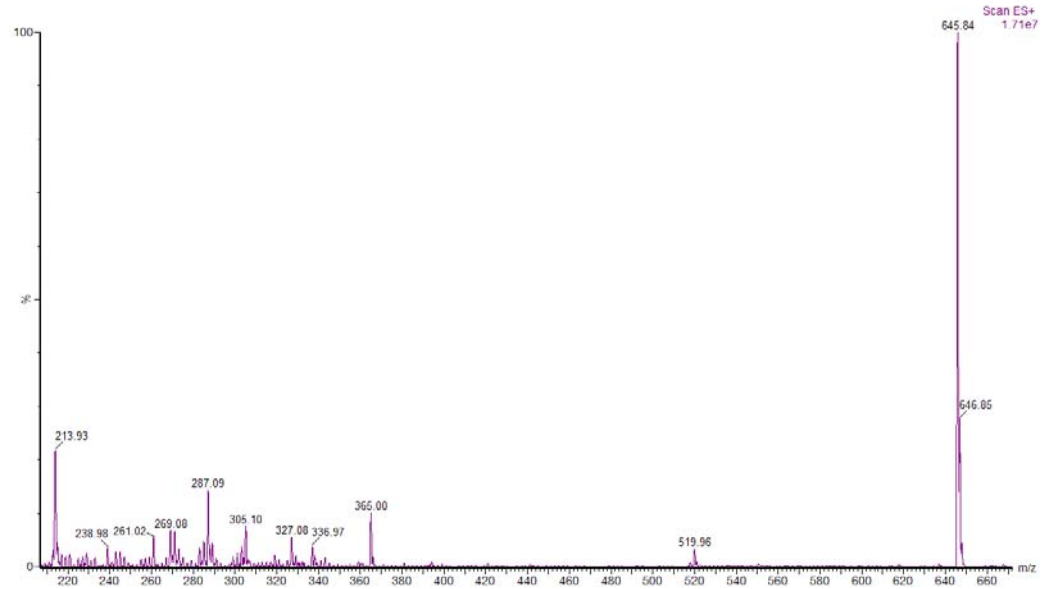

Figure 3.2 – Positive ion mass spectra of (A) valspodar and (B) amiodarone (IS).

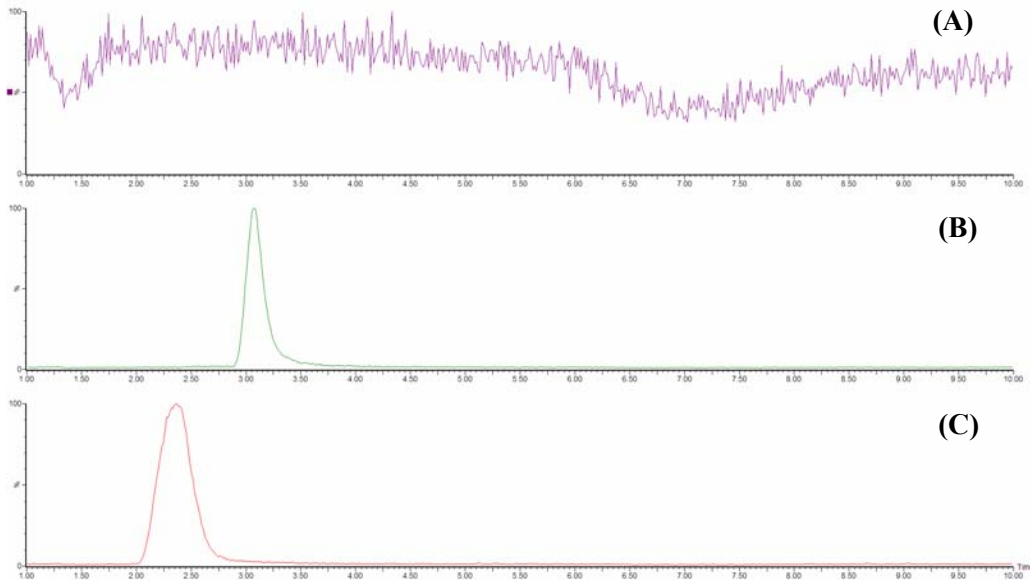

Figure 3.3 – Representative selected ion recording (SIR) chromatograms of (A) blank plasma, (B) amiodarone (*m/z* 645.84; 3.05 min), and (C) valspodar (*m/z* 1214.81; 2.37 min) after extraction from rat plasma.

The average extraction recoveries of valspodar from plasma were 102.7, 79, and 73% for 50, 1000, and 5000 ng/mL of valspodar, respectively. A linear relationship between the peak height ratios and rat plasma concentrations of valspodar was observed within the range of 10-5000 ng/mL ($R^2 > 0.99$). The mean slope and intercept from three replicates of calibration curves on different days were calculated to be 0.00015 and – 0.0033 for valspodar, respectively.

The assay CV% for both intraday and interday assessments were less than 15% except for the lowest concentration used in the calibration and validation samples (10 ng/mL), where the values were between 15-19%. Mean error was less than 10% in all the concentrations above 10 ng/mL (Table 3.1). The low variability in the validation data demonstrated the accuracy and reproducibility of

the developed method. Based on the validation data, the limit of quantification (LOQ) was set at 10 ng/mL; and with an injection volume of 10 μL, the value translates into an on-column amount of 0.1 ng. The limit of detection (LOD) was assessed based on signal-to-noise (S/N) ratio. The concentration of valspodar that is associated with an average S/N ratio of 3:1 was considered the LOD. The LOD of this method was found to be 2.5 ng/mL and based on an injection volume of 10 μL, the corresponding amount injected to the system was 0.025 ng (i.e. 25 pg).

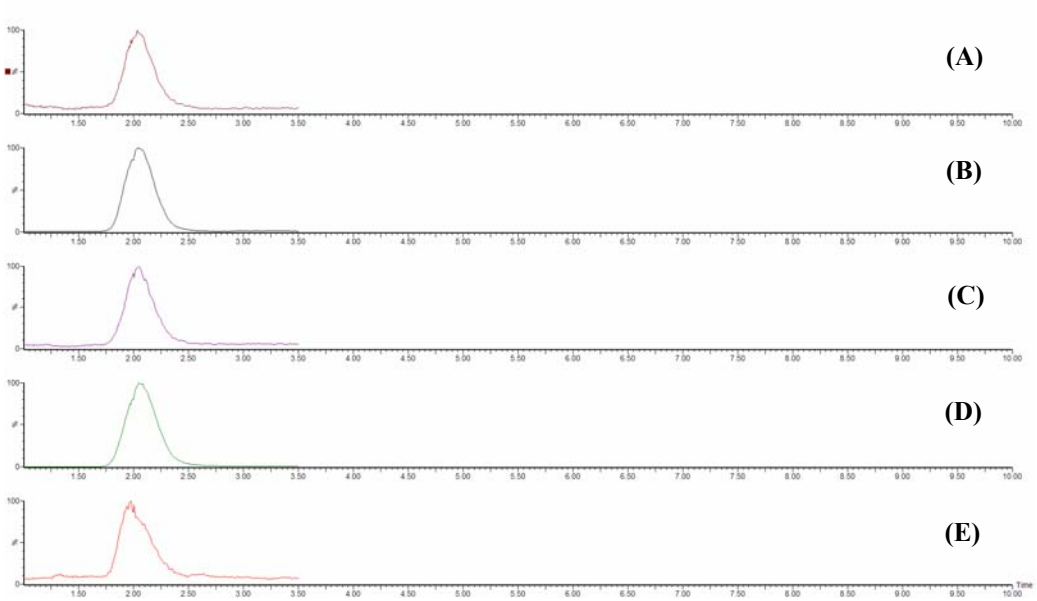

Figure 3.4 – SIR chromatograms of (A) valspodar in methanol (50 ng/mL) (B) valspodar in methanol (1000 ng/mL), (C) rat plasma extract of valspodar (50 ng/mL), (D) rat plasma extract of valspodar (1000 ng/mL), and (E) plasma sample from a rat obtained at 12h following a single iv dose of 5 mg/kg of valspodar.

Table 3.1 – The intraday (n = 5) and interday (n = 3) accuracy and precision of the developed LC/MS method in rat plasma

Nominal concentration, µg/mL	Intraday mean ± SD measured concentrations, µg/mL (intraday CV%)			Interday mean ± SD measured concentrations, µg/mL	Interday CV%	Interday mean error %
0.010	0.010 ± 0.002 (17.4)	0.013 ± 0.002 (15.9)	0.012 ± 0.002 (18.3)	0.012 ± 0.001	17.17	17.76
0.025	0.024 ± 0.002 (9.0)	0.023 ± 0.002 (8.2)	0.025 ± 0.001 (4.6)	0.024 ± 0.001	7.25	-4.41
0.100	0.095 ± 0.005 (5.2)	0.097 ± 0.013 (13.7)	0.106 ± 0.003 (2.5)	0.099 ± 0.005	7.14	-0.83
0.500	0.510 ± 0.013 (2.6)	0.495 ± 0.049 (10.0)	0.535 ± 0.021 (3.9)	0.513 ± 0.020	5.50	2.7
1.000	1.099 ± 0.160 (14.5)	0.970 ± 0.029 (3.0)	1.091 ± 0.067 (6.2)	1.053 ± 0.072	7.89	5.37

3.2.Synthesis of block copolymers and their characterization

PEO_{114}-*b*-PCL_{114} block copolymer (Figure 3.5) was successfully synthesized as previously described (263), and the calculated molecular weight of PCL segment (using ^{1}H NMR) was found to be 12.8 kg/mol, which is very close to the theoretical value of 13.0 kg/mol. Three PEO-*b*-PBCL block copolymers having f_{EO} ranging from 0.18-0.40 (Figure 3.6; Table 3.2) were synthesized by ring-opening polymerization of α-benzyl carboxylate-ε-caprolactone at different ratios to that of methoxy PEO (initiator) using stannous octoate as catalyst. The polymerization reaction yielded PEO-*b*-PBCL copolymers with a unimodal distribution (PDI= 1.13-1.58), as confirmed by gel permeation chromatography (GPC). The PBCL block molecular weights were 8, 16, and 25 kg/mol as determined by ^{1}H NMR corresponding to average degrees of polymerization of 30, 60 and 95 in the hydrophobic block and f_{EO}'s of 0.40, 0.25 and 0.18 for the prepared block copolymers, respectively (Table 3.2).

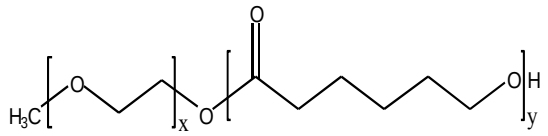

Figure 3.5 – Chemical structure of PEO-*b*-PCL (x = 114; y = 114).

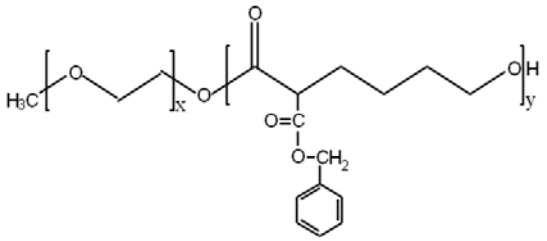

Figure 3.6 – Chemical structure of PEO-*b*-PBCL (x = 114; y = 30, 60, or 95).

Table 3.2 – Characterization of the prepared block copolymers

Block copolymer [a]	Theor mol wt (kg/mol)	M_n (kg/mol)[b]	M_n (kg/mol)[c]	PDI[d]	f_{EO}[e]
PEO_{114}-*b*-PCL_{114}	18.0	17.8	ND	ND	0.28
PEO_{114}-*b*-$PBCL_{30}$	13.0	12.5	14.8	1.32	0.40
PEO_{114}-*b*-$PBCL_{60}$	21.0	19.7	21.1	1.58	0.25
PEO_{114}-*b*-$PBCL_{95}$	30.0	28.5	31.4	1.13	0.18

[a] The number shown as a subscript indicates the polymerization degree of each block determined by ^{1}H NMR. [b] Number-average molecular weight measured by ^{1}H NMR. [c] Number-average molecular weight measured by GPC using PS standards. [d] Polydispersity index (M_w/M_n) determined by GPC. [e] Weight fraction of the PEO block as determined by ^{1}H NMR spectroscopy. ND: not determined.

3.3. Assembly of block copolymers to nano-carriers and their characterization

Previously, in our lab, we have reported on the synthesis and self assembly of PEO-*b*-PCL block copolymers of different molecular weights (263, 393). The assembly of PEO_{114}-*b*-PCL_{114} was triggered through a co-solvent evaporation method as described previously (in section 2.2.3.1.) (393). Assembly of PEO_{114}-*b*-PCL_{114} has led to the formation of nanostructrues with average diameter of 63.0 nm with a low polydispersity (0.14) as determined by dynamic light scattering (DLS) technique (393). The average critical association concentration (CAC) was found to be 46 *n*M (393), as determined by following changes in the fluorescence

excitation spectra of pyrene in the presence of varied concentrations of block copolymers (384).

Assembly of PEO-*b*-PBCL was triggered through a co-solvent evaporation method identical to the one used for PEO-*b*-PCL (244). Assembly of prepared block copolymers led to the formation of nanostructures with average diameters of 104, 95.5, and 74.1 nm for PEO_{114}-*b*-$PBCL_{30}$, PEO_{114}-*b*-$PBCL_{60}$, and PEO_{114}-*b*-$PBCL_{95}$, respectively, as determined by DLS technique. The population of nanostructures prepared for all three block copolymers showed a narrow distribution (polydispersity ≤ 0.15). The average CAC for PEO_{114}-*b*-$PBCL_{30}$, PEO_{114}-*b*-$PBCL_{60}$, and PEO_{114}-*b*-$PBCL_{95}$ was found to be 62, 41, and 23 *n*M, respectively (Table 3.3).

Table 3.3 – Characteristics of prepared PEO-*b*-PBCL nanostructures

Block copolymer	**Diameter (nm)** [a]	**Polydispersity**	**CAC (*n*M)** [b]	I_e/I_m [c]
PEO_{114}-*b*-$PBCL_{30}$	104.0 ± 3.0	0.14 ± 0.02	61.7 ± 3.0	0.055 ± 0.001
PEO_{114}-*b*-$PBCL_{60}$	95.5 ± 2.3	0.15 ± 0.01	41.2 ± 2.7	0.119 ± 0.019
PEO_{114}-*b*-$PBCL_{95}$	74.1 ± 0.9	0.14 ± 0.01	23.5 ± 3.2	0.177 ± 0.006

[a] Average diameter (Z_{ave}) estimated by the DLS technique. [b] Measured from the onset of a rise in the intensity ratio of peaks at 338 nm to peaks at 334 nm in the fluorescence excitation spectra of pyrene plotted vs logarithm of polymer concentration. [c] Intensity ratio (excimer/monomer) from emission spectrum of 1,3-(1,1′ dipyrenyl) propane in the presence of polymeric micelle. Data is presented as mean ± SD (n = 3).

The rigidity of the hydrophobic domain in the prepared nanostructures was estimated by measuring excimer to monomer intensity ratio (I_e/I_m) from the emission spectra of 1,3-(1,1′-dipyrenyl) propane at 373 and 480 nm, respectively. Low excimer to monomer (I_e/I_m) intensity ratios in the emission spectrum of the

dipyrene probe is an indication of a high viscosity (rigidity) of the hydrophobic domain. Increasing the chain length of the hydrophobic block is usually associated with higher rigidity (lower I_e/I_m value) of the core in core/shell type nano-structures (263, 385). Interestingly, I_e/I_m intensity ratios did not decrease as the chain length of PBCL increased. Instead, the polymer with the longest PBCL chain showed the highest I_e/I_m ratios among the three block copolymers (Table 3.3).

Morphology of the assembled structures in the present study was characterized by transmission electron microscopy (TEM). The TEM image of PEO_{114}-*b*-$PBCL_{30}$ shows the formation of spherical micelles with high polydispersity and an average diameter of 60.7 nm (Figure 3.7A). An increase in the molecular weight of PBCL, and subsequent drop in f_{EO} from 0.40 to 0.25, resulted in a mixed population of spherical micelles and vesicles with average diameters of 42.6 and 77.0 nm, respectively (Figures 3.7B and C). A further increase in PBCL block length leading to the preparation of block copolymers with f_{EO} of 0.18, also resulted in the formation of a mixed population of micelles and vesicles with average diameters of 55.8 and 57.4 nm, respectively (Figures 3.7D and E).

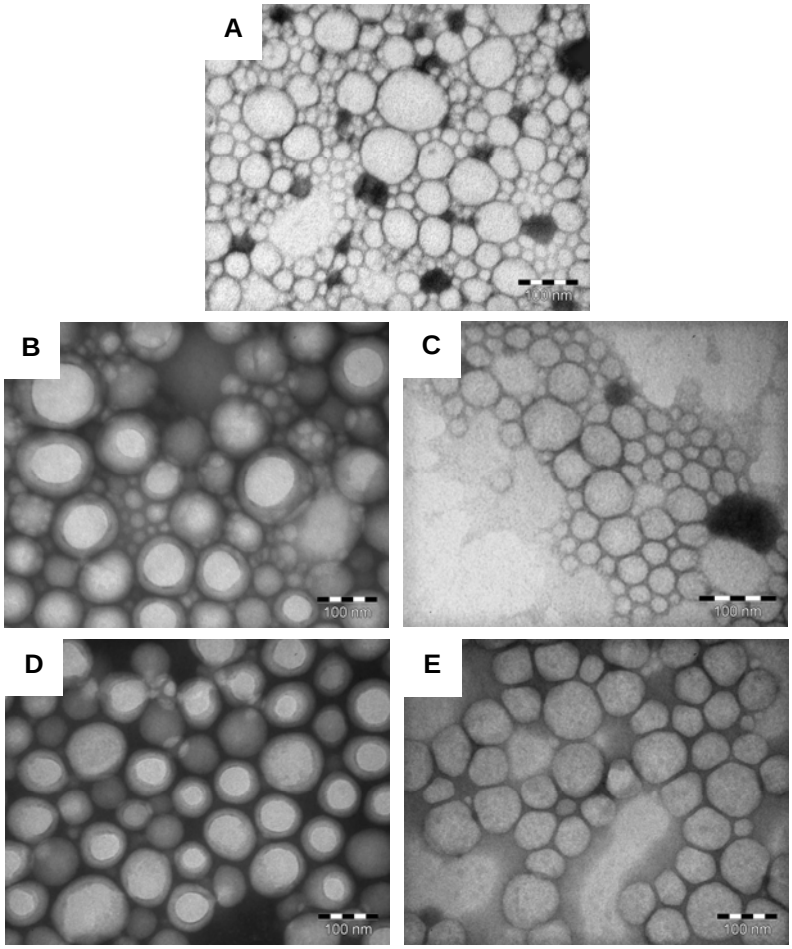

Figure 3.7 – TEM images obtained from 1 mg/mL aqueous solutions of PEO_{114}-*b*-$PBCL_{30}$ micelles (A), PEO_{114}-*b*-$PBCL_{60}$ vesicles and micelles (B & C, respectively), and PEO_{114}-*b*-$PBCL_{95}$ vesicles and micelles (D & E, respectively).

3.4. Encapsulation of valspodar in PEO-*b*-PCL and PEO-*b*-PBCL nanocarriers

Valspodar reached a level of 2.81 mg/mL (4.16 valspodar:polymer mol/mol) when loaded in nanostructures formed from PEO_{114}-b-PCL_{114} (Table 3.4). This corresponded to an encapsulation efficiency of 93.6 %. Valspodar drug loading levels were 2.1, 2.3, and 4.0 mol/mol for PEO_{114}-*b*-$PBCL_{30}$, PEO_{114}-*b*-

$PBCL_{60}$, and PEO_{114}-*b*-$PBCL_{95}$, respectively, which correspond to encapsulation efficiencies of 67.6, 47.3, and 56.8%, respectively (Table 3.4). PEO-*b*-PCL nanocarrriers containing valspodar have shown an average diameter of 62.3 nm. The average diameters of valspodar-loaded PEO-*b*-PBCL nanostructures were 97, 107, and 94 nm, respectively. While the size of PEO_{114}-*b*-$PBCL_{30}$ and PEO_{114}-*b*-$PBCL_{60}$ did not change significantly after drug loading, it significantly increased when valspodar was loaded to PEO_{114}-*b*-$PBCL_{95}$ assemblies. This is likely because PEO_{114}-*b*-$PBCL_{95}$ was associated with the highest *mol/mol* drug loading compared to PEO_{114}-*b*-$PBCL_{30}$ and PEO_{114}-*b*- $PBCL_{60}$ (Table 3.4).

Table 3.4 – Characteristics of valspodar-loaded PEO-*b*-PCL and PEO-*b*-PBCL nanocarriers

Block copolymer	Valspodar Loading (mg/mg)	Valspodar Loading (mol/mol)	Encapsulation Efficiency (%)	Diameter (nm) [a]	Polydispersity
PEO_{114}-*b*-PCL_{114}	0.28 ± 0.01	4.16 ± 0.21	93.6 ± 4.8	62.3 ± 0.70	0.21 ± 0.03
PEO_{114}-*b*-$PBCL_{30}$	0.20 ± 0.01	2.09 ± 0.09	67.6 ± 2.9	96.9 ± 14.5	0.26 ± 0.11
PEO_{114}-*b*-$PBCL_{60}$	0.14 ± 0.01	2.30 ± 0.13	47.3 ± 2.6	107.4 ± 16.1	0.32 ± 0.02
PEO_{114}-*b*-$PBCL_{95}$	0.17 ± 0.01	4.00 ± 0.21	56.8 ± 2.9	93.9 ± 5.5	0.25 ± 0.03

[a] Average diameter (Z_{ave}) estimated by the DLS technique. Data is presented as mean ± SD (n = 3).

3.5. Pharmacokinetics of valspodar-loaded PEO-*b*-PCL and PEO-*b*-PBCL nanocarriers following i.v. administration

Figure 3.8 shows the concentration-time profile of valspodar in plasma following an i.v. dose of 5 mg/kg in rats. The 24-h profile for the Cremophor EL-based formulation (control) shows a rapid decline in plasma concentration in the first two hours representing a distribution phase which was followed by an

elimination phase with an average $t_{1/2}$ of approximately 13 h. On the other hand, valspodar in the PEO-*b*-PCL micellar formulation was associated with a less steep decline in plasma concentration especially at the early time points (up to ~ 6 h) with a terminal phase $t_{1/2}$ of nearly 10 h. The difference in the terminal phase $t_{1/2}$ between the two formulations was not statistically significant. However, valspodar in PEO-*b*-PCL micelles yielded higher plasma concentrations when compared to the Cremophor EL formulation. Non-compartmental analysis of the plasma concentrations showed a significant change in the pharmacokinetic parameters of valspodar in polymeric micelles in comparison to the Cremophor EL formulation (Table 3.5). PEO-*b*-PCL micelles provided ~ 77% higher plasma AUC compared to the Cremophor EL formulation. The PEO-*b*-PCL micelles also significantly decreased the volume of distribution (Vd_{ss}) and clearance (CL) of valspodar by 49 and 34%, respectively. The pharmacokinetic parameters following intravenous administration of valspodar are listed in Table 3.5.

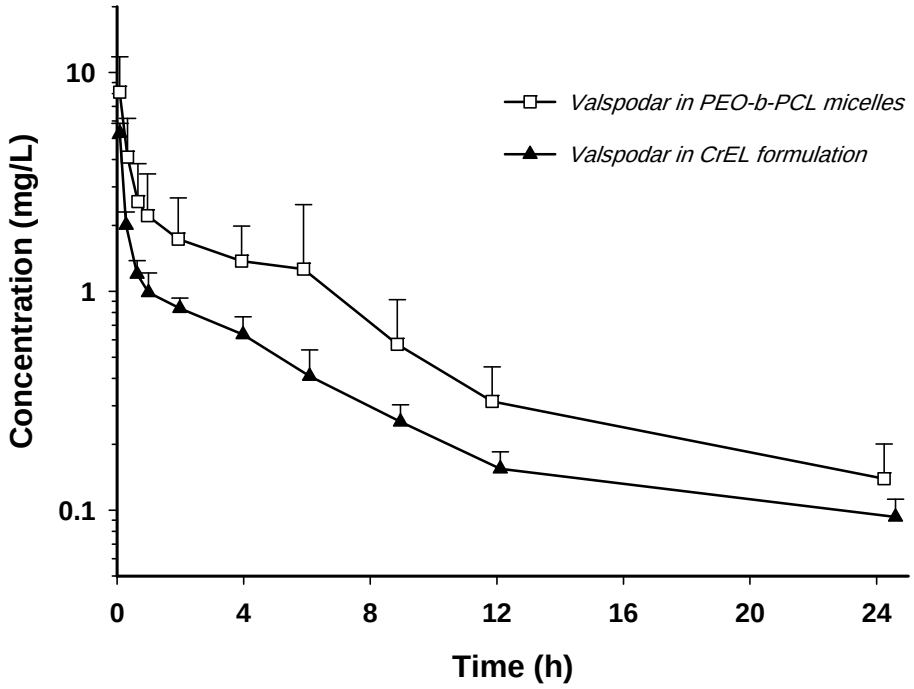

Figure 3.8 – Plasma concentration versus time profile in rat following a single i.v. dose (5 mg/kg) of valspodar control formulation (n = 7) and PEO-*b*-PCL micellar formulation (n = 8). Each data point represents the mean ± SD CrEL: Cremophor EL.

Table 3.5 – Plasma pharmacokinetic parameters (mean ± SD) of valspodar in rats following a single i.v. administration (5 mg/kg)

Parameter	**Valspodar in CrEL** (n = 7)	**Valspodar in PEO-*b*-PCL micelles** (n = 8)
$AUC_{0\text{-}24h}$ (mg·h/L)	9.10 ± 1.38	17.51 ± 8.67*
$AUC_{0\text{-}\infty}$ (mg·h/L)	10.99 ± 1.62	19.43 ± 8.78*
$t_{1/2}$ (h)	12.71 ± 3.40	9.62 ± 3.41
MRT (h)	12.66 ± 3.62	9.54 ± 3.42
CL (L/kg/h)	0.462 ± 0.06	0.303 ± 0.13*
Vd_{ss} (L/kg)	5.83 ± 1.87	3.03 ± 1.78*

* Denotes significant difference between the two groups.

Figure 3.9 shows the concentration-time profile of valspodar for PEO-*b*-PBCL formulations in plasma following an i.v. dose of 5 mg/kg in rats. In the 24-h profile for all the formulations there were rapid declines in plasma concentrations in the first two hours after dosing representing an initial distribution phase. This was followed by a sustained elimination phase with an average $t_{1/2}$ ranging from 9-14 h. Although characterization studies confirmed formation of a population consisting of polymeric vesicles for PEO_{114}-*b*-$PBCL_{60}$ and PEO_{114}-*b*-$PBCL_{95}$, no significant difference in the pharmacokinetic parameters of these formulations compared to PEO_{114}-*b*-$PBCL_{30}$, that has presumably only formed micelles, was observed (Table 3.6).

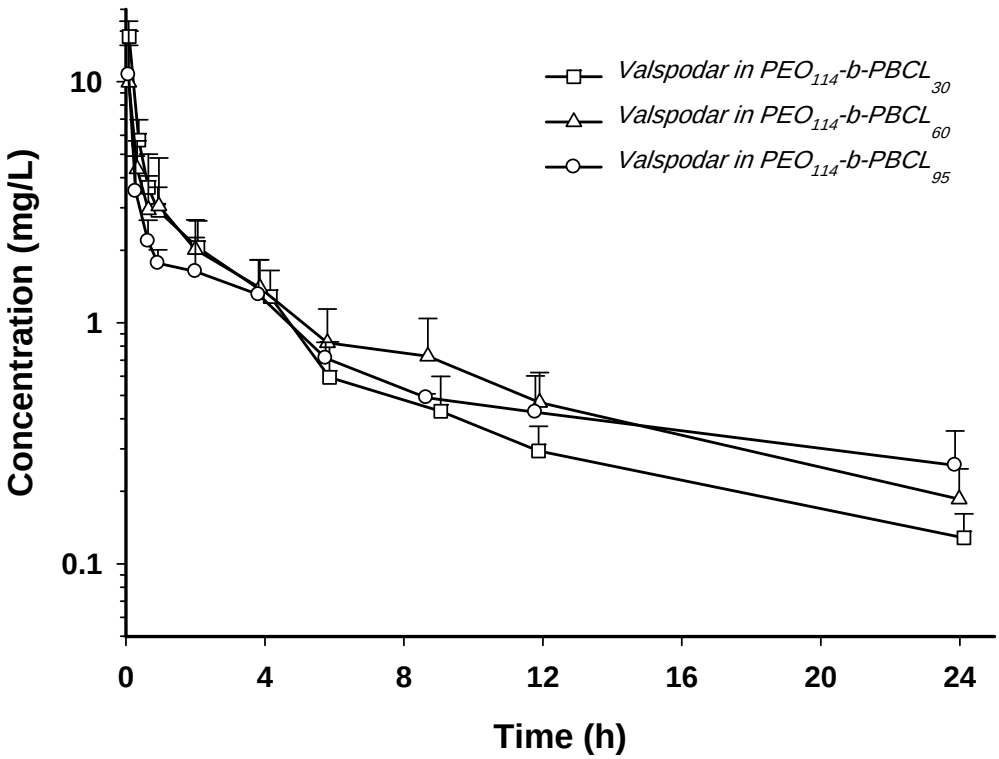

Figure 3.9 – Plasma concentration versus time profile in rat following a single i.v. dose (5 mg/kg) of valspodar in the PEO-*b*-PBCL formulations (n = 3 - 4/group). Data are presented as mean ± SD.

Table 3.6 – Plasma pharmacokinetic parameters (mean ± SD) of valspodar as part of PEO-*b*-PBCL nanocarriers in rats following a single i.v. administration (5 mg/kg; n = 3 - 4/group)

Parameter	PEO_{114}-*b*-$PBCL_{30}$	PEO_{114}-*b*-$PBCL_{60}$	PEO_{114}-*b*-$PBCL_{95}$
$AUC_{0\text{-}24h}$ (mg.h/L)	19.13 ± 3.08	20.02 ± 5.99	17.25 ± 4.70
$AUC_{0\text{-}\infty}$ (mg.h/L)	20.90 ± 3.58	22.50 ± 6.12	22.55 ± 6.82
$t_{1/2}$ (h)	9.56 ± 1.58	8.98 ± 2.92	13.99 ± 1.62
MRT (h)	7.23 ± 0.66	9.64 ± 3.42	15.32 ± 3.26
CL (L/kg/h)	0.244 ± 0.05	0.236 ± 0.07	0.236 ± 0.06
Vd_{ss} (L/kg)	1.75 ± 0.16	2.30 ± 0.99	3.58 ± 1.11

3.6. Pharmacokinetics of valspodar-loaded PEO-*b*-PCL nanocarriers following oral administration

The concentration-time profile of valspodar in plasma following oral dose of 10 mg/kg is shown in Figure 3.10. The 48 h profile shows a rapid absorption phase reaching average C_{max} of 1.17 mg/L and 1.00 mg/L for control formulation and the polymeric micellar formulation, respectively. The median t_{max} was very similar between the two formulations. Mean absolute F for the control and the polymeric micellar formulations were 42.3% and 28.9%, respectively. However, the relative F, where the AUC of the control formulation served as the reference AUC formulation, was 121%. The pharmacokinetic parameters following oral administration of valspodar are listed in Table 3.7.

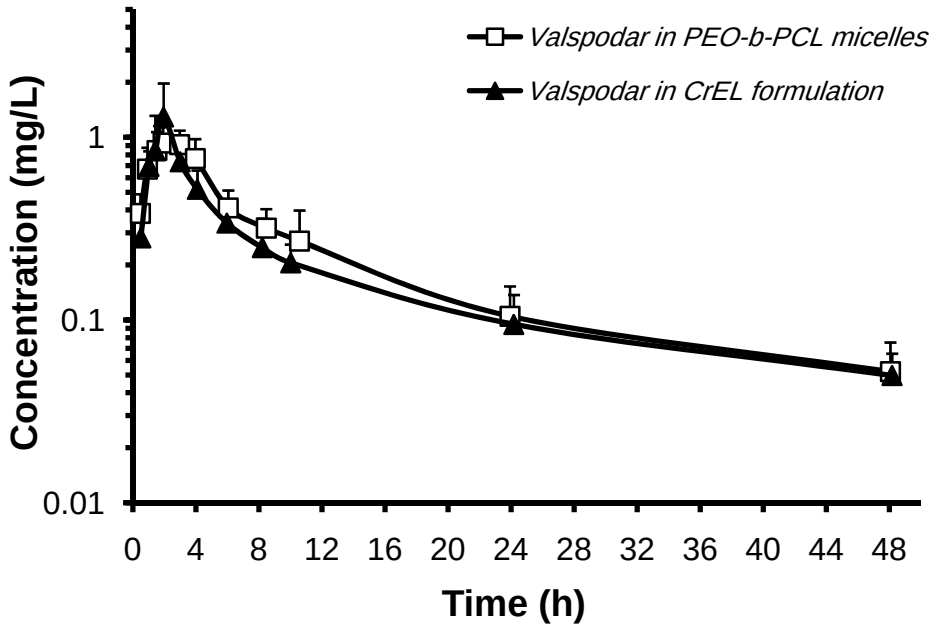

Figure 3.10 – Plasma concentration versus time profile in rat following a single oral dose (10 mg/kg) of valspodar control formulation (n = 6) and PEO-*b*-PCL micellar formulation (n = 5). Each data point represents the mean ± SD

The mean blood CL for the Cremophor EL and PEO-*b*-PCL polymeric micellar formulations were 0.894 L/h/kg and 0.620 L/h/kg, respectively. By using the reported mean hepatic blood flow in rat (392) and assuming that the majority of the CL of valspodar occurs in liver, E was estimated to be 0.27 and f_g was found to be 0.59 for the Cremophor EL formulation. The corresponding values of E and f_g for the PEO-*b*-PCL polymeric micellar formulation were 0.19 and 0.36, respectively.

Table 3.7 – Plasma pharmacokinetic parameters (mean ± SD) of valspodar in rats following a single oral administration (10 mg/kg)

Parameter	**Valspodar in CrEL** (n = 6)	**Valspodar in PEO-*b*-PCL micelles** (n = 5)
$AUC_{0\text{-}48h}$ (mg·h/L)	8.69 ± 1.67	9.54 ± 2.37
$AUC_{0\text{-}\infty}$ (mg·h/L)	9.30 ± 1.83	11.23 ± 2.56
$t_{1/2}$ (h)	14.82 ± 5.02	16.34 ± 4.52
MRT (h)	17.80 ± 4.19	18.70 ± 4.68
CL/F (L/kg/h)	1.09 ± 0.30	0.94 ± 0.27
F	0.423	0.289
C_{max} (mg/L)	1.17 ± 0.70	1.00 ± 0.15
t_{max} (h) [a]	1.96 (1.43-1.97)	1.92 (1.55-3.85)

[a] Data is presented as median (range in parenthesis).

3.7. Determination of valspodar blood to plasma ratio

The mean blood:plasma ratios of valspodar at 0.5 and 2.5 µg/mL were the same with the average values of 0.52 and 0.49 for the Cremophor EL formulation and the PEO-*b*-PCL polymeric micellar formulation, respectively. These values indicate minimal blood-cell partitioning for valspodar and its restriction primarily to the plasma fraction within the blood matrix.

3.8. Determination of valspodar unbound fraction (f_u)

The PEO-*b*-PCL polymeric micellar formulation showed a significantly lower f_u for valspodar (5.59%) compared to the Cremophor EL formulation (14.85%) (Table 3.8).

Table 3.8 – Valspodar unbound fraction (f_u) in rat plasma

Formulation	f_u (%)
Cremophor EL/ethanol	14.85 ± 2.97
PEO-*b*-PCL	5.59 ± 1.12

Data are represented as mean ± SD (n = 3 – 4)

3.9. Pharmacokinetic interaction studies

Figure 3.11 illustrates the plasma concentration-time profile for DOX in the presence and absence of CyA formulations (Figure 3.11A), valspodar formulations (Figure 3.11B), and the drug-free vehicles (Figure 3.11 C). The pharmacokinetics of DOX was characterized by an AUC of 0.546 mg.h/L, a terminal $t_{1/2}$ of 2.84 h, and a total body CL of 9.58 L/h/kg. In the presence of Sandimmune®, there was more than a 250% (2.5-fold) increase in the AUC of DOX. This increase in AUC was due to an over 55% reduction ($p < 0.05$) in the CL of DOX caused by Sandimmune® co-administration. Further, although not significant ($p > 0.05$), the $t_{1/2}$ showed an increase by more than 170% compared to DOX alone. On the other hand, when DOX was co-administered with CyA in the polymeric micelles, the changes in the pharmacokinetic parameters of DOX were less intense. Specifically, there was around 170% increase in the AUC ($p < 0.05$), 40% reduction in CL ($p < 0.05$), and 165% increase in the $t_{1/2}$ ($p > 0.05$) (Table 3.9, Figure 3.12).

When valspodar in its standard formulation (Cremophor EL-based) was co-administered with DOX, the changes in the pharmacokinetics of DOX were comparable to those obtained from co-administration with Sandimmune®. Specifically, a 47% decrease ($p < 0.05$) in CL and an increase ($p < 0.05$) in the AUC and $t_{1/2}$ by 214% and 210%, respectively. In contrast, valspodar in the polymeric micellar formulation did not significantly ($p > 0.05$) alter any of the pharmacokinetic parameters of DOX, as indicated by comparable values, for AUC, $t_{1/2}$, and CL (Table 3.9, Figure 3.12).

To study whether the drug-free vehicles, namely, Cremophor EL/ethanol and unloaded PEO-*b*-PCL polymeric micelles would have any impact on DOX pharmacokinetics, these vehicles were administered to the animals at an equivalent dose to 10 mg/kg CyA. The unloaded PEO-*b*-PCL polymeric micelles did not seem to have any influence on the pharmacokinetic parameters of DOX, as indicated by comparable values, for AUC, $t_{1/2}$, and CL ($p > 0.05$) (Table 3.9, Figure 3.12). However, administration of Cremophor EL/ethanol vehicle caused a 25% decrease ($p < 0.05$) in the DOX CL. Furthermore, there were concomitant increase (although not significant; $p > 0.05$) in the AUC and $t_{1/2}$ by 33 and 53%, respectively (Table 3.9, Figure 3.12).

Doxorubicinol (DOXol), the primary metabolite of DOX, was below detection limits in the plasma for all the groups under study.

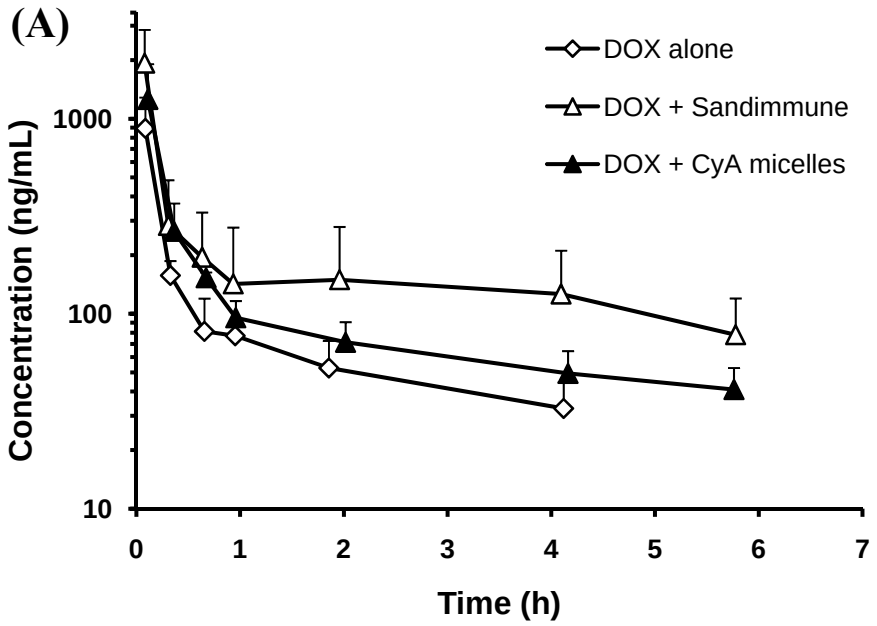
(A)
DOX alone
DOX + Sandimmune
DOX + CyA micelles
Concentration (ng/mL)
1000
100
10
0
1
2
3
4
5
6
7
Time (h)

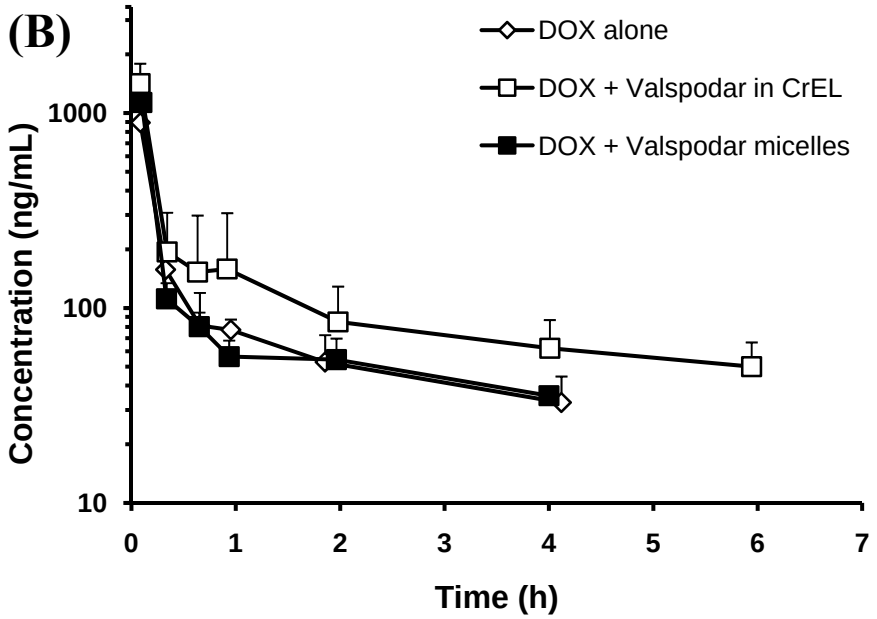
(B)
DOX alone
DOX + Valspodar in CrEL
DOX + Valspodar micelles
Concentration (ng/mL)
1000
100
10
0
1
2
3
4
5
6
7
Time (h)

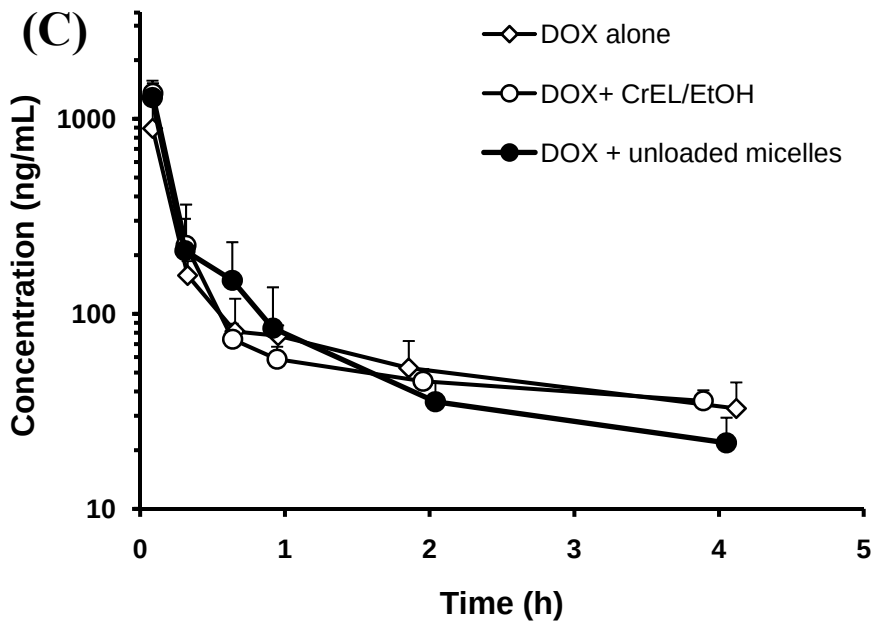

Figure 3.11 – Plasma concentration versus time profiles of DOX (5 mg/kg) in rat, either alone or 30 following a single i.v. administration of (A) CyA (10 mg/kg) either as Sandimmune® or in the polymeric micellar formulation, (B) valspodar (10 mg/kg) either in the standard Cremophor EL/ethanol (CrEL/EtOH) formulation or in the polymeric micellar formulation, or (C) equivalent dose of the vehicles (CrEL/EtOH; unloaded PEO-*b*-PCL micelles. Each data point represents the mean ± SD (n = 6 rats/group).

Table 3.9 – Plasma pharmacokinetic parameters (mean ± SD, n = 6 rats/group) of DOX after a single i.v. dose of 5 mg/kg alone or 30 min following a single i.v. administration of valspodar (10 mg/kg) or CyA (10 mg/kg), or equivalent dose of their vehicles

Parameter	**DOX alone**	**DOX + CrEL/EtOH**	**DOX + Unloaded micelles**	**DOX + Sandimmune®**	**DOX + CyA PEO-*b*-PCL micelles**	**DOX + Valspodar CrEL\EtOH**	**DOX + Valspodar PEO-*b*-PCL micelles**
$AUC_{0\text{-}4h}$ (mg.h/L)	0.398 ± 0.06	0.506 ± 0.09	0.487 ± 0.07	0.824 ± 0.48	0.606 ± 0.17	0.667 ± 0.25	0.461 ± 0.07
$AUC_{0\text{-}\infty}$ (mg.h/L)	0.546 ± 0.12	0.728 ± 0.14	0.553 ± 0.07	1.394 ± 0.66	0.942 ± 0.24	1.170 ± 0.32	0.653 ± 0.15
$t_{1/2}$ (h)	2.84 ± 1.04	4.35 ± 0.32	1.93 ± 0.82	5.07 ± 1.63	4.74 ± 1.52	5.98 ± 1.32	4.09 ± 1.22
CL (L/h/kg)	9.58 ± 2.33	7.15 ± 1.78	9.19 ± 1.26	4.28 ± 1.84	5.55 ± 1.16	4.50 ± 0.99	8.05 ± 2.03

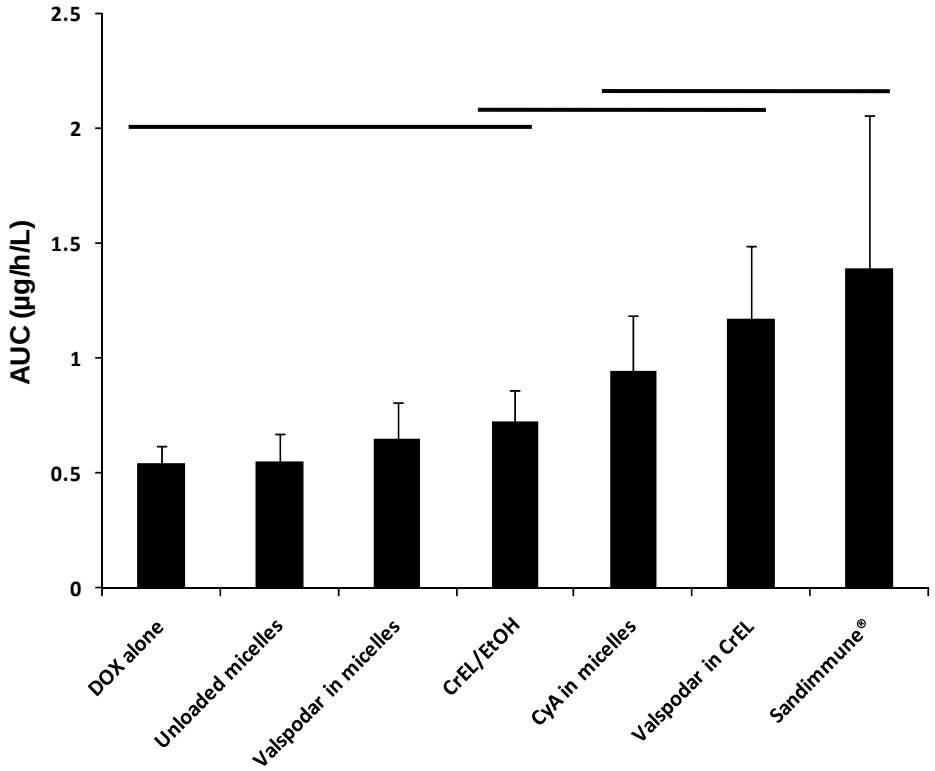
AUC (µg/h/L)
2.5
2
1.5
1
0.5
0
DOX alone
Unloaded micelles
Valspodar in micelles
CrEL/EtOH
CyA in micelles
Valspodar in CrEL
Sandimmune®

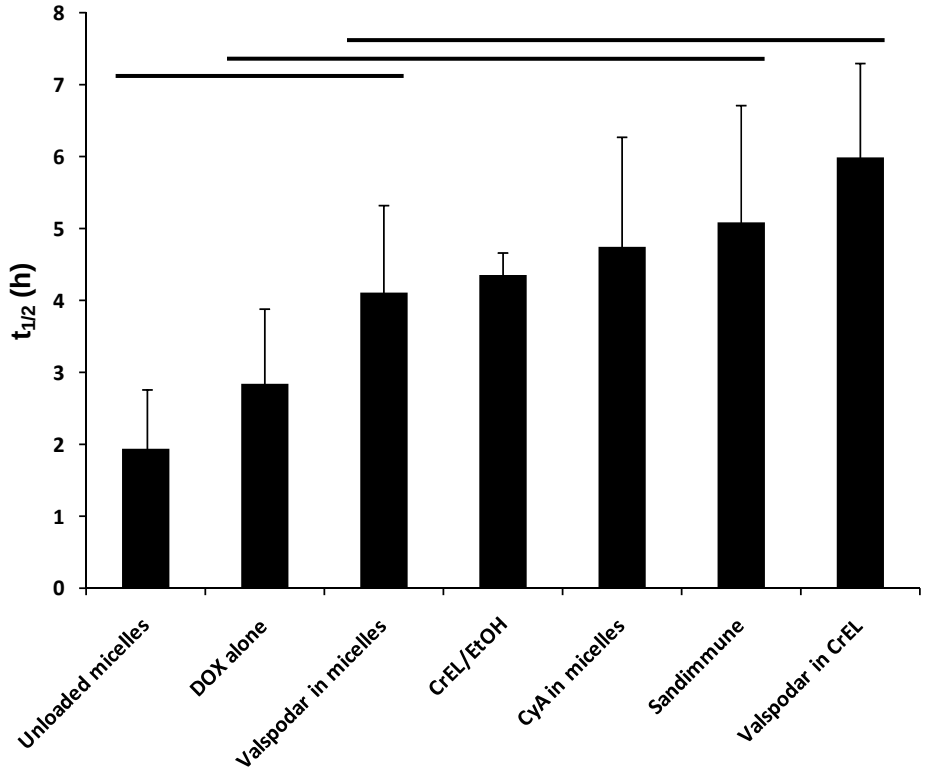
$t_{1/2}$ (h)
8
7
6
5
4
3
2
1
0
Unloaded micelles
DOX alone
Valspodar in micelles
CrEL/EtOH
CyA in micelles
Sandimmune
Valspodar in CrEL

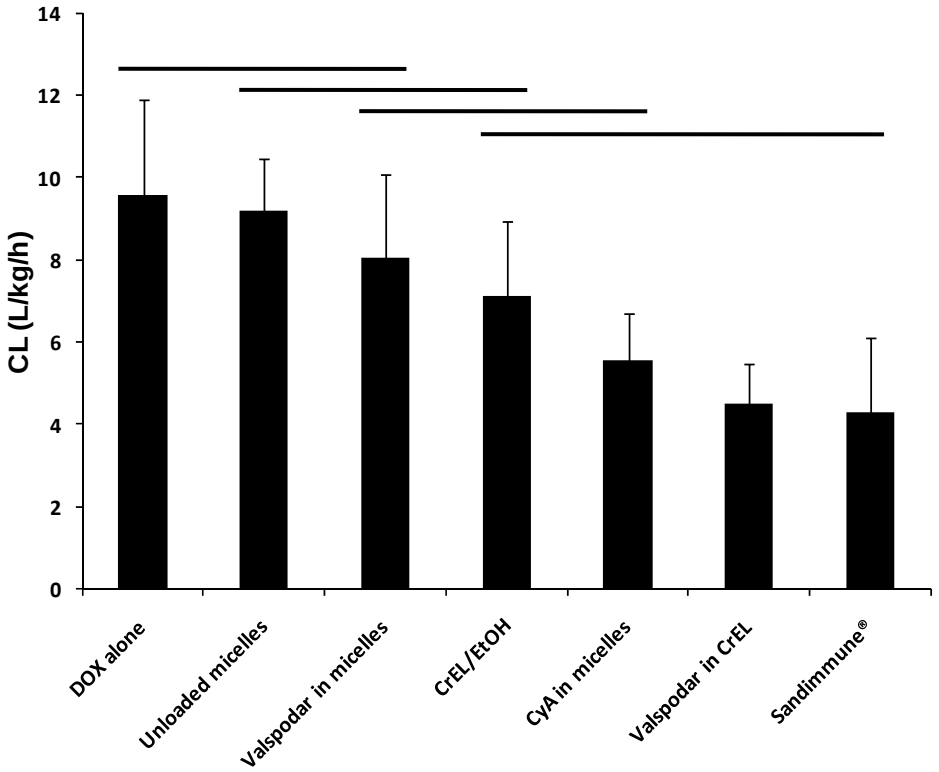

Figure 3.12 – Statistical ranking of different pharmacokinetic parameters of DOX in each group. For each parameter the data are ranked from lowest value to highest. Continuous lines over the data bars indicate lack of significance between groups encompassed by the lines; groups not encompassed within lines are significantly different from those encompassed by the lines (one way ANOVA followed by Bonferroni test, $p < 0.05$). Each bar represents the mean ± SD for the group.

CHAPTER FOUR

DISCUSSION, CONCLUSIONS & FUTURE DIRECTIONS

4.1. Discussion

4.1.1. Valspodar LC/MS assay

Quantitative analysis of valspodar in blood or plasma is usually accomplished through analytical methods based on either RIA (181, 182, 352, 353) or HPLC (354-357). Some of the RIA kits are known to lack specificity toward CyA metabolites especially the major monohydroxylated metabolite (AM9) that also occurs in valspodar metabolism (M9) (358). Therefore, application of the RIA assay methods would likely lead to an over-estimation of valspodar concentrations in blood or plasma. Besides cost, several steps involved in sample preparation and more importantly, the safety issues are among several limitations associated with the use of the RIA methods in general (181, 182). Although HPLC analysis methods do not have the limitations of RIA, most of the reported HPLC assays for valspodar have failed to produce a single peak. This has resulted in a relatively low sensitivity for valspodar analysis by HPLC (354, 356). van Tellingen *et al.* reported that the poor peak shapes and double peaks markedly reduces the sensitivity of the assay, and they had relatively good chromatographic performance only when columns with NovaPak® Phenyl packing material were used (356). The presence of two peaks was attributed to the existence of valspodar keto-enol tautomerism (Figure 3.1 A) (354). Another disadvantage associated with the use of HPLC assays for valspodar is the relatively long analytical run times (valspodar retention time ≥ 15 min).

Generally, when HPLC analysis is conducted using an ordinary detector such as a UV absorbance detector, only retention time information can be considered reliable, which could in some instances be misleading. Typical examples of this would be variations in peak retention time due to faulty preparation of the mobile phase, or peak misidentification due to unanticipated elution of impurities. Therefore, correct quantitation cannot be obtained if the peak of interest is misidentified. One way to address this issue is to use a mass spectrometer (MS) as an HPLC detector. The greatest advantage of using an MS as an HPLC detector is that mass information for each peak can easily be obtained at the same time as the respective retention times. The availability of such mass information provides a powerful means of reducing the possibility of peak misidentification and elution of unanticipated impurities inherent in HPLC analysis. It also allows for better quantitation in the case of overlapping peaks. Therefore, LC/MS is very commonly used in pharmacokinetic studies due to the high sensitivity and exceptional specificity provided by MS detection compared to UV, and the short analysis time.

The mass spectra of valspodar and IS dissolved in methanol with 0.2% ammonium hydroxide are shown in Figure 3.2 A and B, respectively. Valspodar and IS peaks were well separated with retention times of approximately 2.4 and 3.1 min, respectively. A linear relationship between the peak height ratios and rat plasma concentrations of valspodar was observed within the range of 10-5000 ng/mL ($R^2 > 0.99$).

The assay CV% for both intraday and interday assessments were less than 15% except for the lowest concentration used in the calibration and validation samples (10 ng/mL), where the values were between 15-19%. Mean error was less than 10% in all the concentrations above 10 ng/mL (Table 3.1). The low variability in the validation data demonstrated the accuracy and reproducibility of the developed method. The LOQ is the lowest amount of an analyte in a sample that can be quantitatively determined with suitable precision and accuracy (394). Based on the validation data, the LOQ was set at 10 ng/mL; and with an injection volume of 10 μL, the value translates into an on-column amount of 0.1 ng. The LOD is the lowest concentration of an analyte that the bioanalytical procedure can reliably differentiate from background noise (394). The LOD of this method was found to be 2.5 ng/mL and based on an injection volume of 10 μL, the corresponding amount injected to the system was 0.025 ng (i.e. 25 pg).

Previous studies have shown LOQ values in the range of 37.5-75 ng/mL and 50-100 ng/mL for RIA and HPLC methods of valspodar analysis, respectively (182, 355-357). The lower level of LOQ for the LC/MS method is an indication for the higher sensitivity of this method compared to the reported RIA and HPLC methods for valspodar quantification. However, the validation of the developed method refers to an individual instrument; this applies in principle for all LC/MS methods. The need for close quality control in further analytical series should be noted.

4.1.2. Development of block copolymeric based nanocarriers of vaslpodar

4.1.2.1. The PEO-*b*-PCL formulation

The synthesis of PEO-*b*-PCL has been previously optimized in our lab in terms of time, temperature and catalyst concentration (263). Additionally, different PEO-*b*-PCL block copolymers with different molecular weights have been synthesized and fully characterized (263, 393). Moreover, CyA, the structural analog of valspodar, has been encapsulated into micelles prepared from these different PEO-*b*-PCL block copolymers. Micelles prepared from PEO_{5000}-b-PCL_{13000} (PEO_{114}-*b*-PCL_{114}) have been found to be the optimum carrier for CyA in terms of drug loading (3.42 *mol/mol*) (263, 393). Likewise, when a pilot study (n = 1) was conducted using different PEO-*b*-PCL with different molecular weights, results have shown that nanocarriers formed from PEO_{114}-*b*-PCL_{114} were associated with the highest drug loading for valspodar (4.16 *mol/mol*). Therefore, PEO_{114}-*b*-PCL_{114} block copolymer was selected for the current research project. The block copolymer of PEO_{114}-*b*-PCL_{114} was synthesized and the molecular weight of PCL segment (using ^{1}H NMR) was found to be 12,880 g/mol, which is very close to the targeted molecular weight of 13,000 g/mol and to the one previously synthesized in our lab (263, 393).

Through a co-solvent evaporation method, identical to the one used for CyA (374, 381), valspodar was encapsulated in PEO-*b*-PCL micelles effectively. It achieved high drug loading levels (4.16 *mol/mol*) and very efficient

encapsulation (93.6%) in PEO-*b*-PCL micelles (Table 3.4). This loading was superior to what was reported for CyA encapsulation in PEO-*b*-PCL micelles using an identical method (3.42 *mol/mol* CyA loading content and 75.9% encapsulation efficiency) (340, 342). The average diameter of valspodar-loaded PEO-*b*-PCL micelles was 62 nm, which is smaller than the size reported for CyA-loaded micelles (89 nm) (340, 342).

4.1.2.2. The PEO-*b*-PBCL formulation

Our research group has previously reported on the synthesis and characterization of the novel family of self-associating PEO-*b*-PCL based block copolymers carrying pendent benzyl groups on the polyester block (PEO-*b*-PBCL) (244). To test the potential of PEO-*b*-PBCL and their assembled nanostructures as efficient carriers for valspodar, three block copolymers with different molecular weight of the PBCL were synthesized and characterized. The PBCL block molecular weights were 8, 16, and 25 kg/mol as determined by ^{1}H NMR corresponding to average degrees of polymerization of 30, 60 and 95, respectively. The PEO-*b*-PBCL formulations of valsopodar were hypothesized to be more stable *in vivo* due to their lower CMC compared to PEO-*b*-PCL nanocarriers. Since the assembled nanostructures prepared from large molecular weight PEO-*b*-PBCL has not been characterized before, the CAC, the viscosity of the hydrophobic domain, and the morphology of the assembled structures were investigated. Also, the influence of f_{EO} on the morphology of nanostructures formed in water was investigated. Assembly of prepared block copolymers led to

the formation of nanostructures with average diameters of 104, 95.5, and 74.1 nm for PEO_{114}-*b*-$PBCL_{30}$, PEO_{114}-*b*-$PBCL_{60}$, and PEO_{114}-*b*-$PBCL_{95}$, respectively, as determined by DLS technique. The population of nanostructures prepared for all three block copolymers showed a narrow distribution (polydispersity $\leq$ 0.15). Interestingly, the size of the prepared nanostructures decreased with an increase in the chain length of PBCL. This observation was in contrast to observations on the effect of hydrophobic block length on the size of core/shell nanostructures formed from self assembly of block copolymers where an increase in the hydrophobic block molecular weight led to an increase in the size of nanoparticles (395, 396). The CAC of each block copolymer was determined by following changes in the fluorescence excitation spectra of pyrene in the presence of varied concentrations of block copolymers (384). The average CAC for PEO_{114}-*b*-$PBCL_{30}$, PEO_{114}-*b*-$PBCL_{60}$, and PEO_{114}-*b*-$PBCL_{95}$ was found to be 62, 41, and 23 *n*M, respectively (Table 2). For comparison, the CAC we reported recently for PEO_{114}-*b*-$PBCL_{19}$ was 98 *n*M (244). This trend was expected since it is known that increasing the length of the hydrophobic segment of the block copolymer is usually associated with an increased tendency for self assembly of amphiphilic block copolymers reflected by a lower CAC.

The rigidity of the hydrophobic domain in the prepared nanostructures was estimated by measuring excimer to monomer intensity ratio (I_e/I_m) from the emission spectra of 1,3-(1,1′-dipyrenyl) propane at 373 and 480 nm, respectively. Low I_e/I_m intensity ratio in the emission spectrum of the dipyrene probe is an

indication of a high viscosity (rigidity) of the hydrophobic domain. Increasing the chain length of the hydrophobic block is usually associated with higher rigidity (lower I_e/I_m value) of the core in core/shell type nano-structures (263, 385). Interestingly, I_e/I_m intensity ratios did not decrease as the chain length of PBCL increased. Instead, the polymer with the longest PBCL chain showed the highest I_e/I_m ratios among the three block copolymers reflecting the lowest microviscosity (Table 3.3). The increase in the rigidity of the hydrophobic domain is usually associated with slow dissociation of nanostructures and controlled release of the drugs associated with this domain (397).

Amphiphilic block copolymers can self-assemble into different nanostructures with various morphologies (398-400). The size and morphology of the self-assembled structures may depend on parameters such as the nature and composition of the block copolymers, copolymer concentration, preparation method, type of organic solvent, temperature, pH, and additives such as salts, ions, and homopolymer (398, 399, 401, 402). The weight fraction of the hydrophilic block (f_{EO}) in the block copolymer structure, however, is believed to be the major determinant of the morphology of the self-assembled structures (401-404). For instance, Discher et al. have reported self assembly of poly(ethylene oxide)-*b*-poly(butadiene) (PEO-*b*-PBD) or PEO-*b*-poly(ethylethylene) (PEO-*b*-PEE) copolymers, at f_{EO} of 20% to 42%, into fluid-like bilayer-forming vesicles (405, 406). Zupancich et al. who studied the dependence of the morphology of the self-assembled structures of PEO-*b*-poly(γ-

methyl-ε-caprolactone) (PEO-*b*-PMCL) on f_{EO}, reported a continuous evolution of morphologies (404). When block copolymers with f_{EO} values ranging from 0.17 to 0.43 were used, a transition from vesicles to cylinders to spheres was observed as the f_{EO} was raised.

The morphology of the assembled structures in the present study was characterized by TEM. The TEM image of PEO_{114}-*b*-$PBCL_{30}$ shows the formation of spherical micelles with high polydispersity and an average diameter of 60.7 nm (Figure 3.7A). An increase in the molecular weight of PBCL, and subsequent drop in f_{EO} from 0.40 to 0.25, resulted in a mixed population of spherical micelles and vesicles with average diameters of 42.6 and 77.0 nm, respectively (Figures 3.7B and C). A further increase in PBCL block length leading to the preparation of block copolymers with f_{EO} of 0.18, also resulted in the formation of a mixed population of micelles and vesicles with average diameters of 55.8 and 57.4 nm, respectively (Figures 3.7D and E). Our findings are similar to what has previously been reported on the morphology of PEO-*b*-poly(γ-methyl-ε-caprolactone) nanostructures (404). In that study, spherical micelles were evident at f_{EO} = 0.43, whereas the vesicles were observed at f_{EO} = 0.17-0.28. A lower rigidity of the hydrophobic domain in nanostructures formed from the assembly of PEO_{114}-*b*-$PBCL_{60}$ (f_{EO} = 0.25) and PEO_{114}-*b*-$PBCL_{95}$ (f_{EO} = 0.18) in comparison to PEO_{114}-*b*-$PBCL_{30}$ (f_{EO} = 0.40) was observed. As the former two polymers formed a mixed population of spherical micelles and vesicles upon self assembly rather than pure micellar morphology, it appears that

the rigidity of the hydrophobic domain is lower in the vesicular structures. The transition among different morphologies occurs to minimize the free energy in the system and to provide the optimum thermodynamic equilibrium (401, 402). Moreover, polydispersity of the constituent block copolymer molecules from which the assembled structures are comprised may also contribute to the presence of mixed morphologies (402, 404).

Valspodar drug loading levels were 2.1, 2.3, and 4.0 *mol/mol* for PEO_{114}-*b*-$PBCL_{30}$, PEO_{114}-*b*-$PBCL_{60}$, and PEO_{114}-*b*-$PBCL_{95}$, respectively, which correspond to encapsulation efficiencies of 67.6, 47.3, and 56.8%, respectively. The average diameters of valspodar-loaded nanocarriers were 97, 107, and 94 nm, respectively. While the size of PEO_{114}-*b*-$PBCL_{30}$ and PEO_{114}-*b*-$PBCL_{60}$ did not change significantly after drug loading, it significantly increased when valspodar was loaded to PEO_{114}-*b*-$PBCL_{95}$ nanocarriers. This is likely because PEO_{114}-*b*-$PBCL_{95}$ was associated with the highest *mol/mol* drug loading compared to PEO_{114}-*b*-$PBCL_{30}$ and PEO_{114}-*b*- $PBCL_{60}$. Although the nanocarriers of PEO-*b*-PCL have shown a better drug loading compared to PEO-*b*-PBCL, it is worthwhile to investigate the pharmacokinetics of valspodar-loaded PEO-*b*-PBCL and compare it to that of PEO-*b*-PCL to shed the light on the stablility of those formulations *in vivo*.

4.1.2.3. Pharmacokinetics of valspodar-loaded PEO-*b*-PCL and PEO-*b*-PBCL nanocarriers following i.v. administration

In previous studies, Aliabadi et al. have been exploring the potential of PEO-*b*-PCL micelles as vehicles for the solubilization and controlled delivery of CyA as a model P-gp inhibitor (339, 340). The results showed that PEO-*b*-PCL micelles were not only able to solubilize CyA at clinically relevant concentrations but favorably change the plasma protein binding, pharmacokinetic and biodistribution profile of CyA after a single i.v. dose to rats keeping the incorporated CyA mainly in blood circulation and away from sites of CyA toxicity, i.e., kidneys (341, 342). This has led to a reduction in the nephrotoxic side effects of CyA upon multiple dosing of its polymeric micellar formulation compared to the Cremophor EL formulation.

Through a co-solvent evaporation method, identical to the one used for CyA, valspodar was encapsulated in PEO-*b*-PCL micelles effectively. A high level of drug loading was achieved (4.16 mol drug/mol polymer) leading to an aqueous solubility of nearly 2.8 mg/mL. This loading level was significantly higher than the one achieved with CyA at the optimum conditions (3.42 mol drug/mol polymer; aqueous solubility ~ 2.3 mg/mL) (Table 1) (340, 342). This was not surprising since valspodar is a more hydrophobic derivative of CyA and therefore it is perhaps more compatible with the hydrophobic micellar core (PCL). Based on a better compatibility between valspodar and PCL, valspodar was

expected to remain associated with the PEO-*b*-PCL micelles to a higher extent, as well.

Although the PEO-*b*-PCL micellar formulation was able to solubilize more valspodar (compared to CyA) and decrease the f_u of valspodar by ~ 62% compared to the control formulation (Table 3.8), it was unexpectedly less effective in changing the pharmacokinetics of valspodar from what observed for the Cremophor EL formulation. To facilitate the comparison between valspodar and CyA data, valspodar blood AUC, CL, and Vd_{ss} were estimated from its corresponding plasma values by using the blood to plasma ratio data. Following a single i.v. dose of 5 mg/kg to rats, PEO-*b*-PCL polymeric micelles provided ~ 67% higher blood AUC compared to the Cremophor EL formulation (9.5 versus 5.7 mg·h/L, respectively). The blood CL and Vd_{ss} of valspodar were 0.89 L/h/kg and 11.2 L/kg for Cremophor EL, and 0.62 L/h/kg and 6.2 L/kg for PEO-*b*-PCL micelles, respectively, representing reduction of blood CL and Vd_{ss} by 30 and 45%, respectively. However, it has previously been demonstrated that PEO-*b*-PCL micelles were able to change the pharmacokinetics of the encapsulated CyA to a higher extent showing a 90% decrease in blood CL and Vd_{ss} of polymeric micellar CyA in comparison to CyA in Cremophor EL (Sandimmune® formulation) (342). Moreover, the blood AUC of CyA in Sandimmune® was only 12% of the AUC encompassed with the polymeric micellar formulation.

Assuming that the pathway of valspodar elimination is mostly hepatic (168, 364), the hepatic extraction ratio (*E*) for valspodar was found to be nearly

30% lower in the polymeric micellar formulation compared to the Cremophor EL preparation. Since valspodar is a low *E* drug ($E < 0.3$), its clearance is expected to be proportional to the product of the intrinsic clearance of unbound drug and the f_u. Therefore, the lower *E* in the polymeric micellar formulation can be largely attributed to the lower f_u, since it is about 45% lower than the control formulation. Nevertheless, we showed that after i.v. doses, PEO-*b*-PCL micelles were able to significantly lower the clearance and volume of distribution of valspodar and increase the AUC of valspodar in plasma compared to the Cremophor EL formulation.

We have then examined the pharmacokinetics of valspodar as part of PEO-*b*-PBCL formulations. Figure 3.9 shows the concentration-time profile of valspodar in the PEO-*b*-PBCL polymeric micellar formulations in plasma following an i.v. dose of 5 mg/kg in rats. In the 24-h profile for all the formulations there were rapid declines in plasma concentrations in the first two hours after dosing, representing an initial distribution phase. This was followed by an elimination phase with an average $t_{1/2}$ ranging from 9-14 h. Although characterization studies confirmed formation of a population consisting of polymeric vesicles for PEO_{114}-*b*-$PBCL_{60}$ and PEO_{114}-*b*-$PBCL_{95}$, no significant difference in the pharmacokinetic parameters of valspodar in these formulations compared to PEO_{114}-*b*-$PBCL_{30}$, that has presumably only formed micelles, was observed (Table 3.6). This might be attributed to one of these possibilities: (1) the drug is only loaded in the micelle population, (2) the drug loading has influenced

the morphology of the carrier, or (3) the micelles and vesicles were releasing the drug at a similar rate.

The pharmacokinetics of valspodar in PEO-*b*-PBCL formulations has been changed in a manner similar to that of PEO-*b*-PCL. Specifically, PEO-*b*-PBCL formulations provided higher plasma AUC (nearly double) compared to the Cremophor EL formulation. This increase in the AUC was a consequence of the 50% reduction in the CL of valspodar in the PEO-*b*-PBCL formulations. Moreover, the Vd_{ss} of valspodar was reduced in the PEO_{114}-*b*-$PBCL_{30}$, PEO_{114}-*b*-$PBCL_{60}$, and PEO_{114}-*b*-$PBCL_{95}$ by approximately 70 and 62, and 40%, respectively compared to the Cremophor EL formulation. The pharmacokinetic parameters of valspodar in the PEO-*b*-PBCL formulations were comparable to those obtained with PEO_{114}-*b*-PCL_{114} formulation ($p > 0.05$). Therefore, PEO_{114}-*b*-PCL_{114} formulation was used for the pharmacokinetic interaction studies since it provided the highest valspodar encapsulation efficiency (i.e. highest valspodar solubility) compared to the other formulations.

4.1.2.4. Pharmacokinetics of valspodar-loaded PEO-*b*-PCL nanocarriers following oral administration

The potential use of polymeric micelles as oral drug delivery systems has not been widely demonstrated *in vivo*. For instance, Préat and coworkers have investigated the potential of polymeric micelles based on methoxypoly(ethylene

glycol)-poly(ε-caprolactone/trimethylene carbonate) [PEG-p(CL-co-TMC)] for oral administration utilizing risperidone as a model drug (407, 408). They showed that PEG-p(CL-co-TMC) was able to form micelles and reach a bioavailability of 40%, while the absolute bioavailability of drug (risperisdone) was 19% in rats. Moreover, the mechanistic studies suggest that the drug-loaded micelles were absorbed by pinocytosis, whereas the polymeric unimers diffused passively across the membrane concomitantly with micellar endocytosis (409). Furthermore, Pierri and Avgoustakis have studied the *in vitro* degradation and drug-release properties of poly(ethylene glycol)-poly(lactide) (PEG-PLA) micelles using griseofulvin as a model drug (410). They demonstrated that PEG-PLA micelles were stable and exhibited sustained release properties in PBS (pH = 7.4) as well as in simulated gastric (pH = 1.2) and intestinal fluids (pH = 7.5). In this project, we investigated the pharmacokinetics of valspodar-loaded micelles and compared it to the standard Cremophor EL formulation following a single oral dose of 10 mg/kg to rats.

The median t_{max} of valspodar was similar in the formulations (~ 2 h). Likewise, the C_{max} did not differ significantly between the two formulations (Table 3.7). The absolute F% calculated for valspodar in the polymeric micellar formulation (28.9%) was lower than the Cremophor EL formulation (42.3%). This is clearly due to the significantly higher AUC obtained for the i.v. micellar formulation compared to the control formulation (19.4 versus 11.0 mg.h/L), as the relative F% was ~ 120%. The f_g, however, was ~ 47% lower in the polymeric

micellar formulation. It is possible that the lower f_g is due to a lower absorption, suggesting that the polymeric micellar formulation somehow restricts the drug to the confines of the gastrointestinal fluids. The mechanisms involved in micellar transport across intestinal mucosa are not well defined but several studies suggest that cellular uptake of intact polymeric micelles is through fluid-phase endocytosis (pinocytosis) (411-413). In this study, however, it is not known whether the drug-loaded polymeric micelles were stable in the gastrointestinal fluids, and whether the micelles were able to pass the intestinal barrier (as intact micelles) or not. Further studies need to be performed to investigate the route and extent of polymeric micellar absorption from the gastrointestinal tract.

4.1.3. Pharmacokinetic interaction study

Valspodar has been shown to be a potent chemosensitizing agent for a wide variety of cells overexpressing P-gp. Upon *in vivo* administration, valspodar itself is non-toxic at typical MDR-reversing concentrations. However, studies have demonstrated that it increases the toxicity of free DOX in normal mice (414). Valspodar-mediated increases in toxicity have been correlated with alterations in anticancer drug pharmacokinetics and are presumably a consequence of increased anticancer drug accumulation to susceptible target organs (415). This is consistent with the clinical observations, in which valspodar and CyA have been shown to decrease the clearance of free DOX, paclitaxel, and etoposide in Phase I and Phase II trials, which resulted in increased toxic side effects and a need to decrease the anticancer drug dose.

Cyclosporine derivatives including CyA and valspodar are mainly metabolized by human CYP3A enzymes (168, 185). In contrast, metabolism through CYP3A enzymes, if involved, is not a major elimination pathway for DOX (177, 416). Therefore, the observed increases in DOX exposure and reduced CL in the presence of valspodar or CyA cannot be explained solely by a reduction in DOX metabolism by these agents. In humans, biliary excretion is a major route of DOX elimination, where it appears in bile within 5 min after an i.v. bolus administration (417, 418). Moreover, more than 40% of the injected drug is recovered in bile compared with 14% in urine (418). Similar relationships between total biliary and urinary excretion have been observed in preclinical models (419, 420). Therefore, changes in tissue distribution and reduced transport into the bile (179, 414, 421) could explain the increased exposure and reduced CL observed in the preclinical studies and clinical trials. In fact, both CyA and valspodar have been shown to block biliary and renal excretion of anticancer agents, including DOX (179, 422, 423). Moreover, these inhibitory effects have been shown to be dose-dependent.

Krishna and Mayer have shown previously that encapsulation of DOX PEGylated liposomes (Doxil®) can reduce the drug-drug interactions with valspodar, thereby avoiding the anticancer drug dose reductions typically associated with this combination therapy. In addition, combining valspodar with liposomal DOX led to significant improvements in antitumor activity compared

with that achievable with non-encapsulated DOX and valspodar (231, 415). Later, Krishna et al. have evaluated the DOX renal and biliary clearance following i.v. administration of non-encapsulated and liposome-entrapped DOX in a rat model, both in the presence and absence of orally administered valspodar. Significant differences in the renal and biliary handling of DOX arising from administration of non-encapsulated and liposomal DOX formulations were observed. While administration of valspodar with free DOX caused significant reductions in DOX plasma, renal, and biliary clearance, the reductions were very modest for the liposomal formulation of DOX. Krishna et al. have concluded that liposomal delivery of DOX to the liver appears to result in much lower DOX and DOX metabolite exposure over extended periods of time, such that even under conditions of valspodar mediated inhibition of P-gp, the renal and biliary excretion capacity is sufficient to handle the levels exposed to these tissues.

Since chemotherapy protocols usually involve combination therapy, one could argue that if using liposomal DOX would help avoid the drug interactions with CyA or valspodar, then what about the other anticancer agents (P-gp and/or CYP 3A substrates) in the chemotherapy regimen that do not have alternative delivery systems such as Doxil®? Therefore, encapsulation of the P-gp inhibitor inside a delivery system can serve as an alternative approach to avoid the pharmacokinetic interactions with the conventional formulations of anticancer agents.

We hypothesized that encapsulation of valspodar by polymeric nanocarriers can reduce the adverse pharmacokinetic interaction of this drug with DOX upon intravenous co-administration. Indeed, when valspodar was encapsulated inside PEO-*b*-PCL nanocarriers, it did not cause any significant changes on DOX pharmacokinetic parameters upon i.v. co-administration. This is in contrast to valspodar in the Cremophor EL/ethanol formulation, where it caused around 50% reduction in the CL of DOX ($p < 0.05$), which consequently resulted in more than double the AUC and the $t_{1/2}$ ($p < 0.05$). This is despite the fact that valspodar in the micellar formulation was associated with higher plasma concentrations compared to the Cremophor EL/ethanol formulation (Figure 3.8, Table 3.5). Although a similar scenario was seen with CyA, the encapsulation inside the nanocarriers was not able to completely prevent the drug interactions with DOX. Nonetheless, CyA-loaded nanocarriers seemed to have less influence on the pharmacokinetics of DOX compared to the CyA commercially available formulation, Sandimmune®. Specifically, Sandimmune® caused more than 55% reduction in the CL that resulted in more than 250% incease in the AUC of DOX, whereas CyA-loaded nanocarriers showed a 40% reduction in the CL and 170% increase in the AUC. Although these changes were statistically significant when compared to "DOX alone" group, the differences between "DOX *plus* Sandimmune®" and "DOX *plus* CyA nanocarriers" were not statistically significant. This is consistent with the results from biodistribution studies of CyA using the same animal model, since the mean AUC of CyA in polymeric micelles was around 32% lower in liver compared to Sandimmune® (373). Although the

difference was not statistically significant, it might indicate that encapsulation of CyA in PEO-*b*-PCL micelles has reduced its uptake by liver (373).

The reason why the nanocarrier formulation of valspodar, but not CyA, was able to circumvent free drug-DOX interaction is not known. In order to find out the reason behind that, it should be noted that a significant fraction of DOX (~ 30% of dose) is excreted unchanged in the bile and it is reported that P-gp is significantly contributing in this exretion process, but it is not the only transporter involved in this process (424, 425). Several studies have shown that MRP, especially MRP-2, is a major contributor in the biliary excretion of several drugs (substrates) including DOX (425, 426). It has also been reported that CyA is a broad spectrum MDR inhibitor (375), because of its capability of blocking transporters other than P-gp, including MRP, BCRP and LRP. This is in contrast to valspodar which is known to be a more specific P-gp inhibitor (185, 375). Therefore, this may, at least in part, explain why valspodar-loaded nanocarriers, but not CyA-loaded nanocarriers, were able to prevent the pharmacokinetic interaction with DOX.

It has been demonstrated that Cremophor EL can profoundly alter the plasma pharmacokinetics of doxorubicin and etoposide, in animals as well as in humans (376-378). Since Sandimmune® and the clinical formulation of valspodar for i.v. administration also contain substantial amounts of Cremophor EL, it can be postulated that pharmacokinetic interactions with these P-gp inhibitors (184,

353) is at least partially attributed to the use of this vehicle. Indeed, the findings of the current study suggest that Cremophor EL seems to have an impact on the DOX pharmacokinetics. Specifically, upon co-administration with Cremophor EL, the CL of DOX was reduced by 25%. There was also a 33% increase in AUC and 53% increase in the $t_{1/2}$. Although these parameters were not significantly different from those obtained with "DOX alone" group, the values still indicate that Cremophor EL might have an impact on the pharmacokinetics of DOX. This is in contrast to the drug-free PEO-*b*-PCL nanocarriers, which did not seem to have any impact on the DOX pharmacokinetics (Table 3.10).

4.2. Conclusions

In this study, an LC/MS assay method was developed and validated for the quantification of valspodar in rat plasma. The intra- and interday variability (% coefficient of variation) ranged from 2.5% to 18.3% and 5.5% to 17.2%, respectively. The assay quantification limit was 10 ng/mL. The developed method was used for the quantification of valspodar in all biological samples used in the pharmacokinetic studies.

We showed that polymeric nanocarriers of PEO-*b*-PCL and PEO-*b*-PBCL were able to efficiently encapsulate valspodar by a co-solvent evaporation method to achieve a maximum aqueous solubility of 2.8 mg/mL, which is clinically relevant.

The self assembly of PEO-*b*-PBCL at $f_{EO} \leq 0.25$ showed a formation of polymeric vesicles as well as micelles, while those with f_{EO} of 0.40 assembled only to polymeric micelles. Moreover, despite an increase in the molecular weight of block copolymers, PEO-*b*-PBCL block copolymers with $f_{EO} \leq 0.25$ (PEO_{114}-*b*-$PBCL_{60}$ and PEO_{114}-*b*-$PBCL_{95}$) formed smaller particles and showed lower rigidity in their hydrophobic domain compared to those formed from PEO-*b*-PBCL block copolymers with f_{EO} of 0.40 (PEO_{114}-*b*-$PBCL_{30}$). As the former two polymers formed a mixed population of spherical micelles and vesicles upon self assembly rather than pure micellar morphology, it appears that the rigidity of the hydrophobic domain is lower in the vesicular structures.

In this study, we showed that after intravenous doses, PEO-*b*-PCL nanocarriers were able to significantly lower the clearance and volume of distribution of valspodar compared to the Cremophor EL/ethanol formulation. Moreover, following oral administration, the AUC of valspodar in the polymeric micellar formulation was similar to the Cremophor EL formulation. However, PEO-*b*-PCL formulation did not substantially impact the AUC and other pharmacokinetic parameters. The replacement of Cremophor EL with the polymeric micellar formulation of valspodar is not justified at this point, since both formulations have shown similar pharmacokinetics and it is known that Cremophor EL is well tolerated orally. Nevertheless, the results imply a potential

for PEO-*b*-PCL nanocarriers to possibly serve as a suitable vehicle for oral administration of hydrophobic drugs.

We have then examined the pharmacokinetics of valspodar as part of PEO-*b*-PBCL formulations. The pharmacokinetics of valspodar in PEO-*b*-PBCL formulations has been changed in a manner similar to that of PEO-*b*-PCL. Namely, significant reductions in the CL and Vd_{ss} and a significant increase in the AUC of valspodar, compared to the Cremophor EL/ethanol formulation.

In line with the findings of valspodar protein binding study, where encapsulation of valspodar inside the polymeric nanocarriers significantly reduced the f_u compared to the Cremophor EL/ethanol formulation, valspodar-loaded nanocarriers did not have any influence on DOX pharmacokinetics upon i.v. co-administration. This is in contrast to valspodar in its standard Cremophor EL/ethanol formulation, where it caused significant reduction in the CL as well as significant increase in the AUC and $t_{1/2}$ of DOX. To the best of our knowledge this is the first report on the impact of polymeric micellar formulations in reducing the pharmacokinetic interactions between the two co-administered drugs.

4.3. Future directions

The assembly of relatively large molecular weight PEO-*b*-PBCL was shown to form a mixture of polymeric micelles and polymeric vesicles. The use of other techniques such as cryogenic temperature TEM (cryo-TEM) and atomic force microscopy (AFM) would help confirm the results. Moreover, while TEM involves addition of negative stain (such as phosphotungstic acid) to improve the contrast followed by viewing the specimen after drying, in cryo-TEM the specimen is vitrified (thermally fixed) and then examined under the microscope without any additives. Therefore, cryo-TEM provides the advantage of viewing unaltered copolymer assemblies. Since there is a potential for production of vesicles from PEO-*b*-PBCL copolymers, different concentrations of the block copolymers and different methods of preparation should be investigated to optimize the conditions for production of pure vesicles. Moreover, studies on the influence of drug loading on the morphology of the PEO-*b*-PBCL nanocarriers could be a future direction for this project.

We showed that PEO-*b*-PCL and PEO-*b*-PBCL were able to change the pharmacokinetics of valspodar favorably following i.v. administration. Conduction of future biodistribution studies in tumor-bearing animals would give insights into the potential of polymeric nanocarrier formulations for changing the tissue distribution of the drug. It would show whether or not encapsulation of valspodar into the polymeric nancarriers increases the tumor accumulation of the drug and decreases its distribution to the normal tissues.

We showed that the pharmacokinetic parameters of valspodar-loaded PEO-*b*-PCL were comparable to valspodar in the Cremophor EL/ethanol formulation following oral administration. However, it is not known whether the drug-loaded polymeric nanocarriers were stable in the gastrointestinal fluids and whether the nanocarriers were able to pass the intestinal barrier (as intact nanocarrier) or not. Future studies to investigate the route and extent of PEO-*b*-PCL polymeric nanocarriers' absorption from the gastrointestinal tract are needed.

The developed valspodar-loaded nanocarrier formulations have a potential application as a tumor targeted P-gp inhibitor that may increase the efficacy while reducing the toxicity of anticancer drugs upon co-administration. We have shown that valspodar-loaded PEO-*b*-PCL formulation was able to prevent the pharmacokinetic interactions, and presumably the expected toxicity, with DOX. However, conduction of biodistribution, toxicity, and efficacy studies on DOX either in the commercially available formulation or the liposomal formulation in tumor-bearing animal models can clarify the effect of polymeric nanocarrier formulations on the overall therapeutic outcome of tumor targeted P-gp inhibitor in overcoming drug resistance. Moreover, conduction of pharmacokinetic interaction studies with other anticancer drugs that are substrates of P-gp and/or CYP3A such as paclitaxel and etoposide would help confirm the applicability of this approach (i.e. use of polymeric nanocarrier system) to prevent drug-drug interactions.

Stability of the micellar and vesicular structures is one of the challenges in the scale-up and commercialization of their formulations. Aggregation of nanocarriers and loss of the encapsulated drug have been reported with storage of the micellar solutions or after reconstitution of the freeze dried or frozen samples. In this project, all the nanocarrier formulations were prepared freshly just before the experiments to avoid these complications. Future studies on different stabilizing methods (such as lyophilization and spray-drying) and ingredients (such as lyoprotectants), and the assessment of stability of the formulations by periodic analysis of the nanocarrier characteristics could shed the light on proper strategies that would be useful for different nanocarrier formulations.

References

1. Ford JM, Hait WN. Pharmacology of drugs that alter multidrug resistance in cancer. Pharmacol Rev. 1990 Sep;42(3):155-99.
2. Chin KV, Pastan I, Gottesman MM. Function and regulation of the human multidrug resistance gene. Adv Cancer Res. 1993;60:157-80.
3. Hiddemann W, Kern W, Schoch C, Fonatsch C, Heinecke A, Wormann B, et al. Management of acute myeloid leukemia in elderly patients. J Clin Oncol. 1999 Nov;17(11):3569-76.
4. Jamroziak K, Robak T. Pharmacogenomics of MDR1/ABCB1 gene: the influence on risk and clinical outcome of haematological malignancies. Hematology. 2004 Apr;9(2):91-105.
5. Leighton JC, Jr., Goldstein LJ. P-glycoprotein in adult solid tumors. Expression and prognostic significance. Hematol Oncol Clin North Am. 1995 Apr;9(2):251-73.
6. Zhang D, Fan D. Multidrug resistance in gastric cancer: recent research advances and ongoing therapeutic challenges. Expert Rev Anticancer Ther. 2007 Oct;7(10):1369-78.
7. Nelson DA, Tan TT, Rabson AB, Anderson D, Degenhardt K, White E. Hypoxia and defective apoptosis drive genomic instability and tumorigenesis. Genes Dev. 2004 Sep 1;18(17):2095-107.
8. Brizel DM, Scully SP, Harrelson JM, Layfield LJ, Bean JM, Prosnitz LR, et al. Tumor oxygenation predicts for the likelihood of distant metastases in human soft tissue sarcoma. Cancer Res. 1996 Mar 1;56(5):941-3.
9. Brown JM. Tumor hypoxia, drug resistance, and metastases. J Natl Cancer Inst. 1990 Mar 7;82(5):338-9.
10. Harris AL. Hypoxia--a key regulatory factor in tumour growth. Nat Rev Cancer. 2002 Jan;2(1):38-47.
11. Hockel M, Schlenger K, Hockel S, Vaupel P. Hypoxic cervical cancers with low apoptotic index are highly aggressive. Cancer Res. 1999 Sep 15;59(18):4525-8.
12. Nordsmark M, Overgaard M, Overgaard J. Pretreatment oxygenation predicts radiation response in advanced squamous cell carcinoma of the head and neck. Radiother Oncol. 1996 Oct;41(1):31-9.
13. Shannon AM, Bouchier-Hayes DJ, Condron CM, Toomey D. Tumour hypoxia, chemotherapeutic resistance and hypoxia-related therapies. Cancer Treat Rev. 2003 Aug;29(4):297-307.
14. Tredan O, Galmarini CM, Patel K, Tannock IF. Drug resistance and the solid tumor microenvironment. J Natl Cancer Inst. 2007 Oct 3;99(19):1441-54.
15. Young SD, Hill RP. Effects of reoxygenation on cells from hypoxic regions of solid tumors: anticancer drug sensitivity and metastatic potential. J Natl Cancer Inst. 1990 Mar 7;82(5):371-80.
16. Comerford KM, Wallace TJ, Karhausen J, Louis NA, Montalto MC, Colgan SP. Hypoxia-inducible factor-1-dependent regulation of the multidrug resistance (MDR1) gene. Cancer Res. 2002 Jun 15;62(12):3387-94.

17. Jabr-Milane LS, van Vlerken LE, Yadav S, Amiji MM. Multi-functional nanocarriers to overcome tumor drug resistance. Cancer Treat Rev. 2008 Nov;34(7):592-602.
18. Yague E, Arance A, Kubitza L, O'Hare M, Jat P, Ogilvie CM, et al. Ability to acquire drug resistance arises early during the tumorigenesis process. Cancer Res. 2007 Feb 1;67(3):1130-7.
19. Krishna R, Mayer LD. Multidrug resistance (MDR) in cancer. Mechanisms, reversal using modulators of MDR and the role of MDR modulators in influencing the pharmacokinetics of anticancer drugs. Eur J Pharm Sci. 2000 Oct;11(4):265-83.
20. Jones PM, George AM. The ABC transporter structure and mechanism: perspectives on recent research. Cell Mol Life Sci. 2004 Mar;61(6):682-99.
21. Dean M, Fojo T, Bates S. Tumour stem cells and drug resistance. Nat Rev Cancer. 2005 Apr;5(4):275-84.
22. Ejendal KF, Hrycyna CA. Multidrug resistance and cancer: the role of the human ABC transporter ABCG2. Curr Protein Pept Sci. 2002 Oct;3(5):503-11.
23. Leslie EM, Deeley RG, Cole SP. Multidrug resistance proteins: role of P-glycoprotein, MRP1, MRP2, and BCRP (ABCG2) in tissue defense. Toxicol Appl Pharmacol. 2005 May 1;204(3):216-37.
24. Sampath J, Adachi M, Hatse S, Naesens L, Balzarini J, Flatley RM, et al. Role of MRP4 and MRP5 in biology and chemotherapy. AAPS PharmSci. 2002;4(3):E14.
25. Sheehan D, Meade G, Foley VM, Dowd CA. Structure, function and evolution of glutathione transferases: implications for classification of non-mammalian members of an ancient enzyme superfamily. Biochem J. 2001 Nov 15;360(Pt 1):1-16.
26. Hao XY, Widersten M, Ridderstrom M, Hellman U, Mannervik B. Co-variation of glutathione transferase expression and cytostatic drug resistance in HeLa cells: establishment of class Mu glutathione transferase M3-3 as the dominating isoenzyme. Biochem J. 1994 Jan 1;297 (Pt 1):59-67.
27. Lewis AD, Forrester LM, Hayes JD, Wareing CJ, Carmichael J, Harris AL, et al. Glutathione S-transferase isoenzymes in human tumours and tumour derived cell lines. Br J Cancer. 1989 Sep;60(3):327-31.
28. Bernardini S, Bellincampi L, Ballerini S, Ranalli M, Pastore A, Cortese C, et al. Role of GST P1-1 in mediating the effect of etoposide on human neuroblastoma cell line Sh-Sy5y. J Cell Biochem. 2002;86(2):340-7.
29. Zhang D, Lu H, Li J, Shi X, Huang C. Essential roles of ERKs and p38K in up-regulation of GST A1 expression by Maotai content in human hepatoma cell line Hep3B. Mol Cell Biochem. 2006 Dec;293(1-2):161-71.
30. Di Pietro G, Magno LA, Rios-Santos F. Glutathione S-transferases: an overview in cancer research. Expert Opin Drug Metab Toxicol. 2010 Feb;6(2):153-70.
31. Lorusso D, Ferrandina G, Fanfani F, Gagliardi ML, Scambia G. Investigational agents against platinum-resistant ovarian cancer. Expert Opin Investig Drugs. 2007 Mar;16(3):325-36.

32. Vergote I, Finkler N, del Campo J, Lohr A, Hunter J, Matei D, et al. Phase 3 randomised study of canfosfamide (Telcyta, TLK286) versus pegylated liposomal doxorubicin or topotecan as third-line therapy in patients with platinum-refractory or -resistant ovarian cancer. Eur J Cancer. 2009 Sep;45(13):2324-32.
33. Vergote I, Finkler NJ, Hall JB, Melnyk O, Edwards RP, Jones M, et al. Randomized phase III study of canfosfamide in combination with pegylated liposomal doxorubicin compared with pegylated liposomal doxorubicin alone in platinum-resistant ovarian cancer. Int J Gynecol Cancer. 2010 Jul;20(5):772-80.
34. Ball CR, Connors TA, Double JA, Ujhazy V, Whisson ME. Comparison of nitrogen-mustard sensitive and -resistant Yoshida sarcomas. Int J Cancer. 1966 Jul 15;1(4):319-27.
35. Meister A. Glutathione deficiency produced by inhibition of its synthesis, and its reversal; applications in research and therapy. Pharmacol Ther. 1991;51(2):155-94.
36. Meister A. Glutathione, ascorbate, and cellular protection. Cancer Res. 1994 Apr 1;54(7 Suppl):1969s-75s.
37. Champoux JJ. DNA topoisomerases: structure, function, and mechanism. Annu Rev Biochem. 2001;70:369-413.
38. Saavedra RA, Huberman JA. DNA topoisomerases in eukaryotes. Nature. 1985 Sep 5-11;317(6032):22.
39. Wang JC. DNA topoisomerases. Annu Rev Biochem. 1985;54:665-97.
40. Sordet O, Khan QA, Kohn KW, Pommier Y. Apoptosis induced by topoisomerase inhibitors. Curr Med Chem Anticancer Agents. 2003 Jul;3(4):271-90.
41. Beck WT, Morgan SE, Mo YY, Bhat UG. Tumor cell resistance to DNA topoisomerase II inhibitors: new developments. Drug Resist Updat. 1999 Dec;2(6):382-9.
42. Matsumoto Y, Tamiya T, Nagao S. Resistance to topoisomerase II inhibitors in human glioma cell lines overexpressing multidrug resistant associated protein (MRP) 2. J Med Invest. 2005 Feb;52(1-2):41-8.
43. Robert J, Larsen AK. Drug resistance to topoisomerase II inhibitors. Biochimie. 1998 Mar;80(3):247-54.
44. Valkov NI, Sullivan DM. Drug resistance to DNA topoisomerase I and II inhibitors in human leukemia, lymphoma, and multiple myeloma. Semin Hematol. 1997 Oct;34(4 Suppl 5):48-62.
45. Kamath N, Grabowski D, Ford J, Kerrigan D, Pommier Y, Ganapathi R. Overexpression of P-glycoprotein and alterations in topoisomerase II in P388 mouse leukemia cells selected in vivo for resistance to mitoxantrone. Biochem Pharmacol. 1992 Sep 1;44(5):937-45.
46. Withoff S, de Vries EG, Keith WN, Nienhuis EF, van der Graaf WT, Uges DR, et al. Differential expression of DNA topoisomerase II alpha and -beta in P-gp and MRP-negative VM26, mAMSA and mitoxantrone-resistant sublines of the human SCLC cell line GLC4. Br J Cancer. 1996 Dec;74(12):1869-76.

47. Beck WT. Mechanisms of multidrug resistance in human tumor cells. The roles of P-glycoprotein, DNA topoisomerase II, and other factors. Cancer Treat Rev. 1990 Dec;17 Suppl A:11-20.
48. Bugg BY, Danks MK, Beck WT, Suttle DP. Expression of a mutant DNA topoisomerase II in CCRF-CEM human leukemic cells selected for resistance to teniposide. Proc Natl Acad Sci U S A. 1991 Sep 1;88(17):7654-8.
49. Campain JA, Gottesman MM, Pastan I. A novel mutant topoisomerase II alpha present in VP-16-resistant human melanoma cell lines has a deletion of alanine 429. Biochemistry. 1994 Sep 20;33(37):11327-32.
50. Deffie AM, Bosman DJ, Goldenberg GJ. Evidence for a mutant allele of the gene for DNA topoisomerase II in adriamycin-resistant P388 murine leukemia cells. Cancer Res. 1989 Dec 15;49(24 Pt 1):6879-82.
51. Cole SP, Chanda ER, Dicke FP, Gerlach JH, Mirski SE. Non-P-glycoprotein-mediated multidrug resistance in a small cell lung cancer cell line: evidence for decreased susceptibility to drug-induced DNA damage and reduced levels of topoisomerase II. Cancer Res. 1991 Jul 1;51(13):3345-52.
52. Evans CD, Mirski SE, Danks MK, Cole SP. Reduced levels of topoisomerase II alpha and II beta in a multidrug-resistant lung-cancer cell line. Cancer Chemother Pharmacol. 1994;34(3):242-8.
53. Ritke MK, Murray NR, Allan WP, Fields AP, Yalowich JC. Hypophosphorylation of topoisomerase II in etoposide (VP-16)-resistant human leukemia K562 cells associated with reduced levels of beta II protein kinase C. Mol Pharmacol. 1995 Nov;48(5):798-805.
54. Xu Y, Villalona-Calero MA. Irinotecan: mechanisms of tumor resistance and novel strategies for modulating its activity. Ann Oncol. 2002 Dec;13(12):1841-51.
55. Tan KB, Mattern MR, Eng WK, McCabe FL, Johnson RK. Nonproductive rearrangement of DNA topoisomerase I and II genes: correlation with resistance to topoisomerase inhibitors. J Natl Cancer Inst. 1989 Nov 15;81(22):1732-5.
56. Eder JP, Chan V, Wong J, Wong YW, Ara G, Northey D, et al. Sequence effect of irinotecan (CPT-11) and topoisomerase II inhibitors in vivo. Cancer Chemother Pharmacol. 1998;42(4):327-35.
57. Kim R, Hirabayashi N, Nishiyama M, Jinushi K, Toge T, Okada K. Experimental studies on biochemical modulation targeting topoisomerase I and II in human tumor xenografts in nude mice. Int J Cancer. 1992 Mar 12;50(5):760-6.
58. Crump M, Lipton J, Hedley D, Sutton D, Shepherd F, Minden M, et al. Phase I trial of sequential topotecan followed by etoposide in adults with myeloid leukemia: a National Cancer Institute of Canada Clinical Trials Group Study. Leukemia. 1999 Mar;13(3):343-7.
59. Houghton JA, Cheshire PJ, Hallman JD, 2nd, Lutz L, Luo X, Li Y, et al. Evaluation of irinotecan in combination with 5-fluorouracil or etoposide in xenograft models of colon adenocarcinoma and rhabdomyosarcoma. Clin Cancer Res. 1996 Jan;2(1):107-18.
60. Vey N, Kantarjian H, Beran M, O'Brien S, Cortes J, Koller C, et al. Combination of topotecan with cytarabine or etoposide in patients with refractory

or relapsed acute myeloid leukemia: results of a randomized phase I/II study. Invest New Drugs. 1999;17(1):89-95.
61. Crump M, Couban S, Meyer R, Rudinskas L, Zanke B, Gluck S, et al. Phase II study of sequential topotecan and etoposide in patients with intermediate grade non-Hodgkin's lymphoma: a National Cancer Institute of Canada Clinical Trials Group study. Leuk Lymphoma. 2002 Aug;43(8):1581-7.
62. Salerno S, Da Settimo F, Taliani S, Simorini F, La Motta C, Fornaciari G, et al. Recent advances in the development of dual topoisomerase I and II inhibitors as anticancer drugs. Curr Med Chem. 2010;17(35):4270-90.
63. Denny WA, Baguley BC. Dual topoisomerase I/II inhibitors in cancer therapy. Curr Top Med Chem. 2003;3(3):339-53.
64. Moffitt KL, Martin SL, Walker B. From sentencing to execution--the processes of apoptosis. J Pharm Pharmacol. 2010 May;62(5):547-62.
65. Levine AJ. p53, the cellular gatekeeper for growth and division. Cell. 1997 Feb 7;88(3):323-31.
66. Lowe SW, Ruley HE, Jacks T, Housman DE. p53-dependent apoptosis modulates the cytotoxicity of anticancer agents. Cell. 1993 Sep 24;74(6):957-67.
67. Qin H, Yu T, Qing T, Liu Y, Zhao Y, Cai J, et al. Regulation of apoptosis and differentiation by p53 in human embryonic stem cells. J Biol Chem. 2007 Feb 23;282(8):5842-52.
68. Tsujimoto Y, Cossman J, Jaffe E, Croce CM. Involvement of the bcl-2 gene in human follicular lymphoma. Science. 1985 Jun 21;228(4706):1440-3.
69. Ackermann EJ, Taylor JK, Narayana R, Bennett CF. The role of antiapoptotic Bcl-2 family members in endothelial apoptosis elucidated with antisense oligonucleotides. J Biol Chem. 1999 Apr 16;274(16):11245-52.
70. Reed JC. Regulation of apoptosis by bcl-2 family proteins and its role in cancer and chemoresistance. Curr Opin Oncol. 1995 Nov;7(6):541-6.
71. Korsmeyer SJ, Wei MC, Saito M, Weiler S, Oh KJ, Schlesinger PH. Pro-apoptotic cascade activates BID, which oligomerizes BAK or BAX into pores that result in the release of cytochrome c. Cell Death Differ. 2000 Dec;7(12):1166-73.
72. Duronio V. The life of a cell: apoptosis regulation by the PI3K/PKB pathway. Biochem J. 2008 Nov 1;415(3):333-44.
73. Liu Y, Mei C, Sun L, Li X, Liu M, Wang L, et al. The PI3K-Akt pathway regulates calpain 6 expression, proliferation, and apoptosis. Cell Signal. 2011 Jan 19.
74. Turco MC, Romano MF, Petrella A, Bisogni R, Tassone P, Venuta S. NF-kappaB/Rel-mediated regulation of apoptosis in hematologic malignancies and normal hematopoietic progenitors. Leukemia. 2004 Jan;18(1):11-7.
75. Chang F, Steelman LS, Shelton JG, Lee JT, Navolanic PM, Blalock WL, et al. Regulation of cell cycle progression and apoptosis by the Ras/Raf/MEK/ERK pathway (Review). Int J Oncol. 2003 Mar;22(3):469-80.
76. Bossi G, Lapi E, Strano S, Rinaldo C, Blandino G, Sacchi A. Mutant p53 gain of function: reduction of tumor malignancy of human cancer cell lines through abrogation of mutant p53 expression. Oncogene. 2006 Jan 12;25(2):304-9.

77. Chan KT, Lung ML. Mutant p53 expression enhances drug resistance in a hepatocellular carcinoma cell line. Cancer Chemother Pharmacol. 2004 Jun;53(6):519-26.
78. Oren M, Rotter V. Mutant p53 gain-of-function in cancer. Cold Spring Harb Perspect Biol. 2010 Feb;2(2):a001107.
79. Guo XN, Rajput A, Rose R, Hauser J, Beko A, Kuropatwinski K, et al. Mutant PIK3CA-bearing colon cancer cells display increased metastasis in an orthotopic model. Cancer Res. 2007 Jun 15;67(12):5851-8.
80. Jhawer M, Goel S, Wilson AJ, Montagna C, Ling YH, Byun DS, et al. PIK3CA mutation/PTEN expression status predicts response of colon cancer cells to the epidermal growth factor receptor inhibitor cetuximab. Cancer Res. 2008 Mar 15;68(6):1953-61.
81. Kolasa IK, Rembiszewska A, Felisiak A, Ziolkowska-Seta I, Murawska M, Moes J, et al. PIK3CA amplification associates with resistance to chemotherapy in ovarian cancer patients. Cancer Biol Ther. 2009 Jan;8(1):21-6.
82. Wang J, Kuropatwinski K, Hauser J, Rossi MR, Zhou Y, Conway A, et al. Colon carcinoma cells harboring PIK3CA mutations display resistance to growth factor deprivation induced apoptosis. Mol Cancer Ther. 2007 Mar;6(3):1143-50.
83. Wee S, Jagani Z, Xiang KX, Loo A, Dorsch M, Yao YM, et al. PI3K pathway activation mediates resistance to MEK inhibitors in KRAS mutant cancers. Cancer Res. 2009 May 15;69(10):4286-93.
84. Kanaseki T, Torigoe T, Hirohashi Y, Hirai I, Himi T, Sato N. Identification of germline mutation of PTEN gene and analysis of apoptosis resistance of the lymphocytes in a patient with Cowden disease. Pathobiology. 2002;70(1):34-9.
85. Lin PY, Fosmire SP, Park SH, Park JY, Baksh S, Modiano JF, et al. Attenuation of PTEN increases p21 stability and cytosolic localization in kidney cancer cells: a potential mechanism of apoptosis resistance. Mol Cancer. 2007;6:16.
86. Montiel-Duarte C, Cordeu L, Agirre X, Roman-Gomez J, Jimenez-Velasco A, Jose-Eneriz ES, et al. Resistance to Imatinib Mesylate-induced apoptosis in acute lymphoblastic leukemia is associated with PTEN down-regulation due to promoter hypermethylation. Leuk Res. 2008 May;32(5):709-16.
87. Gotz R. Inter-cellular adhesion disruption and the RAS/RAF and beta-catenin signalling in lung cancer progression. Cancer Cell Int. 2008;8:7.
88. Santarpia L, El-Naggar AK, Cote GJ, Myers JN, Sherman SI. Phosphatidylinositol 3-kinase/akt and ras/raf-mitogen-activated protein kinase pathway mutations in anaplastic thyroid cancer. J Clin Endocrinol Metab. 2008 Jan;93(1):278-84.
89. Seth R, Crook S, Ibrahem S, Fadhil W, Jackson D, Ilyas M. Concomitant mutations and splice variants in KRAS and BRAF demonstrate complex perturbation of the Ras/Raf signalling pathway in advanced colorectal cancer. Gut. 2009 Sep;58(9):1234-41.
90. Foster BA, Coffey HA, Morin MJ, Rastinejad F. Pharmacological rescue of mutant p53 conformation and function. Science. 1999 Dec 24;286(5449):2507-10.

91. Sebolt-Leopold JS. MEK inhibitors: a therapeutic approach to targeting the Ras-MAP kinase pathway in tumors. Curr Pharm Des. 2004;10(16):1907-14.
92. Serra V, Markman B, Scaltriti M, Eichhorn PJ, Valero V, Guzman M, et al. NVP-BEZ235, a dual PI3K/mTOR inhibitor, prevents PI3K signaling and inhibits the growth of cancer cells with activating PI3K mutations. Cancer Res. 2008 Oct 1;68(19):8022-30.
93. Leber B, Geng F, Kale J, Andrews DW. Drugs targeting Bcl-2 family members as an emerging strategy in cancer. Expert Rev Mol Med. 2010;12:e28.
94. Nguyen M, Marcellus RC, Roulston A, Watson M, Serfass L, Murthy Madiraju SR, et al. Small molecule obatoclax (GX15-070) antagonizes MCL-1 and overcomes MCL-1-mediated resistance to apoptosis. Proc Natl Acad Sci U S A. 2007 Dec 4;104(49):19512-7.
95. Bunney TD, Katan M. Phosphoinositide signalling in cancer: beyond PI3K and PTEN. Nat Rev Cancer. 2010 May;10(5):342-52.
96. Cleary JM, Shapiro GI. Development of phosphoinositide-3 kinase pathway inhibitors for advanced cancer. Curr Oncol Rep. 2010 Mar;12(2):87-94.
97. Boller YC, Brandes LM, Russell RL, Lin ZP, Patierno SR, Kennedy KA. Prostaglandin A1 inhibits stress-induced NF-kappaB activation and reverses resistance to topoisomerase II inhibitors. Oncol Res. 2000;12(9-10):383-95.
98. Wang W, McLeod HL, Cassidy J. Disulfiram-mediated inhibition of NF-kappaB activity enhances cytotoxicity of 5-fluorouracil in human colorectal cancer cell lines. Int J Cancer. 2003 Apr 20;104(4):504-11.
99. Zhu BS, Xing CG, Lin F, Fan XQ, Zhao K, Qin ZH. Blocking NF-kappaB nuclear translocation leads to p53-related autophagy activation and cell apoptosis. World J Gastroenterol. 2011 Jan 28;17(4):478-87.
100. Zhou H, Liu Y, Cheung LH, Kim S, Zhang W, Mohamedali KA, et al. Characterization and mechanistic studies of a novel melanoma-targeting construct containing IkappaBa for specific inhibition of nuclear factor-kappaB activity. Neoplasia. 2011 Oct;12(10):766-77.
101. Juliano RL, Ling V. A surface glycoprotein modulating drug permeability in Chinese hamster ovary cell mutants. Biochim Biophys Acta. 1976 Nov 11;455(1):152-62.
102. Thomas H, Coley HM. Overcoming multidrug resistance in cancer: an update on the clinical strategy of inhibiting p-glycoprotein. Cancer Control. 2003 Mar-Apr;10(2):159-65.
103. Gottesman MM, Pastan I. Biochemistry of multidrug resistance mediated by the multidrug transporter. Annu Rev Biochem. 1993;62:385-427.
104. Schinkel AH. The physiological function of drug-transporting P-glycoproteins. Semin Cancer Biol. 1997 Jun;8(3):161-70.
105. Lee CH, Bradley G, Zhang JT, Ling V. Differential expression of P-glycoprotein genes in primary rat hepatocyte culture. J Cell Physiol. 1993 Nov;157(2):392-402.
106. Lin JH, Yamazaki M. Role of P-glycoprotein in pharmacokinetics: clinical implications. Clin Pharmacokinet. 2003;42(1):59-98.
107. Ruetz S, Gros P. Phosphatidylcholine translocase: A physiological role for the mdr2 gene. Cell. 1994;77(7):1071-81.

108. van Helvoort A, Smith AJ, Sprong H, Fritzsche I, Schinkel AH, Borst P, et al. MDR1 P-glycoprotein is a lipid translocase of broad specificity, while MDR3 P-glycoprotein specifically translocates phosphatidylcholine; 1996.
109. Shustik C, Dalton W, Gros P. P-glycoprotein-mediated multidrug resistance in tumor cells: biochemistry, clinical relevance and modulation. Mol Aspects Med. 1995;16(1):1-78.
110. Seelig A, Landwojtowicz E. Structure-activity relationship of P-glycoprotein substrates and modifiers. Eur J Pharm Sci. 2000 Nov;12(1):31-40.
111. Osterberg T, Norinder U. Theoretical calculation and prediction of P-glycoprotein-interacting drugs using MolSurf parametrization and PLS statistics. Eur J Pharm Sci. 2000;10(4):295-303.
112. Zhou SF. Structure, function and regulation of P-glycoprotein and its clinical relevance in drug disposition. Xenobiotica. 2008 Jul;38(7-8):802-32.
113. Varma MVS, Obach RS, Rotter C, Miller HR, Chang G, Steyn SJ, et al. Physicochemical Space for Optimum Oral Bioavailability: Contribution of Human Intestinal Absorption and First-Pass Elimination. J Med Chem. 2003.
114. Ambudkar SV, Dey S, Hrycyna CA, Ramachandra M, Pastan I, Gottesman MM. Biochemical, cellular, and pharmacological aspects of the multidrug transporter. Annu Rev Pharmacol Toxicol. 1999;39:361-98.
115. Sonveaux N, Shapiro AB, Goormaghtigh E, Ling V, Ruysschaert JM. Secondary and tertiary structure changes of reconstituted P-glycoprotein. A Fourier transform attenuated total reflection infrared spectroscopy analysis. J Biol Chem. 1996 Oct 4;271(40):24617-24.
116. Sauna ZE, Smith MM, Muller M, Kerr KM, Ambudkar SV. The mechanism of action of multidrug-resistance-linked P-glycoprotein. J Bioenerg Biomembr. 2001 Dec;33(6):481-91.
117. Rosenberg MF, Kamis AB, Callaghan R, Higgins CF, Ford RC. Three-dimensional structures of the mammalian multidrug resistance P-glycoprotein demonstrate major conformational changes in the transmembrane domains upon nucleotide binding. J Biol Chem. 2003 Mar 7;278(10):8294-9.
118. Bellamy WT. P-glycoproteins and multidrug resistance. Annu Rev Pharmacol Toxicol. 1996;36:161-83.
119. Higgins CF, Callaghan R, Linton KJ, Rosenberg MF, Ford RC. Structure of the multidrug resistance P-glycoprotein. Semin Cancer Biol. 1997 Jun;8(3):135-42.
120. Cordon-Cardo C, O'Brien JP, Casals D, Rittman-Grauer L, Biedler JL, Melamed MR, et al. Multidrug-resistance gene (P-glycoprotein) is expressed by endothelial cells at blood-brain barrier sites. Proc Natl Acad Sci U S A. 1989 Jan;86(2):695-8.
121. Ho RH, Kim RB. Transporters and drug therapy: implications for drug disposition and disease. Clin Pharmacol Ther. 2005 Sep;78(3):260-77.
122. Thiebaut F, Tsuruo T, Hamada H, Gottesman MM, Pastan I, Willingham MC. Cellular localization of the multidrug-resistance gene product P-glycoprotein in normal human tissues. Proc Natl Acad Sci U S A. 1987 Nov;84(21):7735-8.

123. Hsing S, Gatmaitan Z, Arias IM. The function of Gp170, the multidrug-resistance gene product, in the brush border of rat intestinal mucosa. Gastroenterology. 1992 Mar;102(3):879-85.
124. Wacher VJ, Wu CY, Benet LZ. Overlapping substrate specificities and tissue distribution of cytochrome P450 3A and P-glycoprotein: implications for drug delivery and activity in cancer chemotherapy. Mol Carcinog. 1995 Jul;13(3):129-34.
125. Benet LZ, Cummins CL. The drug efflux-metabolism alliance: biochemical aspects. Adv Drug Deliv Rev. 2001 Oct 1;50 Suppl 1:S3-11.
126. Zhang Y, Benet LZ. The gut as a barrier to drug absorption: combined role of cytochrome P450 3A and P-glycoprotein. Clin Pharmacokinet. 2001;40(3):159-68.
127. Cummins CL, Mangravite LM, Benet LZ. Characterizing the expression of CYP3A4 and efflux transporters (P-gp, MRP1, and MRP2) in CYP3A4-transfected Caco-2 cells after induction with sodium butyrate and the phorbol ester 12-O-tetradecanoylphorbol-13-acetate. Pharm Res. 2001 Aug;18(8):1102-9.
128. Synold TW, Dussault I, Forman BM. The orphan nuclear receptor SXR coordinately regulates drug metabolism and efflux. Nat Med. 2001 May;7(5):584-90.
129. Kusuhara H, Suzuki H, Sugiyama Y. The role of P-glycoprotein and canalicular multispecific organic anion transporter in the hepatobiliary excretion of drugs. J Pharm Sci. 1998 Sep;87(9):1025-40.
130. Matheny CJ, Lamb MW, Brouwer KR, Pollack GM. Pharmacokinetic and pharmacodynamic implications of P-glycoprotein modulation. Pharmacotherapy. 2001 Jul;21(7):778-96.
131. Ernest S, Rajaraman S, Megyesi J, Bello-Reuss EN. Expression of MDR1 (multidrug resistance) gene and its protein in normal human kidney. Nephron. 1997;77(3):284-9.
132. Okamura N, Hirai M, Tanigawara Y, Tanaka K, Yasuhara M, Ueda K, et al. Digoxin-cyclosporin A interaction: modulation of the multidrug transporter P-glycoprotein in the kidney. J Pharmacol Exp Ther. 1993 Sep;266(3):1614-9.
133. Joo F. Endothelial cells of the brain and other organ systems: some similarities and differences. Prog Neurobiol. 1996 Feb;48(3):255-73.
134. van Asperen J, Mayer U, van Tellingen O, Beijnen JH. The functional role of P-glycoprotein in the blood-brain barrier. J Pharm Sci. 1997 Aug;86(8):881-4.
135. Drion N, Lemaire M, Lefauconnier JM, Scherrmann JM. Role of P-glycoprotein in the blood-brain transport of colchicine and vinblastine. J Neurochem. 1996 Oct;67(4):1688-93.
136. Tsuji A, Terasaki T, Takabatake Y, Tenda Y, Tamai I, Yamashima T, et al. P-glycoprotein as the drug efflux pump in primary cultured bovine brain capillary endothelial cells. Life Sci. 1992;51(18):1427-37.
137. Goldstein LJ, Galski H, Fojo A, Willingham M, Lai SL, Gazdar A, et al. Expression of a multidrug resistance gene in human cancers. J Natl Cancer Inst. 1989 Jan 18;81(2):116-24.

138. Sekine I, Shimizu C, Nishio K, Saijo N, Tamura T. A literature review of molecular markers predictive of clinical response to cytotoxic chemotherapy in patients with breast cancer. Int J Clin Oncol. 2009 Apr;14(2):112-9.
139. O'Driscoll L, Clynes M. Biomarkers and multiple drug resistance in breast cancer. Curr Cancer Drug Targets. 2006 Aug;6(5):365-84.
140. Trock BJ, Leonessa F, Clarke R. Multidrug resistance in breast cancer: a meta-analysis of MDR1/gp170 expression and its possible functional significance. J Natl Cancer Inst. 1997 Jul 2;89(13):917-31.
141. Goda K, Bacso Z, Szabo G. Multidrug resistance through the spectacle of P-glycoprotein. Curr Cancer Drug Targets. 2009 May;9(3):281-97.
142. Johnstone RW, Ruefli AA, Smyth MJ. Multiple physiological functions for multidrug transporter P-glycoprotein? Trends Biochem Sci. 2000 Jan;25(1):1-6.
143. Ruth AC, Roninson IB. Effects of the multidrug transporter P-glycoprotein on cellular responses to ionizing radiation. Cancer Res. 2000 May 15;60(10):2576-8.
144. Tainton KM, Smyth MJ, Jackson JT, Tanner JE, Cerruti L, Jane SM, et al. Mutational analysis of P-glycoprotein: suppression of caspase activation in the absence of ATP-dependent drug efflux. Cell Death Differ. 2004 Sep;11(9):1028-37.
145. Gouaze-Andersson V, Cabot MC. Glycosphingolipids and drug resistance. Biochim Biophys Acta. 2006 Dec;1758(12):2096-103.
146. Gouaze-Andersson V, Yu JY, Kreitenberg AJ, Bielawska A, Giuliano AE, Cabot MC. Ceramide and glucosylceramide upregulate expression of the multidrug resistance gene MDR1 in cancer cells. Biochim Biophys Acta. 2007 Dec;1771(12):1407-17.
147. Pallis M, Russell N. P-glycoprotein plays a drug-efflux-independent role in augmenting cell survival in acute myeloblastic leukemia and is associated with modulation of a sphingomyelin-ceramide apoptotic pathway. Blood. 2000 May 1;95(9):2897-904.
148. Aouali N, Eddabra L, Macadre J, Morjani H. Immunosuppressors and reversion of multidrug-resistance. Crit Rev Oncol Hematol. 2005 Oct;56(1):61-70.
149. Mimeault M, Hauke R, Batra SK. Recent advances on the molecular mechanisms involved in the drug resistance of cancer cells and novel targeting therapies. Clin Pharmacol Ther. 2008 May;83(5):673-91.
150. Cabot MC, Han TY, Giuliano AE. The multidrug resistance modulator SDZ PSC 833 is a potent activator of cellular ceramide formation. FEBS Lett. 1998 Jul 17;431(2):185-8.
151. Wang H, Giuliano AE, Cabot MC. Enhanced de novo ceramide generation through activation of serine palmitoyltransferase by the P-glycoprotein antagonist SDZ PSC 833 in breast cancer cells. Mol Cancer Ther. 2002 Jul;1(9):719-26.
152. Ford JM, Hait WN. Pharmacologic circumvention of multidrug resistance. Cytotechnology. 1993;12(1-3):171-212.

153. Wang SW, Monagle J, McNulty C, Putnam D, Chen H. Determination of P-glycoprotein inhibition by excipients and their combinations using an integrated high-throughput process. J Pharm Sci. 2004 Nov;93(11):2755-67.
154. Watanabe T, Nakayama Y, Naito M, Oh-hara T, Itoh Y, Tsuruo T. Cremophor EL reversed multidrug resistance in vitro but not in tumor-bearing mouse models. Anticancer Drugs. 1996 Nov;7(8):825-32.
155. Lampidis TJ, Krishan A, Planas L, Tapiero H. Reversal of intrinsic resistance to adriamycin in normal cells by verapamil. Cancer Drug Deliv. 1986 Fall;3(4):251-9.
156. Alaoui-Jamali MA, Schecter RL, Rustum YM, Centurioni MG, Lehnert S, Batist G. In vivo reversal of doxorubicin resistance by a new tiapamil analog Ro11-2933. J Pharmacol Exp Ther. 1993 Mar;264(3):1299-304.
157. Boesch D, Muller K, Pourtier-Manzanedo A, Loor F. Restoration of daunomycin retention in multidrug-resistant P388 cells by submicromolar concentrations of SDZ PSC 833, a nonimmunosuppressive cyclosporin derivative. Exp Cell Res. 1991 Sep;196(1):26-32.
158. Krishna R, de Jong G, Mayer LD. Pulsed exposure of SDZ PSC 833 to multidrug resistant P388/ADR and MCF7/ADR cells in the absence of anticancer drugs can fully restore sensitivity to doxorubicin. Anticancer Res. 1997 Sep-Oct;17(5A):3329-34.
159. Dale IL, Tuffley W, Callaghan R, Holmes JA, Martin K, Luscombe M, et al. Reversal of P-glycoprotein-mediated multidrug resistance by XR9051, a novel diketopiperazine derivative. Br J Cancer. 1998 Oct;78(7):885-92.
160. Dantzig AH, Shepard RL, Cao J, Law KL, Ehlhardt WJ, Baughman TM, et al. Reversal of P-glycoprotein-mediated multidrug resistance by a potent cyclopropyldibenzosuberane modulator, LY335979. Cancer Res. 1996 Sep 15;56(18):4171-9.
161. Peck RA, Hewett J, Harding MW, Wang YM, Chaturvedi PR, Bhatnagar A, et al. Phase I and pharmacokinetic study of the novel MDR1 and MRP1 inhibitor biricodar administered alone and in combination with doxorubicin. J Clin Oncol. 2001 Jun 15;19(12):3130-41.
162. Baguley BC. Multiple drug resistance mechanisms in cancer. Mol Biotechnol. 2010 Nov;46(3):308-16.
163. Fox E, Bates SE. Tariquidar (XR9576): a P-glycoprotein drug efflux pump inhibitor. Expert Rev Anticancer Ther. 2007 Apr;7(4):447-59.
164. Coley HM. Overcoming multidrug resistance in cancer: clinical studies of p-glycoprotein inhibitors. Methods Mol Biol. 2010;596:341-58.
165. Kusunoki N, Takara K, Tanigawara Y, Yamauchi A, Ueda K, Komada F, et al. Inhibitory effects of a cyclosporin derivative, SDZ PSC 833, on transport of doxorubicin and vinblastine via human P-glycoprotein. Jpn J Cancer Res. 1998 Nov;89(11):1220-8.
166. Lemaire M, Bruelisauer A, Guntz P, Sato H. Dose-dependent brain penetration of SDZ PSC 833, a novel multidrug resistance-reversing cyclosporin, in rats. Cancer Chemother Pharmacol. 1996;38(5):481-6.

167. Watanabe T, Tsuge H, Oh-Hara T, Naito M, Tsuruo T. Comparative study on reversal efficacy of SDZ PSC 833, cyclosporin A and verapamil on multidrug resistance in vitro and in vivo. Acta Oncol. 1995;34(2):235-41.
168. Fischer V, Rodriguez-Gascon A, Heitz F, Tynes R, Hauck C, Cohen D, et al. The multidrug resistance modulator valspodar (PSC 833) is metabolized by human cytochrome P450 3A. Implications for drug-drug interactions and pharmacological activity of the main metabolite. Drug Metab Dispos. 1998 Aug;26(8):802-11.
169. Pourtier-Manzanedo A, Didier AD, Muller CD, Loor F. SDZ PSC 833 and SDZ 280-446 are the most active of various resistance-modifying agents in restoring rhodamine-123 retention within multidrug resistant P388 cells. Anticancer Drugs. 1992 Aug;3(4):419-25.
170. Archinal-Mattheis A, Rzepka RW, Watanabe T, Kokubu N, Itoh Y, Combates NJ, et al. Analysis of the interactions of SDZ PSC 833 ([3'-keto-Bmt1]-Val2]-Cyclosporine), a multidrug resistance modulator, with P-glycoprotein. Oncol Res. 1995;7(12):603-10.
171. Atadja P, Watanabe T, Xu H, Cohen D. PSC-833, a frontier in modulation of P-glycoprotein mediated multidrug resistance. Cancer Metastasis Rev. 1998 Jun;17(2):163-8.
172. Jette L, Murphy GF, Beliveau R. Drug binding to P-glycoprotein is inhibited in normal tissues following SDZ-PSC 833 treatment. Int J Cancer. 1998 May 29;76(5):729-37.
173. Naito M, Watanabe T, Tsuge H, Koyama T, Oh-hara T, Tsuruo T. Potentiation of the reversal activity of SDZ PSC833 on multi-drug resistance by an anti-P-glycoprotein monoclonal antibody MRK-16. Int J Cancer. 1996 Jul 29;67(3):435-40.
174. Uchiyama-Kokubu N, Watanabe T, Cohen D. Intracellular levels of two cyclosporin derivatives valspodar (PSC 833) and cyclosporin a closely associated with multidrug resistance-modulating activity in sublines of human colorectal adenocarcinoma HCT-15. Jpn J Cancer Res. 2001 Oct;92(10):1116-26.
175. Smith AJ, Mayer U, Schinkel AH, Borst P. Availability of PSC833, a substrate and inhibitor of P-glycoproteins, in various concentrations of serum. J Natl Cancer Inst. 1998 Aug 5;90(15):1161-6.
176. Watanabe T, Kokubu N, Charnick SB, Naito M, Tsuruo T, Cohen D. Interaction of cyclosporin derivatives with the ATPase activity of human P-glycoprotein. Br J Pharmacol. 1997 Sep;122(2):241-8.
177. Kivisto KT, Kroemer HK, Eichelbaum M. The role of human cytochrome P450 enzymes in the metabolism of anticancer agents: implications for drug interactions. Br J Clin Pharmacol. 1995 Dec;40(6):523-30.
178. Song S, Suzuki H, Kawai R, Sugiyama Y. Effect of PSC 833, a P-glycoprotein modulator, on the disposition of vincristine and digoxin in rats. Drug Metab Dispos. 1999 Jun;27(6):689-94.
179. Speeg KV, Maldonado AL. Effect of the nonimmunosuppressive cyclosporin analog SDZ PSC-833 on colchicine and doxorubicin biliary secretion by the rat in vivo. Cancer Chemother Pharmacol. 1994;34(2):133-6.

180. Achira M, Suzuki H, Ito K, Sugiyama Y. Comparative studies to determine the selective inhibitors for P-glycoprotein and cytochrome P4503A4. AAPS PharmSci. 1999;1(4):E18.
181. Bates S, Kang M, Meadows B, Bakke S, Choyke P, Merino M, et al. A Phase I study of infusional vinblastine in combination with the P-glycoprotein antagonist PSC 833 (valspodar). Cancer. 2001 Sep 15;92(6):1577-90.
182. Fracasso PM, Westervelt P, Fears CL, Rosen DM, Zuhowski EG, Cazenave LA, et al. Phase I study of paclitaxel in combination with a multidrug resistance modulator, PSC 833 (Valspodar), in refractory malignancies. J Clin Oncol. 2000 Mar;18(5):1124-34.
183. Patnaik A, Warner E, Michael M, Egorin MJ, Moore MJ, Siu LL, et al. Phase I dose-finding and pharmacokinetic study of paclitaxel and carboplatin with oral valspodar in patients with advanced solid tumors. J Clin Oncol. 2000 Nov 1;18(21):3677-89.
184. Boote DJ, Dennis IF, Twentyman PR, Osborne RJ, Laburte C, Hensel S, et al. Phase I study of etoposide with SDZ PSC 833 as a modulator of multidrug resistance in patients with cancer. J Clin Oncol. 1996 Feb;14(2):610-8.
185. Loor F. Valspodar: current status and perspectives. Expert Opin Investig Drugs. 1999 Jun;8(6):807-35.
186. Sonneveld P, Marie JP, Huisman C, Vekhoff A, Schoester M, Faussat AM, et al. Reversal of multidrug resistance by SDZ PSC 833, combined with VAD (vincristine, doxorubicin, dexamethasone) in refractory multiple myeloma. A phase I study. Leukemia. 1996 Nov;10(11):1741-50.
187. Kolitz JE, George SL, Marcucci G, Vij R, Powell BL, Allen SL, et al. P-glycoprotein inhibition using valspodar (PSC-833) does not improve outcomes for patients younger than age 60 years with newly diagnosed acute myeloid leukemia: Cancer and Leukemia Group B study 19808. Blood. 2010 Sep 2;116(9):1413-21.
188. O'Brien MM, Lacayo NJ, Lum BL, Kshirsagar S, Buck S, Ravindranath Y, et al. Phase I study of valspodar (PSC-833) with mitoxantrone and etoposide in refractory and relapsed pediatric acute leukemia: a report from the Children's Oncology Group. Pediatr Blood Cancer. 2010 May;54(5):694-702.
189. Baekelandt M, Lehne G, Trope CG, Szanto I, Pfeiffer P, Gustavssson B, et al. Phase I/II trial of the multidrug-resistance modulator valspodar combined with cisplatin and doxorubicin in refractory ovarian cancer. J Clin Oncol. 2001 Jun 15;19(12):2983-93.
190. Fracasso PM, Brady MF, Moore DH, Walker JL, Rose PG, Letvak L, et al. Phase II study of paclitaxel and valspodar (PSC 833) in refractory ovarian carcinoma: a gynecologic oncology group study. J Clin Oncol. 2001 Jun 15;19(12):2975-82.
191. Friedenberg WR, Rue M, Blood EA, Dalton WS, Shustik C, Larson RA, et al. Phase III study of PSC-833 (valspodar) in combination with vincristine, doxorubicin, and dexamethasone (valspodar/VAD) versus VAD alone in patients with recurring or refractory multiple myeloma (E1A95): a trial of the Eastern Cooperative Oncology Group. Cancer. 2006 Feb 15;106(4):830-8.
192. Gruber A, Bjorkholm M, Brinch L, Evensen S, Gustavsson B, Hedenus M, et al. A phase I/II study of the MDR modulator Valspodar (PSC 833) combined

with daunorubicin and cytarabine in patients with relapsed and primary refractory acute myeloid leukemia. Leuk Res. 2003 Apr;27(4):323-8.
193. Riehm H, Biedler JL. Potentiation of drug effect by Tween 80 in Chinese hamster cells resistant to actinomycin D and daunomycin. Cancer Res. 1972 Jun;32(6):1195-200.
194. Mayer LD, Shabbits JA. The role for liposomal drug delivery in molecular and pharmacological strategies to overcome multidrug resistance. Cancer Metastasis Rev. 2001;20(1-2):87-93.
195. Rahman A, Husain SR, Siddiqui J, Verma M, Agresti M, Center M, et al. Liposome-mediated modulation of multidrug resistance in human HL-60 leukemia cells. J Natl Cancer Inst. 1992 Dec 16;84(24):1909-15.
196. Sadava D, Coleman A, Kane SE. Liposomal daunorubicin overcomes drug resistance in human breast, ovarian and lung carcinoma cells. J Liposome Res. 2002 Nov;12(4):301-9.
197. Thierry AR, Dritschilo A, Rahman A. Effect of liposomes on P-glycoprotein function in multidrug resistant cells. Biochem Biophys Res Commun. 1992 Sep 16;187(2):1098-105.
198. Warren L, Jardillier JC, Malarska A, Akeli MG. Increased accumulation of drugs in multidrug-resistant cells induced by liposomes. Cancer Res. 1992 Jun 1;52(11):3241-5.
199. Riganti C, Voena C, Kopecka J, Corsetto PA, Montorfano G, Enrico E, et al. Liposome-Encapsulated Doxorubicin Reverses Drug Resistance by Inhibiting P-Glycoprotein in Human Cancer Cells. Mol Pharm. 2011 May 5.
200. Krieger ML, Konold A, Wiese M, Jaehde U, Bendas G. Targeted doxorubicin-liposomes as a tool to circumvent P-gp-mediated resistance in ovarian carcinoma cells. Int J Clin Pharmacol Ther. 2010 Jul;48(7):442-4.
201. Booser DJ, Esteva FJ, Rivera E, Valero V, Esparza-Guerra L, Priebe W, et al. Phase II study of liposomal annamycin in the treatment of doxorubicin-resistant breast cancer. Cancer Chemother Pharmacol. 2002 Jul;50(1):6-8.
202. Hu YP, Henry-Toulme N, Robert J. Failure of liposomal encapsulation of doxorubicin to circumvent multidrug resistance in an in vitro model of rat glioblastoma cells. Eur J Cancer. 1995;31A(3):389-94.
203. Rivera E, Valero V, Esteva FJ, Syrewicz L, Cristofanilli M, Rahman Z, et al. Lack of activity of stealth liposomal doxorubicin in the treatment of patients with anthracycline-resistant breast cancer. Cancer Chemother Pharmacol. 2002 Apr;49(4):299-302.
204. Wang Y, Eksborg S, Lewensohn R, Lindberg A, Liliemark E. In vitro cellular accumulation and cytotoxicity of liposomal and conventional formulations of daunorubicin and doxorubicin in resistant K562 cells. Anticancer Drugs. 1999 Nov;10(10):921-8.
205. Li X, Lu WL, Liang GW, Ruan GR, Hong HY, Long C, et al. Effect of stealthy liposomal topotecan plus amlodipine on the multidrug-resistant leukaemia cells in vitro and xenograft in mice. Eur J Clin Invest. 2006 Jun;36(6):409-18.

206. Wang J, Goh B, Lu W, Zhang Q, Chang A, Liu XY, et al. In vitro cytotoxicity of Stealth liposomes co-encapsulating doxorubicin and verapamil on doxorubicin-resistant tumor cells. Biol Pharm Bull. 2005 May;28(5):822-8.
207. Wu J, Lu Y, Lee A, Pan X, Yang X, Zhao X, et al. Reversal of multidrug resistance by transferrin-conjugated liposomes co-encapsulating doxorubicin and verapamil. J Pharm Pharm Sci. 2007;10(3):350-7.
208. Alakhov V, Moskaleva E, Batrakova EV, Kabanov AV. Hypersensitization of multidrug resistant human ovarian carcinoma cells by pluronic P85 block copolymer. Bioconjug Chem. 1996 Mar-Apr;7(2):209-16.
209. Venne A, Li S, Mandeville R, Kabanov A, Alakhov V. Hypersensitizing effect of pluronic L61 on cytotoxic activity, transport, and subcellular distribution of doxorubicin in multiple drug-resistant cells. Cancer Res. 1996 Aug 15;56(16):3626-9.
210. Alakhov V, Klinski E, Li S, Pietrzynski G, Venne A, Batrakova E, et al. Block copolymer-based formulation of doxorubicin. From cell screen to clinical trials. Colloids and Surfaces B: Biointerfaces. 1999;16(1-4):113-34.
211. Batrakova EV, Dorodnych TY, Klinskii EY, Kliushnenkova EN, Shemchukova OB, Goncharova ON, et al. Anthracycline antibiotics non-covalently incorporated into the block copolymer micelles: in vivo evaluation of anti-cancer activity. Br J Cancer. 1996 Nov;74(10):1545-52.
212. Batrakova EV, Li S, Brynskikh AM, Sharma AK, Li Y, Boska M, et al. Effects of pluronic and doxorubicin on drug uptake, cellular metabolism, apoptosis and tumor inhibition in animal models of MDR cancers. J Control Release. 2010 May 10;143(3):290-301.
213. Valle JW, Armstrong A, Newman C, Alakhov V, Pietrzynski G, Brewer J, et al. A phase 2 study of SP1049C, doxorubicin in P-glycoprotein-targeting pluronics, in patients with advanced adenocarcinoma of the esophagus and gastroesophageal junction. Invest New Drugs. 2010 Feb 24.
214. Yokoyama M. Polymeric micelles as a new drug carrier system and their required considerations for clinical trials. Expert Opin Drug Deliv. 2010 Feb;7(2):145-58.
215. Valle JW, Lawrance J, Brewer J, Clayton A, Corrie P, Alakhov V, et al. A phase II, window study of SP1049C as first-line therapy in inoperable metastatic adenocarcinoma of the oesophagus. 2004 ASCO Annual Meeting 2004.
216. Zastre J, Jackson J, Bajwa M, Liggins R, Iqbal F, Burt H. Enhanced cellular accumulation of a P-glycoprotein substrate, rhodamine-123, by Caco-2 cells using low molecular weight methoxypolyethylene glycol-block-polycaprolactone diblock copolymers. Eur J Pharm Biopharm. 2002 Nov;54(3):299-309.
217. Elamanchili P, McEachern C, Burt H. Reversal of multidrug resistance by methoxypolyethylene glycol-block-polycaprolactone diblock copolymers through the inhibition of P-glycoprotein function. J Pharm Sci. 2009 Mar;98(3):945-58.
218. Batrakova EV, Li S, Alakhov VY, Miller DW, Kabanov AV. Optimal structure requirements for pluronic block copolymers in modifying P-glycoprotein drug efflux transporter activity in bovine brain microvessel endothelial cells. J Pharmacol Exp Ther. 2003 Feb;304(2):845-54.

219. Zastre JA, Jackson JK, Wong W, Burt HM. P-glycoprotein efflux inhibition by amphiphilic diblock copolymers: relationship between copolymer concentration and substrate hydrophobicity. Mol Pharm. 2008 Jul-Aug;5(4):643-53.
220. Batrakova E, Lee S, Li S, Venne A, Alakhov V, Kabanov A. Fundamental relationships between the composition of pluronic block copolymers and their hypersensitization effect in MDR cancer cells. Pharm Res. 1999 Sep;16(9):1373-9.
221. Miller DW, Batrakova EV, Waltner TO, Alakhov V, Kabanov AV. Interactions of pluronic block copolymers with brain microvessel endothelial cells: evidence of two potential pathways for drug absorption. Bioconjug Chem. 1997 Sep-Oct;8(5):649-57.
222. Astier A, Doat B, Ferrer MJ, Benoit G, Fleury J, Rolland A, et al. Enhancement of adriamycin antitumor activity by its binding with an intracellular sustained-release form, polymethacrylate nanospheres, in U-937 cells. Cancer Res. 1988 Apr 1;48(7):1835-41.
223. Omelyanenko V, Kopeckova P, Gentry C, Kopecek J. Targetable HPMA copolymer-adriamycin conjugates. Recognition, internalization, and subcellular fate. J Control Release. 1998 Apr 30;53(1-3):25-37.
224. Hu CM, Zhang L. Therapeutic nanoparticles to combat cancer drug resistance. Curr Drug Metab. 2009 Oct;10(8):836-41.
225. de Verdiere AC, Dubernet C, Nemati F, Soma E, Appel M, Ferte J, et al. Reversion of multidrug resistance with polyalkylcyanoacrylate nanoparticles: towards a mechanism of action. Br J Cancer. 1997;76(2):198-205.
226. Pepin X, Attali L, Domrault C, Gallet S, Metreau JM, Reault Y, et al. On the use of ion-pair chromatography to elucidate doxorubicin release mechanism from polyalkylcyanoacrylate nanoparticles at the cellular level. J Chromatogr B Biomed Sci Appl. 1997 Nov 21;702(1-2):181-91.
227. Kopecek J, Kopeckova P, Minko T, Lu Z. HPMA copolymer-anticancer drug conjugates: design, activity, and mechanism of action. Eur J Pharm Biopharm. 2000 Jul;50(1):61-81.
228. Dong X, Mumper RJ. Nanomedicinal strategies to treat multidrug-resistant tumors: current progress. Nanomedicine (Lond). 2010 Jun;5(4):597-615.
229. Advani R, Lum BL, Fisher GA, Halsey J, Chin DL, Jacobs CD, et al. A phase I trial of liposomal doxorubicin, paclitaxel and valspodar (PSC-833), an inhibitor of multidrug resistance. Ann Oncol. 2005 Dec;16(12):1968-73.
230. Fracasso PM, Blum KA, Ma MK, Tan BR, Wright LP, Goodner SA, et al. Phase I study of pegylated liposomal doxorubicin and the multidrug-resistance modulator, valspodar. Br J Cancer. 2005 Jul 11;93(1):46-53.
231. Krishna R, Mayer LD. Liposomal doxorubicin circumvents PSC 833-free drug interactions, resulting in effective therapy of multidrug-resistant solid tumors. Cancer Res. 1997 Dec 1;57(23):5246-53.
232. Krishna R, McIntosh N, Riggs KW, Mayer LD. Doxorubicin encapsulated in sterically stabilized liposomes exhibits renal and biliary clearance properties that are independent of valspodar (PSC 833) under conditions that significantly

inhibit nonencapsulated drug excretion. Clin Cancer Res. 1999 Oct;5(10):2939-47.
233. Jones M, Leroux J. Polymeric micelles - a new generation of colloidal drug carriers. Eur J Pharm Biopharm. 1999 Sep;48(2):101-11.
234. Aliabadi HM, Lavasanifar A. Polymeric micelles for drug delivery. Expert Opin Drug Deliv. 2006 Jan;3(1):139-62.
235. Mahmud A, Xiong XB, Aliabadi HM, Lavasanifar A. Polymeric micelles for drug targeting. J Drug Target. 2007 Nov;15(9):553-84.
236. Kwon GS, Kataoka K. Block copolymer micelles as long-circulating drug vehicles. Advanced Drug Delivery Reviews. 1995;16(2-3):295-309.
237. Yu BG, Okano T, Kataoka K, Kwon G. Polymeric micelles for drug delivery: solubilization and haemolytic activity of amphotericin B. J Control Release. 1998 Apr 30;53(1-3):131-6.
238. Zhang X, Jackson JK, Burt HM. Development of amphiphilic diblock copolymers as micellar carriers of taxol. International Journal of Pharmaceutics. 1996;132(1-2):195-206.
239. Maeda H. SMANCS and polymer-conjugated macromolecular drugs: advantages in cancer chemotherapy. Adv Drug Deliv Rev. 2001 Mar 1;46(1-3):169-85.
240. Allen TM, Hansen C, Martin F, Redemann C, Yau-Young A. Liposomes containing synthetic lipid derivatives of poly(ethylene glycol) show prolonged circulation half-lives in vivo. Biochim Biophys Acta. 1991 Jul 1;1066(1):29-36.
241. Gregoriadis G. Liposome research in drug delivery: the early days. J Drug Target. 2008 Aug;16(7):520-4.
242. Chung JE, Yokoyama M, Okano T. Inner core segment design for drug delivery control of thermo-responsive polymeric micelles. J Control Release. 2000 Mar 1;65(1-2):93-103.
243. Lavasanifar A, Samuel J, Kwon GS. The effect of fatty acid substitution on the in vitro release of amphotericin B from micelles composed of poly(ethylene oxide)-block-poly(N-hexyl stearate-L-aspartamide). J Control Release. 2002 Feb 19;79(1-3):165-72.
244. Mahmud A, Xiong XB, Lavasanifar A. Novel self-associating poly(ethylene oxide)-block-poly(epsilon-caprolactone) block copolymers with functional side groups on the polyester block for drug delivery. Macromolecules. 2006 Dec;39(26):9419-28.
245. Yoo HS, Lee EA, Park TG. Doxorubicin-conjugated biodegradable polymeric micelles having acid-cleavable linkages. J Control Release. 2002 Jul 18;82(1):17-27.
246. Yoo HS, Lee KH, Oh JE, Park TG. In vitro and in vivo anti-tumor activities of nanoparticles based on doxorubicin-PLGA conjugates. J Control Release. 2000 Sep 3;68(3):419-31.
247. Dufresne MH, Elsabahy M, Leroux JC. Characterization of polyion complex micelles designed to address the challenges of oligonucleotide delivery. Pharm Res. 2008 Sep;25(9):2083-93.
248. Harada A, Togawa H, Kataoka K. Physicochemical properties and nuclease resistance of antisense-oligodeoxynucleotides entrapped in the core of

polyion complex micelles composed of poly(ethylene glycol)-poly(L-lysine) block copolymers. Eur J Pharm Sci. 2001 Apr;13(1):35-42.
249. Harada-Shiba M, Yamauchi K, Harada A, Takamisawa I, Shimokado K, Kataoka K. Polyion complex micelles as vectors in gene therapy--pharmacokinetics and in vivo gene transfer. Gene Ther. 2002 Mar;9(6):407-14.
250. Itaka K, Yamauchi K, Harada A, Nakamura K, Kawaguchi H, Kataoka K. Polyion complex micelles from plasmid DNA and poly(ethylene glycol)-poly(L-lysine) block copolymer as serum-tolerable polyplex system: physicochemical properties of micelles relevant to gene transfection efficiency. Biomaterials. 2003 Nov;24(24):4495-506.
251. Jeong YI, Kim SH, Jung TY, Kim IY, Kang SS, Jin YH, et al. Polyion complex micelles composed of all-trans retinoic acid and poly (ethylene glycol)-grafted-chitosan. J Pharm Sci. 2006 Nov;95(11):2348-60.
252. Luo Y, Yao X, Yuan J, Ding T, Gao Q. Preparation and drug controlled-release of polyion complex micelles as drug delivery systems. Colloids Surf B Biointerfaces. 2009 Feb 1;68(2):218-24.
253. Wakebayashi D, Nishiyama N, Itaka K, Miyata K, Yamasaki Y, Harada A, et al. Polyion complex micelles of pDNA with acetal-poly(ethylene glycol)-poly(2-(dimethylamino)ethyl methacrylate) block copolymer as the gene carrier system: physicochemical properties of micelles relevant to gene transfection efficacy. Biomacromolecules. 2004 Nov-Dec;5(6):2128-36.
254. Wakebayashi D, Nishiyama N, Yamasaki Y, Itaka K, Kanayama N, Harada A, et al. Lactose-conjugated polyion complex micelles incorporating plasmid DNA as a targetable gene vector system: their preparation and gene transfecting efficiency against cultured HepG2 cells. J Control Release. 2004 Mar 24;95(3):653-64.
255. Wang CH, Wang WT, Hsiue GH. Development of polyion complex micelles for encapsulating and delivering amphotericin B. Biomaterials. 2009 Jul;30(19):3352-8.
256. Yang KW, Li XR, Yang ZL, Li PZ, Wang F, Liu Y. Novel polyion complex micelles for liver-targeted delivery of diammonium glycyrrhizinate: in vitro and in vivo characterization. J Biomed Mater Res A. 2009 Jan;88(1):140-8.
257. Rapoport N. Stabilization and activation of Pluronic micelles for tumor-targeted drug delivery. Colloids and Surfaces B: Biointerfaces. 1999;16:93-111.
258. Batrakova EV, Li S, Miller DW, Kabanov AV. Pluronic P85 increases permeability of a broad spectrum of drugs in polarized BBMEC and Caco-2 cell monolayers. Pharm Res. 1999 Sep;16(9):1366-72.
259. Kwon GS, Naito M, Yokoyama M, Okano T, Sakurai Y, Kataoka K. Physical entrapment of adriamycin in AB block copolymer micelles. Pharm Res. 1995 Feb;12(2):192-5.
260. Kim SC, Kim DW, Shim YH, Bang JS, Oh HS, Wan Kim S, et al. In vivo evaluation of polymeric micellar paclitaxel formulation: toxicity and efficacy. J Control Release. 2001 May 14;72(1-3):191-202.
261. Kwon G, Naito M, Yokoyama M, Okano T, Sakurai Y, Kataoka K. Block copolymer micelles for drug delivery: loading and release of doxorubicin. Journal of Controlled Release. 1997;48(2-3):195-201.

262. Kataoka K, Matsumoto T, Yokoyama M, Okano T, Sakurai Y, Fukushima S, et al. Doxorubicin-loaded poly(ethylene glycol)-poly(beta-benzyl-L-aspartate) copolymer micelles: their pharmaceutical characteristics and biological significance. J Control Release. 2000 Feb 14;64(1-3):143-53.
263. Aliabadi HM, Mahmud A, Sharifabadi AD, Lavasanifar A. Micelles of methoxy poly(ethylene oxide)-b-poly(epsilon-caprolactone) as vehicles for the solubilization and controlled delivery of cyclosporine A. J Control Release. 2005 May 18;104(2):301-11.
264. Shuai X, Merdan T, Schaper AK, Xi F, Kissel T. Core-cross-linked polymeric micelles as paclitaxel carriers. Bioconjug Chem. 2004 May-Jun;15(3):441-8.
265. Hu J, Johnston KP, Williams RO, 3rd. Nanoparticle engineering processes for enhancing the dissolution rates of poorly water soluble drugs. Drug Dev Ind Pharm. 2004 Mar;30(3):233-45.
266. Kipp JE. The role of solid nanoparticle technology in the parenteral delivery of poorly water-soluble drugs. Int J Pharm. 2004 Oct 13;284(1-2):109-22.
267. Gelderblom H, Verweij J, Nooter K, Sparreboom A. Cremophor EL: the drawbacks and advantages of vehicle selection for drug formulation. Eur J Cancer. 2001 Sep;37(13):1590-8.
268. van Zuylen L, Verweij J, Sparreboom A. Role of formulation vehicles in taxane pharmacology. Invest New Drugs. 2001 May;19(2):125-41.
269. Lee J, Lee SC, Acharya G, Chang CJ, Park K. Hydrotropic solubilization of paclitaxel: analysis of chemical structures for hydrotropic property. Pharm Res. 2003 Jul;20(7):1022-30.
270. Choucair A, Eisenberg A. Interfacial solubilization of model amphiphilic molecules in block copolymer micelles. J Am Chem Soc. 2003 Oct 1;125(39):11993-2000.
271. Liu J, Xiao Y, Allen C. Polymer-drug compatibility: a guide to the development of delivery systems for the anticancer agent, ellipticine. J Pharm Sci. 2004 Jan;93(1):132-43.
272. Yokoyama M, Okano T, Sakurai Y, Kataoka K. Improved synthesis of adriamycin-conjugated poly (ethylene oxide)-poly (aspartic acid) block copolymer and formation of unimodal micellar structure with controlled amount of physically entrapped adriamycin. Journal of Controlled Release. 1994;32(3):269-77.
273. Adams ML, Kwon GS. Relative aggregation state and hemolytic activity of amphotericin B encapsulated by poly(ethylene oxide)-block-poly(N-hexyl-L-aspartamide)-acyl conjugate micelles: effects of acyl chain length. J Control Release. 2003 Feb 21;87(1-3):23-32.
274. Lavasanifar A, Samuel J, Kwon GS. Micelles self-assembled from poly(ethylene oxide)-block-poly(N-hexyl stearate L-aspartamide) by a solvent evaporation method: effect on the solubilization and haemolytic activity of amphotericin B. J Control Release. 2001 Nov 9;77(1-2):155-60.
275. Liu J, Lee H, Allen C. Formulation of drugs in block copolymer micelles: drug loading and release. Curr Pharm Des. 2006;12(36):4685-701.

276. Zuleger S, Lippold BC. Polymer particle erosion controlling drug release. I. Factors influencing drug release and characterization of the release mechanism. Int J Pharm. 2001 Apr 17;217(1-2):139-52.
277. Li Y, Kwon GS. Methotrexate esters of poly(ethylene oxide)-block-poly(2-hydroxyethyl-L-aspartamide). Part I: Effects of the level of methotrexate conjugation on the stability of micelles and on drug release. Pharm Res. 2000 May;17(5):607-11.
278. Nishiyama N, Okazaki S, Cabral H, Miyamoto M, Kato Y, Sugiyama Y, et al. Novel cisplatin-incorporated polymeric micelles can eradicate solid tumors in mice. Cancer Res. 2003 Dec 15;63(24):8977-83.
279. Matsumura Y, Maeda H. A new concept for macromolecular therapeutics in cancer chemotherapy: mechanism of tumoritropic accumulation of proteins and the antitumor agent smancs. Cancer Res. 1986 Dec;46(12 Pt 1):6387-92.
280. Fang J, Nakamura H, Maeda H. The EPR effect: Unique features of tumor blood vessels for drug delivery, factors involved, and limitations and augmentation of the effect. Adv Drug Deliv Rev. 2011 Mar 18;63(3):136-51.
281. Maeda H, Fang J, Inutsuka T, Kitamoto Y. Vascular permeability enhancement in solid tumor: various factors, mechanisms involved and its implications. Int Immunopharmacol. 2003 Mar;3(3):319-28.
282. Maeda H. The enhanced permeability and retention (EPR) effect in tumor vasculature: the key role of tumor-selective macromolecular drug targeting. Adv Enzyme Regul. 2001;41:189-207.
283. Wang GL, Jiang BH, Rue EA, Semenza GL. Hypoxia-inducible factor 1 is a basic-helix-loop-helix-PAS heterodimer regulated by cellular O2 tension. Proc Natl Acad Sci U S A. 1995 Jun 6;92(12):5510-4.
284. Jubb AM, Oates AJ, Holden S, Koeppen H. Predicting benefit from anti-angiogenic agents in malignancy. Nat Rev Cancer. 2006 Aug;6(8):626-35.
285. Senger DR, Galli SJ, Dvorak AM, Perruzzi CA, Harvey VS, Dvorak HF. Tumor cells secrete a vascular permeability factor that promotes accumulation of ascites fluid. Science. 1983 Feb 25;219(4587):983-5.
286. Jain RK. Delivery of molecular and cellular medicine to solid tumors. Adv Drug Deliv Rev. 2001 Mar 1;46(1-3):149-68.
287. Matsumura Y, Kimura M, Yamamoto T, Maeda H. Involvement of the kinin-generating cascade in enhanced vascular permeability in tumor tissue. Jpn J Cancer Res. 1988 Dec;79(12):1327-34.
288. Doi K, Akaike T, Horie H, Noguchi Y, Fujii S, Beppu T, et al. Excessive production of nitric oxide in rat solid tumor and its implication in rapid tumor growth. Cancer. 1996 Apr 15;77(8 Suppl):1598-604.
289. Maeda H, Noguchi Y, Sato K, Akaike T. Enhanced vascular permeability in solid tumor is mediated by nitric oxide and inhibited by both new nitric oxide scavenger and nitric oxide synthase inhibitor. Jpn J Cancer Res. 1994 Apr;85(4):331-4.
290. Reichman HR, Farrell CL, Del Maestro RF. Effects of steroids and nonsteroid anti-inflammatory agents on vascular permeability in a rat glioma model. J Neurosurg. 1986 Aug;65(2):233-7.

291. Wu J, Akaike T, Hayashida K, Okamoto T, Okuyama A, Maeda H. Enhanced vascular permeability in solid tumor involving peroxynitrite and matrix metalloproteinases. Jpn J Cancer Res. 2001 Apr;92(4):439-51.
292. Maeda H, Bharate GY, Daruwalla J. Polymeric drugs for efficient tumor-targeted drug delivery based on EPR-effect. Eur J Pharm Biopharm. 2009 Mar;71(3):409-19.
293. Kashiwagi S, Tsukada K, Xu L, Miyazaki J, Kozin SV, Tyrrell JA, et al. Perivascular nitric oxide gradients normalize tumor vasculature. Nat Med. 2008;14(3):255-7.
294. Bergers G, Benjamin LE. Tumorigenesis and the angiogenic switch. Nat Rev Cancer. 2003 Jun;3(6):401-10.
295. Hobbs SK, Monsky WL, Yuan F, Roberts WG, Griffith L, Torchilin VP, et al. Regulation of transport pathways in tumor vessels: role of tumor type and microenvironment. Proc Natl Acad Sci U S A. 1998 Apr 14;95(8):4607-12.
296. Yuan F, Dellian M, Fukumura D, Leunig M, Berk DA, Torchilin VP, et al. Vascular permeability in a human tumor xenograft: molecular size dependence and cutoff size. Cancer Res. 1995 Sep 1;55(17):3752-6.
297. Maki S, Konno T, Maeda H. Image enhancement in computerized tomography for sensitive diagnosis of liver cancer and semiquantitation of tumor selective drug targeting with oily contrast medium. Cancer. 1985 Aug 15;56(4):751-7.
298. Konno T, Maeda H, Iwai K, Maki S, Tashiro S, Uchida M, et al. Selective targeting of anti-cancer drug and simultaneous image enhancement in solid tumors by arterially administered lipid contrast medium. Cancer. 1984 Dec 1;54(11):2367-74.
299. Chau Y, Dang NM, Tan FE, Langer R. Investigation of targeting mechanism of new dextran-peptide-methotrexate conjugates using biodistribution study in matrix-metalloproteinase-overexpressing tumor xenograft model. J Pharm Sci. 2006 Mar;95(3):542-51.
300. Xiong XB, Huang Y, Lu WL, Zhang X, Zhang H, Nagai T, et al. Enhanced intracellular delivery and improved antitumor efficacy of doxorubicin by sterically stabilized liposomes modified with a synthetic RGD mimetic. J Control Release. 2005 Oct 3;107(2):262-75.
301. Shenoy D, Little S, Langer R, Amiji M. Poly(ethylene oxide)-modified poly(beta-amino ester) nanoparticles as a pH-sensitive system for tumor-targeted delivery of hydrophobic drugs: part 2. In vivo distribution and tumor localization studies. Pharm Res. 2005 Dec;22(12):2107-14.
302. Jun YJ, Kim JI, Jun MJ, Sohn YS. Selective tumor targeting by enhanced permeability and retention effect. Synthesis and antitumor activity of polyphosphazene-platinum (II) conjugates. J Inorg Biochem. 2005 Aug;99(8):1593-601.
303. Greish K, Nagamitsu A, Fang J, Maeda H. Copoly(styrene-maleic acid)-pirarubicin micelles: high tumor-targeting efficiency with little toxicity. Bioconjug Chem. 2005 Jan-Feb;16(1):230-6.

304. Gao ZG, Lee DH, Kim DI, Bae YH. Doxorubicin loaded pH-sensitive micelle targeting acidic extracellular pH of human ovarian A2780 tumor in mice. J Drug Target. 2005 Aug;13(7):391-7.
305. Lu Y, Mahato RI, Seki T, Fang J, Maeda H. Tumor-Targeted Macromolecular Drug Delivery Based on the Enhanced Permeability and Retention Effect in Solid Tumor. Pharmaceutical Perspectives of Cancer Therapeutics: Springer New York; 2009. p. 93-120.
306. Torchilin V. Tumor delivery of macromolecular drugs based on the EPR effect. Adv Drug Deliv Rev. 2011 Mar 18;63(3):131-5.
307. Torchilin VP, Lukyanov AN, Gao Z, Papahadjopoulos-Sternberg B. Immunomicelles: targeted pharmaceutical carriers for poorly soluble drugs. Proc Natl Acad Sci U S A. 2003 May 13;100(10):6039-44.
308. Park EK, Kim SY, Lee SB, Lee YM. Folate-conjugated methoxy poly(ethylene glycol)/poly(epsilon-caprolactone) amphiphilic block copolymeric micelles for tumor-targeted drug delivery. J Control Release. 2005 Dec 5;109(1-3):158-68.
309. Akimoto J, Nakayama M, Sakai K, Okano T. Temperature-induced intracellular uptake of thermoresponsive polymeric micelles. Biomacromolecules. 2009 Jun 8;10(6):1331-6.
310. Cheng C, Wei H, Zhu JL, Chang C, Cheng H, Li C, et al. Functionalized thermoresponsive micelles self-assembled from biotin-PEG-b-P(NIPAAm-co-HMAAm)-b-PMMA for tumor cell target. Bioconjug Chem. 2008 Jun;19(6):1194-201.
311. Koo H, Lee H, Lee S, Min KH, Kim MS, Lee DS, et al. In vivo tumor diagnosis and photodynamic therapy via tumoral pH-responsive polymeric micelles. Chem Commun (Camb). 2010 Aug 21;46(31):5668-70.
312. Wang CH, Wang CH, Hsiue GH. Polymeric micelles with a pH-responsive structure as intracellular drug carriers. J Control Release. 2005 Nov 2;108(1):140-9.
313. Husseini GA, Pitt WG. Ultrasonic-activated micellar drug delivery for cancer treatment. J Pharm Sci. 2009 Mar;98(3):795-811.
314. Luo J, Xiao K, Li Y, Lee JS, Shi L, Tan YH, et al. Well-defined, size-tunable, multifunctional micelles for efficient paclitaxel delivery for cancer treatment. Bioconjug Chem. 2010 Jul 21;21(7):1216-24.
315. Tsai HC, Chang WH, Lo CL, Tsai CH, Chang CH, Ou TW, et al. Graft and diblock copolymer multifunctional micelles for cancer chemotherapy and imaging. Biomaterials. 2010 Mar;31(8):2293-301.
316. Xiong XB, Ma Z, Lai R, Lavasanifar A. The therapeutic response to multifunctional polymeric nano-conjugates in the targeted cellular and subcellular delivery of doxorubicin. Biomaterials. 2010 Feb;31(4):757-68.
317. Xiong XB, Mahmud A, Uludag H, Lavasanifar A. Multifunctional polymeric micelles for enhanced intracellular delivery of doxorubicin to metastatic cancer cells. Pharm Res. 2008 Nov;25(11):2555-66.
318. Nakanishi T, Fukushima S, Okamoto K, Suzuki M, Matsumura Y, Yokoyama M, et al. Development of the polymer micelle carrier system for doxorubicin. J Control Release. 2001 Jul 6;74(1-3):295-302.

319. Matsumura Y, Hamaguchi T, Ura T, Muro K, Yamada Y, Shimada Y, et al. Phase I clinical trial and pharmacokinetic evaluation of NK911, a micelle-encapsulated doxorubicin. Br J Cancer. 2004 Nov 15;91(10):1775-81.
320. Danson S, Ferry D, Alakhov V, Margison J, Kerr D, Jowle D, et al. Phase I dose escalation and pharmacokinetic study of pluronic polymer-bound doxorubicin (SP1049C) in patients with advanced cancer. Br J Cancer. 2004 Jun 1;90(11):2085-91.
321. Zhang X, Burt HM, Mangold G, Dexter D, Von Hoff D, Mayer L, et al. Anti-tumor efficacy and biodistribution of intravenous polymeric micellar paclitaxel. Anticancer Drugs. 1997 Aug;8(7):696-701.
322. Ehrlich A, Booher S, Becerra Y, Borris DL, Figg WD, Turner ML, et al. Micellar paclitaxel improves severe psoriasis in a prospective phase II pilot study. J Am Acad Dermatol. 2004 Apr;50(4):533-40.
323. Kim DW, Kim SY, Kim HK, Kim SW, Shin SW, Kim JS, et al. Multicenter phase II trial of Genexol-PM, a novel Cremophor-free, polymeric micelle formulation of paclitaxel, with cisplatin in patients with advanced non-small-cell lung cancer. Ann Oncol. 2007 Dec;18(12):2009-14.
324. Kim TY, Kim DW, Chung JY, Shin SG, Kim SC, Heo DS, et al. Phase I and pharmacokinetic study of Genexol-PM, a cremophor-free, polymeric micelle-formulated paclitaxel, in patients with advanced malignancies. Clin Cancer Res. 2004 Jun 1;10(11):3708-16.
325. Lee KS, Chung HC, Im SA, Park YH, Kim CS, Kim SB, et al. Multicenter phase II trial of Genexol-PM, a Cremophor-free, polymeric micelle formulation of paclitaxel, in patients with metastatic breast cancer. Breast Cancer Res Treat. 2008 Mar;108(2):241-50.
326. Hamaguchi T, Kato K, Yasui H, Morizane C, Ikeda M, Ueno H, et al. A phase I and pharmacokinetic study of NK105, a paclitaxel-incorporating micellar nanoparticle formulation. Br J Cancer. 2007 Jul 16;97(2):170-6.
327. Wilson RH, Plummer R, Adam J, Eatock MM, Boddy AV, Griffin M, et al. Phase I and pharmacokinetic study of NC-6004, a new platinum entity of cisplatin-conjugated polymer forming micelles. 2008 ASCO Annual Meeting 2008.
328. Hamaguchi T, Matsumura Y, Suzuki M, Shimizu K, Goda R, Nakamura I, et al. NK105, a paclitaxel-incorporating micellar nanoparticle formulation, can extend in vivo antitumour activity and reduce the neurotoxicity of paclitaxel. Br J Cancer. 2005 Apr 11;92(7):1240-6.
329. Koizumi F, Kitagawa M, Negishi T, Onda T, Matsumoto S, Hamaguchi T, et al. Novel SN-38-incorporating polymeric micelles, NK012, eradicate vascular endothelial growth factor-secreting bulky tumors. Cancer Res. 2006 Oct 15;66(20):10048-56.
330. Uchino H, Matsumura Y, Negishi T, Koizumi F, Hayashi T, Honda T, et al. Cisplatin-incorporating polymeric micelles (NC-6004) can reduce nephrotoxicity and neurotoxicity of cisplatin in rats. Br J Cancer. 2005 Sep 19;93(6):678-87.
331. Labet M, Thielemans W. Synthesis of polycaprolactone: a review. Chem Soc Rev. 2009 Dec;38(12):3484-504.

332. Allen C, Eisenberg A, Mrsic J, Maysinger D. PCL-b-PEO micelles as a delivery vehicle for FK506: assessment of a functional recovery of crushed peripheral nerve. Drug Deliv. 2000 Jul-Sep;7(3):139-45.
333. Allen C, Han J, Yu Y, Maysinger D, Eisenberg A. Polycaprolactone-b-poly(ethylene oxide) copolymer micelles as a delivery vehicle for dihydrotestosterone. J Control Release. 2000 Feb 3;63(3):275-86.
334. Zhang N, Guo S. Studies on a kind of new biodegradable material, polycaprolactone and developments in medical area. Journal of Biomedical Engineering. 2003 Dec;20(4):746-9.
335. Joshi P, Madras G. Degradation of polycaprolactone in supercritical fluids. Polymer Degradation and Stability. 2008;93(10):1901-8.
336. Sinha VR, Bansal K, Kaushik R, Kumria R, Trehan A. Poly-epsilon-caprolactone microspheres and nanospheres: an overview. Int J Pharm. 2004 Jun 18;278(1):1-23.
337. Chen DR, Bei JZ, Wang SG. Polycaprolactone microparticles and their biodegradation. Polymer Degradation and Stability. 2000;67(3):455-9.
338. Shi B, Fang C, You MX, Zhang Y, Fu S, Pei Y. Stealth MePEG-PCL micelles: effects of polymer composition on micelle physicochemical characteristics, in vitro drug release, in vivo pharmacokinetics in rats and biodistribution in S180 tumor bearing mice. Colloid and Polymer Science. 2005;283(9):954-67.
339. Aliabadi HM, Mahmud A, Sharifabadi AD, Lavasanifar A. Micelles of methoxy poly(ethylene oxide)-b-poly(epsilon-caprolactone) as vehicles for the solubilization and controlled delivery of Cyclosporine A. Journal of Controlled Release. 2005 May 18;104(2):301-11.
340. Aliabadi HM, Elhasi S, Mahmud A, Gulamhusein R, Mahdipoor P, Lavasanifar A. Encapsulation of hydrophobic drugs in polymeric micelles through co-solvent evaporation: The effect of solvent composition on micellar properties and drug loading. Int J Pharm. 2007 Feb 1;329(1-2):158-65.
341. Aliabadi HM, Brocks DR, Lavasanifar A. Polymeric micelles for the solubilization and delivery of cyclosporine A: pharmacokinetics and biodistribution. Biomaterials. 2005 Dec;26(35):7251-9.
342. Aliabadi HM, Brocks DR, Mahdipoor P, Lavasanifar A. A novel use of an in vitro method to predict the in vivo stability of block copolymer based nano-containers. Journal of Controlled Release. 2007 Sep 11;122(1):63-70.
343. Discher BM, Won YY, Ege DS, Lee JC, Bates FS, Discher DE, et al. Polymersomes: tough vesicles made from diblock copolymers. Science. 1999 May 14;284(5417):1143-6.
344. Discher DE, Ahmed F. Polymersomes. Annu Rev Biomed Eng. 2006;8:323-41.
345. Jain JP, Ayen WY, Kumar N. Self assembling polymers as polymersomes for drug delivery. Curr Pharm Des. 2011;17(1):65-79.
346. Aicher L, Meier G, Norcross AJ, Jakubowski J, Varela MC, Cordier A, et al. Decrease in kidney calbindin-D 28kDa as a possible mechanism mediating cyclosporine A- and FK-506-induced calciuria and tubular mineralization. Biochem Pharmacol. 1997 Mar 7;53(5):723-31.

347. Boesch D, Gaverieaux C, Jachez B, Loor F. In vivo circumvention of P-glycoprotein-mediated multidrug resistance of tumor cells with SDZ PSC 833. Cancer Res. 1991 1991;51:4226-33.
348. Cagliero E, Ferracini R, Morello E, Scotlandi K, Manara MC, Buracco P, et al. Reversal of multidrug-resistance using Valspodar (PSC 833) and doxorubicin in osteosarcoma. Oncol Rep. 2004 Nov;12(5):1023-31.
349. Chico I, Kang MH, Bergan R, Abraham J, Bakke S, Meadows B, et al. Phase I study of infusional paclitaxel in combination with the P-glycoprotein antagonist PSC 833. J Clin Oncol. 2001 Feb 1;19(3):832-42.
350. Dorr R, Karanes C, Spier C, Grogan T, Greer J, Moore J, et al. Phase I/II study of the P-glycoprotein modulator PSC 833 in patients with acute myeloid leukemia. J Clin Oncol. 2001 Mar 15;19(6):1589-99.
351. Krishna R, Mayer LD. Modulation of P-glycoprotein (PGP) mediated multidrug resistance (MDR) using chemosensitizers: recent advances in the design of selective MDR modulators. Curr Med Chem Anticancer Agents. 2001 Aug;1(2):163-74.
352. Kovarik JM, Mueller EA, Richard F, Tetzloff W. Optimizing the absorption of valspodar, a P-glycoprotein modulator, Part II: Quantifying its pharmacokinetic variability and refining the bioavailability estimate. J Clin Pharmacol. 1997 Nov;37(11):1009-14.
353. Kornblau SM, Estey E, Madden T, Tran HT, Zhao S, Consoli U, et al. Phase I study of mitoxantrone plus etoposide with multidrug blockade by SDZ PSC-833 in relapsed or refractory acute myelogenous leukemia. J Clin Oncol. 1997 May;15(5):1796-802.
354. Scott MG, Hock KG, Crimmins DL, Fracasso PM. HPLC method for monitoring SDZ PSC 833 in whole blood. Clin Chem. 1997 Mar;43(3):505-10.
355. Lush RM, Meadows B, Fojo AT, Kalafsky G, Smith HT, Bates S, et al. Initial pharmacokinetics and bioavailability of PSC 833, a P-glycoprotein antagonist. J Clin Pharmacol. 1997 Feb;37(2):123-8.
356. van Tellingen O, Kemper M, Tijssen F, van Asperen J, Nooijen WJ, Beijnen JH. High-performance liquid chromatographic bio-analysis of PSC 833 in human and murine plasma. J Chromatogr B Biomed Sci Appl. 1998 Nov 20;719(1-2):251-7.
357. Mueller EA, Kovarik JM, Uresin Y, Preisig-Fluckiger SS, Hensel S, Lucker PW, et al. Optimizing the absorption of valspodar, a P-glycoprotein modulator, Part I: Selecting an oral formulation and exploring its clinical pharmacokinetics/dynamics. J Clin Pharmacol. 1997 Nov;37(11):1001-8.
358. Yatscoff RW, Copeland KR, Faraci CJ. Abbott TDx monoclonal antibody assay evaluated for measuring cyclosporine in whole blood. Clin Chem. 1990 Nov;36(11):1969-73.
359. Ma MK, McLeod HL, Westervelt P, Fracasso PM. Pharmacokinetic study of infusional valspodar. J Clin Pharmacol. 2002 Apr;42(4):412-8.
360. Drewe J, Ball HA, Beglinger C, Peng B, Kemmler A, Schachinger H, et al. Effect of P-glycoprotein modulation on the clinical pharmacokinetics and adverse effects of morphine. Br J Clin Pharmacol. 2000 Sep;50(3):237-46.

361. Cufer T, Vrhovec I, Pfeifer M, Skrk J, Borstnar S, Sikic BI. Effect of the multidrug resistance modulator valspodar on serum cortisol levels in rabbits. Cancer Chemother Pharmacol. 1998;41(6):517-21.
362. Ptachcinski RJ, Venkataramanan R, Burckart GJ, Gray JA, Van Thiel DH, Sanghvi A, et al. Cyclosporine kinetics in healthy volunteers. J Clin Pharmacol. 1987 Mar;27(3):243-8.
363. Desrayaud S, De Lange EC, Lemaire M, Bruelisauer A, De Boer AG, Breimer DD. Effect of the Mdr1a P-glycoprotein gene disruption on the tissue distribution of SDZ PSC 833, a multidrug resistance-reversing agent, in mice. J Pharmacol Exp Ther. 1998 May;285(2):438-43.
364. Vickers AEM, Alegret M, Jimenez RM, Pflimlin V, Fisher R, Spaans C, et al. Changes in human liver and kidney slice function related to potential side-effects in the presence of biotransformation of four cyclosporin derivatives - CSA, IMM, OG, and PSC. In Vitro & Molecular Toxicology-a Journal of Basic and Applied Research. 1998 Sum;11(2):119-32.
365. Mayer U, Wagenaar E, Dorobek B, Beijnen JH, Borst P, Schinkel AH. Full blockade of intestinal P-glycoprotein and extensive inhibition of blood-brain barrier P-glycoprotein by oral treatment of mice with PSC833. Journal of Clinical Investigation. 1997 Nov;100(10):2430-6.
366. Simon N, Dailly E, Combes O, Malaurie E, Lemaire M, Tillement JP, et al. Role of lipoproteins in the plasma binding of SDZ PSC 833, a novel multidrug resistance-reversing cyclosporin. Br J Clin Pharmacol. 1998 Feb;45(2):173-5.
367. Urien S, Zini R, Lemaire M, Tillement JP. Assessment of cyclosporine A interactions with human plasma lipoproteins in vitro and in vivo in the rat. J Pharmacol Exp Ther. 1990 Apr;253(1):305-9.
368. Loor F. Cyclosporins and Related Fungal Products in the Reversal of P-Glycoprotein-mediated Multidrug resistance. In: Gupta S, Tsuruo T, editors. Multidrug Resistance in Cancer Cells: John Wiley & Sons Ltd; 1996. p. 385-412.
369. Gaveriaux C, Boesch D, Boelsterli JJ, Bollinger P, Eberle MK, Hiestand P, et al. Overcoming multidrug resistance in Chinese hamster ovary cells in vitro by cyclosporin A (Sandimmune) and non-immunosuppressive derivatives. Br J Cancer. 1989 Dec;60(6):867-71.
370. Keller RP, Altermatt HJ, Donatsch P, Zihlmann H, Laissue JA, Hiestand PC. Pharmacologic interactions between the resistance-modifying cyclosporine SDZ PSC 833 and etoposide (VP 16-213) enhance in vivo cytostatic activity and toxicity. Int J Cancer. 1992 May 28;51(3):433-8.
371. Sonneveld P, Schoester M, de Leeuw K. Clinical modulation of multidrug resistance in multiple myeloma: effect of cyclosporine on resistant tumor cells. J Clin Oncol. 1994 1994;12:1584-91.
372. Giaccone G, Linn SC, Welink J, Catimel G, Stieltjes H, van der Vijgh WJ, et al. A dose-finding and pharmacokinetic study of reversal of multidrug resistance with SDZ PSC 833 in combination with doxorubicin in patients with solid tumors. Clin Cancer Res. 1997 Nov;3(11):2005-15.
373. Aliabadi HM, Brocks DR, Lavasanifar A. Polymeric micelles for the solubilization and delivery of cyclosporine A: pharmacokinetics and biodistribution. Biomaterials. 2005 Dec;26(35):7251-9.

374. Aliabadi HM, Elhasi S, Brocks DR, Lavasanifar A. Polymeric micellar delivery reduces kidney distribution and nephrotoxic effects of Cyclosporine A after multiple dosing. J Pharm Sci. 2008 May;97(5):1916-26.
375. Qadir M, O'Loughlin KL, Fricke SM, Williamson NA, Greco WR, Minderman H, et al. Cyclosporin A is a broad-spectrum multidrug resistance modulator. Clin Cancer Res. 2005 Mar 15;11(6):2320-6.
376. Ellis AG, Crinis NA, Webster LK. Inhibition of etoposide elimination in the isolated perfused rat liver by Cremophor EL and Tween 80. Cancer Chemother Pharmacol. 1996;38(1):81-7.
377. Millward MJ, Webster LK, Rischin D, Stokes KH, Toner GC, Bishop JF, et al. Phase I trial of cremophor EL with bolus doxorubicin. Clin Cancer Res. 1998 Oct;4(10):2321-9.
378. Webster LK, Cosson EJ, Stokes KH, Millward MJ. Effect of the paclitaxel vehicle, Cremophor EL, on the pharmacokinetics of doxorubicin and doxorubicinol in mice. Br J Cancer. 1996 Feb;73(4):522-4.
379. Onetto N, Dougan M, Hellmann S, Gustafson N, Burroughs J, Florezyk A, et al. Safety Profile. In: McGuire WP, Rowinsky EK, editors. Paclitaxel in Cancer treatment. New York: Marcel Dekker Inc; 1995. p. 175-86.
380. Brat DJ, Windebank AJ, Brimijoin S. Emulsifier for intravenous cyclosporin inhibits neurite outgrowth, causes deficits in rapid axonal transport and leads to structural abnormalities in differentiating N1E.115 neuroblastoma. J Pharmacol Exp Ther. 1992 May;261(2):803-10.
381. Aliabadi HM, Brocks DR, Mahdipoor P, Lavasanifar A. A novel use of an in vitro method to predict the in vivo stability of block copolymer based nano-containers. J Control Release. 2007 Sep 11;122(1):63-70.
382. Chimalakonda AP, Shah RB, Mehvar R. High-performance liquid chromatographic analysis of cyclosporin A in rat blood and liver using a commercially available internal standard. J Chromatogr B Analyt Technol Biomed Life Sci. 2002 May 25;772(1):107-14.
383. Batalini C, Bieber LW, . Model studies on the synthesis of the natural meroterpenoid cordiaquinone A. Eclética Química. 2001;26:69-76.
384. Wilhelm M, Zhao CL, Wang YC, Xu RL, Winnik MA, Mura JL, et al. Polymer Micelle Formation .3. Poly(Styrene-Ethylene Oxide) Block Copolymer Micelle Formation in Water - a Fluorescence Probe Study. Macromolecules. 1991 Mar 4;24(5):1033-40.
385. Lavasanifar A, Samuel J, Kwon GS. The effect of alkyl core structure on micellar properties of poly(ethylene oxide)-block-poly(L-aspartamide) derivatives. Colloids Surf B Biointerfaces. 2001 Oct;22(2):115-26.
386. Brocks DR. Stereoselective pharmacokinetics of desbutylhalofantrine, a metabolite of halofantrine, in the rat after administration of the racemic metabolite or parent drug. Biopharm Drug Dispos. 2000 Dec;21(9):365-71.
387. Brocks DR, Ala S, Aliabadi HM. The effect of increased lipoprotein levels on the pharmacokinetics of cyclosporine A in the laboratory rat. Biopharm Drug Dispos. 2006 Jan;27(1):7-16.

388. Schuhmacher J, Buhner K, Witt-Laido A. Determination of the free fraction and relative free fraction of drugs strongly bound to plasma proteins. J Pharm Sci. 2000 Aug;89(8):1008-21.
389. Brocks DR, Wasan KM. The influence of lipids on stereoselective pharmacokinetics of halofantrine: Important implications in food-effect studies involving drugs that bind to lipoproteins. J Pharm Sci. 2002 Aug;91(8):1817-26.
390. Binkhathlan Z, Somayaji V, Brocks DR, Lavasanifar A. Development of a liquid chromatography-mass spectrometry (LC/MS) assay method for the quantification of PSC 833 (Valspodar) in rat plasma. J Chromatogr B Analyt Technol Biomed Life Sci. 2008 Jun 15;869(1-2):31-7.
391. Chiou WL. Critical evaluation of the potential error in pharmacokinetic studies of using the linear trapezoidal rule method for the calculation of the area under the plasma level--time curve. J Pharmacokinet Biopharm. 1978 Dec;6(6):539-46.
392. Davies B, Morris T. Physiological parameters in laboratory animals and humans. Pharm Res. 1993 Jul;10(7):1093-5.
393. Aliabadi HM, Elhasi S, Mahmud A, Gulamhusein R, Mahdipoor P, Lavasanifar A. Encapsulation of hydrophobic drugs in polymeric micelles through co-solvent evaporation: the effect of solvent composition on micellar properties and drug loading. Int J Pharm. 2007 Feb 1;329(1-2):158-65.
394. FDA. Guidance for industry; bioanalytical method validation. Rockville: U.S. Department of Health and Human Services; 2001.
395. Halperin A. Polymeric Micelles - a Star Model. Macromolecules. 1987 Nov;20(11):2943-6.
396. Nagarajan R, Ganesh K. Block Copolymer Self-Assembly in Selective Solvents - Theory of Solubilization in Spherical Micelles. Macromolecules. 1989 Nov;22(11):4312-25.
397. Yamamoto T, Yokoyama M, Opanasopit P, Hayama A, Kawano K, Maitani Y. What are determining factors for stable drug incorporation into polymeric micelle carriers? Consideration on physical and chemical characters of the micelle inner core. J Control Release. 2007 Oct 18;123(1):11-8.
398. Bhargava P, Zheng JX, Li P, Quirk RP, Harris FW, Cheng SZD. Self-assembled polystyrene-block-poly(ethylene oxide) micelle morphologies in solution. Macromolecules. 2006 Jul 11;39(14):4880-8.
399. Choucair A, Eisenberg A. Control of amphiphilic block copolymer morphologies using solution conditions. Eur Phys J E. 2003 Jan;10(1):37-44.
400. Geng Y, Ahmed F, Bhasin N, Discher DE. Visualizing worm micelle dynamics and phase transitions of a charged diblock copolymer in water. J Phys Chem B. 2005 Mar 10;109(9):3772-9.
401. Zhang LF, Eisenberg A. Multiple morphologies and characteristics of "crew-cut" micelle-like aggregates of polystyrene-b-poly(acrylic acid) diblock copolymers in aqueous solutions. J Am Chem Soc. 1996 Apr 3;118(13):3168-81.
402. Jain S, Bates FS. On the origins of morphological complexity in block copolymer surfactants. Science. 2003 Apr 18;300(5618):460-4.
403. Won YY, Brannan AK, Davis HT, Bates FS. Cryogenic transmission electron microscopy (cryo-TEM) of micelles and vesicles formed in water by

polyethylene oxide)-based block copolymers. Journal of Physical Chemistry B. 2002 Apr 4;106(13):3354-64.
404. Zupancich JA, Bates FS, Hillmyer MA. Aqueous dispersions of poly(ethylene oxide)-b-poly(gamma-methyl-epsilon-caprolactone) block copolymers. Macromolecules. 2006 Jun 27;39(13):4286-8.
405. Discher BM, Won YY, Ege DS, Lee JCM, Bates FS, Discher DE, et al. Polymersomes: Tough vesicles made from diblock copolymers. Science. 1999 May 14;284(5417):1143-6.
406. Discher DE, Ahmed F. Polymersomes. Annu Rev Biomed Eng. 2006;8:323-41.
407. Mathot F, van Beijsterveldt L, Preat V, Brewster M, Arien A. Intestinal uptake and biodistribution of novel polymeric micelles after oral administration. J Control Release. 2006 Mar 10;111(1-2):47-55.
408. Ould-Ouali L, Noppe M, Langlois X, Willems B, Te Riele P, Timmerman P, et al. Self-assembling PEG-p(CL-co-TMC) copolymers for oral delivery of poorly water-soluble drugs: a case study with risperidone. J Control Release. 2005 Feb 16;102(3):657-68.
409. Mathot F, des Rieux A, Arien A, Schneider YJ, Brewster M, Preat V. Transport mechanisms of mmePEG750P(CL-co-TMC) polymeric micelles across the intestinal barrier. J Control Release. 2007 Dec 20;124(3):134-43.
410. Pierri E, Avgoustakis K. Poly(lactide)-poly(ethylene glycol) micelles as a carrier for griseofulvin. J Biomed Mater Res A. 2005 Dec 1;75(3):639-47.
411. Allen C, Yu Y, Eisenberg A, Maysinger D. Cellular internalization of PCL(20)-b-PEO(44) block copolymer micelles. Biochim Biophys Acta. 1999 Sep 21;1421(1):32-8.
412. Luo L, Tam J, Maysinger D, Eisenberg A. Cellular internalization of poly(ethylene oxide)-b-poly(epsilon-caprolactone) diblock copolymer micelles. Bioconjug Chem. 2002 Nov-Dec;13(6):1259-65.
413. Nam YS, Kang HS, Park JY, Park TG, Han SH, Chang IS. New micelle-like polymer aggregates made from PEI-PLGA diblock copolymers: micellar characteristics and cellular uptake. Biomaterials. 2003 May;24(12):2053-9.
414. Gonzalez O, Colombo T, De Fusco M, Imperatori L, Zucchetti M, D'Incalci M. Changes in doxorubicin distribution and toxicity in mice pretreated with the cyclosporin analogue SDZ PSC 833. Cancer Chemother Pharmacol. 1995;36(4):335-40.
415. Krishna R, St-Louis M, Mayer LD. Increased intracellular drug accumulation and complete chemosensitization achieved in multidrug-resistant solid tumors by co-administering valspodar (PSC 833) with sterically stabilized liposomal doxorubicin. Int J Cancer. 2000 Jan 1;85(1):131-41.
416. Goeptar AR, Te Koppele JM, Lamme EK, Pique JM, Vermeulen NP. Cytochrome P450 2B1-mediated one-electron reduction of adriamycin: a study with rat liver microsomes and purified enzymes. Mol Pharmacol. 1993 Dec;44(6):1267-77.
417. Cusack BJ, Young SP, Driskell J, Olson RD. Doxorubicin and doxorubicinol pharmacokinetics and tissue concentrations following bolus

injection and continuous infusion of doxorubicin in the rabbit. Cancer Chemother Pharmacol. 1993;32(1):53-8.
418. Riggs CE, Jr., Benjamin RS, Serpick AA, Bachur NR. Bilary disposition of adriamycin. Clin Pharmacol Ther. 1977 Aug;22(2):234-41.
419. Tavoloni N, Guarino AM. Biliary and urinary excretion of adriamycin in anesthetized rats. Pharmacology. 1980;20(5):256-67.
420. Yesair DW, Schwartzbach E, Shuck D, Denine EP, Asbell MA. Comparative pharmacokinetics of daunomycin and adriamycin in several animal species. Cancer Res. 1972 Jun;32(6):1177-83.
421. Colombo T, Zucchetti M, D'Incalci M. Cyclosporin A markedly changes the distribution of doxorubicin in mice and rats. J Pharmacol Exp Ther. 1994 Apr;269(1):22-7.
422. Speeg KV, Maldonado AL, Liaci J, Muirhead D. Effect of cyclosporine on colchicine secretion by a liver canalicular transporter studied in vivo. Hepatology. 1992 May;15(5):899-903.
423. Speeg KV, Maldonado AL, Liaci J, Muirhead D. Effect of cyclosporine on colchicine secretion by the kidney multidrug transporter studied in vivo. J Pharmacol Exp Ther. 1992 Apr;261(1):50-5.
424. Suzuki T, Zhao YL, Nadai M, Naruhashi K, Shimizu A, Takagi K, et al. Gender-related differences in expression and function of hepatic P-glycoprotein and multidrug resistance-associated protein (Mrp2) in rats. Life Sci. 2006 Jun 27;79(5):455-61.
425. Vlaming ML, Mohrmann K, Wagenaar E, de Waart DR, Elferink RP, Lagas JS, et al. Carcinogen and anticancer drug transport by Mrp2 in vivo: studies using Mrp2 (Abcc2) knockout mice. J Pharmacol Exp Ther. 2006 Jul;318(1):319-27.
426. Yamaguchi S, Zhao YL, Nadai M, Yoshizumi H, Cen X, Torita S, et al. Involvement of the drug transporters p glycoprotein and multidrug resistance-associated protein Mrp2 in telithromycin transport. Antimicrob Agents Chemother. 2006 Jan;50(1):80-7.